The architecture of Recent brachiopod shells: diversity of biocrystal and biopolymer assemblages in rhynchonellide, terebratulide, thecideide and craniide shells

Maria Simonet Roda, Erika Griesshaber, Lucia Angiolini, Claire Rollion-Bard, Elizabeth M Harper, Maria Aleksandra Bitner, Sara Milner Garcia, Facheng Ye, Daniela Henkel, Vreni Häussermann, et al.

Marine Biology (2022) 169:4
https://doi.org/10.1007/s00227-021-03962-4

REVIEW, CONCEPT, AND SYNTHESIS

The architecture of Recent brachiopod shells: diversity of biocrystal and biopolymer assemblages in rhynchonellide, terebratulide, thecideide and craniide shells

Maria Simonet Roda[1] · Erika Griesshaber[1] · Lucia Angiolini[2] · Claire Rollion-Bard[3,4] · Elizabeth M. Harper[5] · Maria Aleksandra Bitner[6] · Sara Milner Garcia[3,4] · Facheng Ye[7] · Daniela Henkel[8] · Vreni Häussermann[9] · Anton Eisenhauer[8] · Helmut Gnägi[10] · Uwe Brand[11] · Alan Logan[12] · Wolfgang W. Schmahl[1]

Received: 13 May 2021 / Accepted: 23 August 2021

Abstract

Biological hard tissues are a rich source of design concepts for the generation of advanced materials. They represent the most important library of information on the evolution of life and its environmental conditions. Organisms produce soft and hard tissues in a bottom-up process, a construction principle that is intrinsic to biologically secreted materials. This process emerged early on in the geological record, with the onset of biological mineralization. The phylum Brachiopoda is a marine animal group that has an excellent and continuous fossil record from the early Cambrian to the Recent. Throughout this time interval, the Brachiopoda secreted phosphate and carbonate shells and populated many and highly diverse marine habitats. This required great flexibility in the adaptation of soft and hard tissues to the different marine environments and living conditions. This review presents, juxtaposes and discusses the main modes of mineral and biopolymer organization in Recent, carbonate shell-producing, brachiopods. We describe shell tissue characteristics for taxa of the orders Rhynchonellida, Terebratulida, Thecideida and Craniida. We highlight modes of calcite and organic matrix assembly at the macro-, micro-, and nano-scales based on results obtained by Electron Backscatter Diffraction, Atomic Force Microscopy, Field Emission Scanning Electron Microscopy and Scanning Transmission Electron Microscopy. We show variation in composite hard tissue organization for taxa with different lifestyles, visualize nanometer-scale calcite assemblies for rhynchonellide and terebratulide fibers, highlight thecideide shell microstructure, texture and chemistry characteristics, and discuss the feasibility to use thecideide shells as archives of proxies for paleoenvironment and paleoclimate reconstructions.

Keywords Diversity of brachiopod crystal and biopolymer assembly · Determinants of microstructure and texture · Brachiopod microstructure and lifestyle · Brachiopod microstructure and environment · EBSD · AFM

Responsible Editor: A.G. Checa.

✉ Erika Griesshaber
e.griesshaber@lrz.uni-muenchen.de

[1] Department of Earth and Environmental Sciences, LMU Munich, Munich, Germany

[2] Dipartimento di Scienze della Terra "A. Desio", Università degli Studi di Milano, Milan, Italy

[3] Université de Paris, Institut de physique du globe de Paris, CNRS, 75005 Paris, France

[4] Present Address: Laboratoire des Sciences du Climat et de l'Environnement, LSCE, Gif sur Yvette, France

[5] Department of Earth Sciences, University of Cambridge, Cambridge CB2 3EQ, UK

[6] Institute of Paleobiology, Polish Academy of Sciences, 00-818 Warsaw, Poland

[7] School of Earth, Atmospheric and Life Sciences, University of Wollongong, Wollongong, NSW 2522, Australia

[8] GEOMAR-Helmholtz Centre for Ocean Research, Marine Biogeochemistry/Marine Geosystems, Kiel, Germany

[9] Huinay Scientific Field Station, Casilla 462, Puerto Montt, Chile

[10] Diatome Ltd, Helmstraße 1, 2560 Nidau, Switzerland

[11] Department of Earth Sciences, Brock University, St. Catharines, ON L2S 3A1, Canada

[12] Centre for Coastal Studies, University of New Brunswick, Saint John, NB E2L 4L5, Canada

Published online: 20 November 2021

Introduction

Brachiopods are bi-valved lophophorates and form a group of marine sessile organisms that secrete either phosphatic (Linguliformea) or calcitic (Craniiformea, Rhynchonelliformea) shells. An important function of these shells is to protect the soft-part anatomy housed between the posteriorly connected ventral and dorsal valves. In addition to protection, the valves also render hydrodynamic control of water flow through the shell for nutrition (Shiino and Suzuki 2010; Shiino and Angiolini 2014). Unlike many bivalves, brachiopod valves are not mirror images of each other; although each valve has a mirror plane (Rudwick 1959, 1970; Schmahl et al. 2012).

Mantle tissue underlies the shell and consists of an outer and an inner epithelium, with the outer epithelium being responsible for shell secretion (Simonet Roda et al. 2019b). The lophophore, the feeding and respiratory apparatus of brachiopods, is located in the anterior shell region and occupies the largest part of the mantle cavity. Other organs are positioned more posteriorly and use the least space of the cavity between the valves (e.g. James et al. 1992). Brachiopod shells grow mainly at commissural margins and, to a lesser extent, along inner shell surfaces (e.g. Williams 1966; Rosenberg et al. 1988; Baumgarten et al. 2014).

Brachiopods have an excellent fossil record (Curry and Brunton 2007; Carlson 2016; Harper et al. 2017). The first species of both phosphate and carbonate shell-producing orders appeared in the early Cambrian. During the Ordovician the phylum diversified (e.g. Carlson 2016; Harper et al. 2017) so that by the end of the Ordovician a wide range of lifestyles, shell structures and morphologies had evolved (e.g. Williams 1997; Harper and Drachen 2010; Harper et al. 2015, 2017; Finnegan et al. 2016). Loss of about 90% of species during the end-Permian mass extinction (He et al. 2019) severely impacted the taxonomic, morphological, functional and ecological diversity of brachiopods (e.g. Curry and Brunton 2007; Carlson 2016). Nonetheless, some brachiopods of the orders of the Lingulida, Craniida, Rhynchonellida, and Terebratulida survived the end-Permian extinction and subsequently diversified. The Thecideida appeared after the end-Permian crisis in the Triassic (Carlson 2016).

Extant brachiopods belong to three subphyla: Linguliformea, Craniiformea and Rhynchonelliformea (Williams et al. 1996). These diverged at the beginning of the Phanerozoic and developed distinct shell structures, morphologies, mineralogies, anatomies, ontogenies and lifestyles (Ushatinskaya 2008; Holmer et al. 2011; Carlson 2016; Harper et al. 2017). For example, when considering only macroscopic shell features, Linguliformea and Craniiformea have no articulatory structures, while Rhynchonelliformea have a well developed tooth and socket system. Linguliformea secrete organophosphatic shells, Craniiformea form organocarbonate shells, while Rhynchonelliformea secrete low Mg-calcite organocarbonate shells. Three subphyla are present since the early Cambrian, although the extant rhynchonelliform orders have fossil records that date back to the Early Ordovician for the Rhynchonellida, to the Devonian for the Terebratulida and to the Triassic for the Thecideida (Williams et al. 1996; Carlson 2016; Harper et al. 2017).

Species of the five extant brachiopod orders populate today shallow to moderately deep, rarely abyssal, sea floor environments and live in a wide range of marine habitats (e.g. Richardson 1997a, b; Emig 1997a, b; Logan 2007; Peck et al. 1997; Peck 2007; Peck and Harper 2010; Emig et al. 2013; Cross et al. 2015, 2016, 2018; Harper et al. 2017; Emig 2017; Bitner 2010, 2019). The geological record shows that brachiopods were and are able to colonize diverse marine environments. They may live in the open ocean as well as in sheltered, even cryptic habitats, and settle within, as well as on hard rock substrates. When living on the sea floor, brachiopods are either attached to hard substrata by a pedicle or are cemented by their ventral valve, or lie free on the sediment surface. Almost all linguliforms burrow and live within the sediment. Accordingly, representatives of the five extant brachiopod orders have different modes of larval development, differ significantly in soft-tissue anatomy, shell morphology, shell chemistry, shell microstructure and texture, as well as in the amount, type and fabric of organic material intercalated into the shell calcite. Thus today, we observe a large diversity in brachiopod body plans as well as in morphological, structural and chemical shell features.

The aim of this review is to highlight, juxtapose and discuss shell microstructure, texture and chemical diversity for Recent calcite-shelled brachiopods. We do not intend to summarize diversity in overall shell morphology or brachiopod biology. For the latter see the excellent review by James et al. (1992). Rather, we aim to give a comprehensive overview of the nano- and microstructure, texture, biopolymer content and distribution for representatives of all four extant calcite-shell producing brachiopod orders: the Terebratulida, Rhynchonellida, Thecideida and Craniida. We investigated twenty Recent brachiopod taxa (Table S1): two rhynchonellide, one craniide, three thecideide and fourteen terebratulide species and base our results and conclusions on Electron Backscatter Diffraction Measurements (EBSD), complemented by AFM, STEM and FE-SEM imaging of fractured and etched shell cross-sectional surfaces and geochemical results obtained by Ion Microprobe and LA-ICP-MS analyses. A number of studies in the last decades address Recent brachiopod shell structure, microstructure and texture (e.g. Rudwick 1959, 1970; Williams 1973, 1997; Williams and Cusack 2007; Schmahl et al. 2004, 2008, 2012; Griesshaber et al. 2005, 2007; Cusack and Williams 2007; England et al. 2007; Pérez-Huerta et al. 2007;

Merkel et al. 2007, 2009; Cusack et al. 2008; Checa et al. 2009; Goetz et al. 2009, 2011; Gaspard and Nouet 2016; Ye et al. 2018a, b). However, these rarely deal with the composite (biomineral and biopolymer) nature of the shell or the nanoscale arrangement of the calcite material. In addition, these studies concentrated on either one or only a few, predominantly, rhynchonellide or/and terebratulide species. In particular, the shell microstructure and texture of Recent Thecideida and Craniida is, so far, little explored, which is done in this study.

We discuss in this article the following:

1. Differences in microstructure and texture for representatives of the different calcite-shelled orders.
2. Differences in shell structure between thecideide species and the primary shell-layer of rhynchonellide and terebratulide taxa.
3. Shell microstructures and textures of Recent Craniida.
4. Microstructure and texture of the brachiopod brachidium.
5. The mode of organic substance intercalation in the different shell layers of rhynchonellide, terebratulide, thecideide and craniide taxa.
6. The nanometer-scale structure of Recent rhynchonellide and terebratulide fibers.
7. The presence of a sparse network of thin biopolymer fibrils within rhynchonellide and terebratulide fibers.
8. Paleoenvironmental reconstructions based on brachiopod shells relies strongly on the preservation state of the fibrous shell layer. We place major attention on the fibers and summarize the present knowledge of calcite organization within the fibrous shell layer of rhynchonellide and terebratulide taxa.

This review is divided into seven sections:

First (Sect. 1), we demonstrate the distinctness in shell calcite organization for representatives of the Terebratulida, Rhynchonellida, Thecideida and Craniida.

As second (Sect. 2), we describe characteristics of the biocrystals, in particular, the diversity of crystal morphologies and, subsequently, as third (Sect. 3), the distribution pattern of organic substance within the shells.

Then (Sect. 4), we focus on the internal structure of brachiopod fibers, discuss nanometer-scale features of terebratulide and rhynchonellide fiber calcite and highlight, in particular, (1) their hierarchical internal structuring and (2) demonstrate for the first time that fibers incorporate a network of thin organic fibrils.

In the next section (Sect. 5), we provide details for terebratulide, rhynchonellide, thecideide and craniide representatives modes of shell calcite assembly and describe characteristics of shell texture. We show that shells of Recent calcitic brachiopods are constructed of seven types of biocrystals: dendrites, fibers, columns, platelets, laminae, acicles and polygons.

Subsequently (Sect. 6), we discuss Recent thecideide shells in greater detail and highlight differences/similarities in shell microstructure and chemistry between thecideide and terebratulide species.

Our review concludes (Sect. 7), with a summary where we discuss for Recent calcitic brachiopods: (1) microstructural adaptations to environments, (2) the advantage of a hierarchical and composite hard tissue for the animal, (3) determinants of brachiopod microstructure and texture fabrication, and (4) characteristics of thecideide shell microstructures in view of their applicability for paleoenvironment reconstructions.

Materials and methods

Materials

We investigated the following Recent brachiopod specimens (Table S1 in the supplementary section): *Megerlia truncata* (Linnaeus, 1767) (Terebratulida), *Magellania venosa* (Dixon, 1789) (Terebratulida), *Terebratulina septentrionalis* (Couthouy, 1838) (Terebratulida), *Terebratalia transversa* (Sowerby, 1846) (Terebratulida), *Magellania flavescens* (Lamarck, 1819) (Terebratulida), *Terebratulina crossei* Davidson, 1882 (Terebratulina), *Terebratalia* sp. (Terebratulida), *Calloria inconspicua* (Sowerby, 1846) (Terebratulida), *Magasella sanguinea* (Leach, 1814) (Terebratulida), *Laqueus rubellus* (Sowerby, 1870) (Terebratulida), *Liothyrella uva* (Broderip, 1833) (Terebratulida), *Liothyrella neozelanica* Thomson, 1918 (Terebratulida), *Gryphus vitreus* (Born, 1778) (Terebratulida), *Magellania fragilis* Smith, 1907 (Terebratulida), *Terebratulina retusa* (Linnaeus, 1758) (Terebratulida), *Notosaria nigricans* (Soweby, 1846) (Rhynchonellida), *Neorhynchia strebeli* (Dall, 1908) (Rhynchonellida), *Kakanuiella chathamensis* Lüter, 2005 (Thecideida), *Pajaudina atlantica* Logan, 1988 (Thecideida), *Thecidellina blochmanni* Dall, 1920 (Thecideida) and *Novocrania anomala* (Müller, 1776) (Craniida); 14 terebratulide, 2 rhynchonellide, 3 thecideide and 1 craniide species. As species of a specific order show similar shell structural patterns, we show here characteristics for select specimens (underlined in Table S1), and we give references for structural information on the other specimens listed in Table S1, supplementary section.

Terminology

In this study, we may use the terms *mineral units or biocrystals* for fibers, columns, acicles, and granules. The outermost, mineralized, shell layer of terebratulide,

rhynchonellide and craniide shells is called, following the terminology used in the literature, primary or outer shell layer. For what are called secondary and tertiary shell layers in the literature, we use the terms fibrous (for the secondary layer) and columnar (for the tertiary layer). It has been shown for some three-layered Recent brachiopods that fibrous layers may alternate with columnar layers (Goetz et al. 2009 and this study) within the secondary layer. Accordingly, the simple numbering of the two inner shell layers into secondary and tertiary ones is not appropriate. When we refer to the different shell layers we use our terminology, but give in parentheses 'secondary/tertiary', the conventional brachiopod shell layer terminology. Other terms such as distal/proximal fiber regions/surfaces and 'proximal membrane', lining the proximal surface of a fiber are indicated and defined in Fig. 15C, D.

Methods

Microstructure and texture analyses

Electron Backscatter Diffraction measurements (EBSD) We base microstructure and texture characterization on Electron Backscatter Diffraction (EBSD) measurements (for further information on microstructure and texture analysis see Engler and Randle (2009), Schwartz et al. 2000; Wilkinson and Britton 2012; Stojakovic 2012). The basics of calcite crystallograpy and twinning patterns of calcite are covered by Brock (1993) and Richards (1999).

EBSD measurements for this study were performed in step increments between 300 and 500 nm. The microstructure is shown with coloured EBSD maps, where similar colours visualize similar crystal orientations, while, different colours indicate differences in crystal orientation. The term texture relates to the varieties of crystal orientations within a material and is given with pole figures.

For EBSD measurements shell samples were embedded in epoxy resin. The embedded samples were subjected to several sequential mechanical grinding and polishing steps. The last two steps consisted of etch-polishing with colloidal alumina in a vibratory polisher and, subsequently, by ion polishing with an Ar beam in an ion polisher. For EBSD measurements the samples were coated with 4–6 nm of carbon. Measurements were carried out with a Hitachi SU5000 field emission SEM, equipped with an Oxford Instruments EBSD detector. During measurements, the SEM was operated at 20 and 15 kV; Kikuchi patterns were indexed with the CHANNEL 5 HKL software.

Information obtained from EBSD measurements is presented as band contrast measurement images and as colour-coded crystal orientation maps with corresponding pole figures. The latter give either individual data points or, in the contoured version, the strength of the clustering of poles. When we show the contoured data, we use the lowest possible degree for half width and cluster size: a half width of 5° and a cluster size of 3°, respectively. The half width controls the extent of the spread of the poles over the surface of the project sphere. A cluster comprises data with the same orientation.

We use two colour-codes for showing calcite orientation in EBSD maps. These are given in appendix figures, Figs. S12E and S13A. The relevant colour-code for a particular EBSD map is given in the appropriate figure caption.

Terminology

1. *EBSD band contrast* gives the signal strength of the EBSD-Kikuchi diffraction pattern and is displayed as the grey-scale component in a map. The strength of the EBSD signal is high when a crystal is detected (bright in the map), whereas it is weak or absent when a polymer is scanned, such as organic matter (dark/black in the map).
2. *Crystal co-orientation statistics* are derived from Kikuchi diffraction patterns measured at each image pixel of an EBSD map. The degree of calcite co-orientation within as well as between mineral units/crystals is obtained from orientational density distribution measurements. Thus, calcite co-orientation is given with the contoured version of the pole figures and by the MUD value.
3. *The MUD (multiple of uniform (random) distribution) value* is calculated using the Oxford Instruments CHANNEL 5 EBSD software. A high MUD indicates high crystal co-orientation, while low MUD values reflect low to random crystallite or/and mineral unit co-orientation. With a half width of 5 and a cluster size of 3 an MUD value above 700 indicates very high crystallite co-orientation strength, as it is the case for a single crystal.
4. *Pole figures* are stereographic projections of the orientations of crystallographic axes or plane normals measured on all pixels of an EBSD map. They can either display individual data points or orientational probability density distributions. We display the pole figures in the same spatial orientation as the corresponding EBSD map using the data points on the lower hemisphere of the stereographic projection.
5. The term *texture* relates to the distribution of crystal orientations within a material and is illustrated by pole figures, showing either colour-coded orientation data or contoured versions of density distributions of c- and *a**-axes poles.
6. A *fiber texture or axial texture* is present when the measured orientations have a one-dimensional orientational order. For brachiopod shell calcite usually the *c*-axes of the individual crystals are co-oriented, showing a cluster concentration around one particular direction in the {001}

(=*c*-axis) pole figure, whereas the {100} (=*a**-axes) scatter in orientation is on the great circle. The latter is perpendicular to the *c*-axes orientations (e.g. Figs. 19E, F, 21C).

7. A *three dimensional texture* or *three dimensional orientational order* is present when all crystallographic axes in the investigated map are co-oriented, such that there is a concentrated cluster of data points around one particular direction in the *c*-axes pole figure but also distinct clustering on the great circle perpendicular to this direction in the *a**-axes pole figure. Since, for calcite, the *c*-axis is a unique direction and bears the $\bar{3}$ symmetry axis, there are six maxima in the *a**-axis pole figure. However, only three of those are usually visible in the pole figure because data of only one hemisphere are displayed in the stereographic projection (e.g. Fig. 22E–H).
8. The term *microstructure* refers to the sum of grains, their sizes, morphologies, modes of interlinkage, co- and misorientations and is shown with coloured EBSD maps. Similar colours visualize similar crystal orientations, different colours indicate differences in crystal orientation.

Imaging with Field-Emission Scanning Electron microscopy (FE-SEM)

To visualize the distribution pattern of the organic substance within shells, we etched them in cross-sections. First, flat surfaces were obtained by cutting and polishing the samples with glass and diamond knives. The surfaces were then etched with a 0.1 M HEPES buffer (pH 6.5) and 2.5% glutaraldehyde solutions for 90 and 120 s, respectively. Etching was terminated by rinsing the samples three times in 100% isopropanol for 10 s each. Subsequently, samples were critical-point dried and etched surfaces were coated with 4–6 nm of Pt/Pd. SE or/and BSE images were taken at 4 kV, with a Hitachi SU5000 FE-SEM; the used contrast (SE or BSE contrast) is given in the figure caption.

Imaging with Atomic Force Microscopy (AFM)

The sub-micrometer and nanostructure of brachiopod shell calcite were visualized by AFM. Samples were measured in contact mode with a JPK NanoWizard II AFM using silicon cantilevers. The lateral and vertical deflection traces were measured and processed with the NanoWizard® IP image processing software and the Gwyddion free and open-source software. We used the "Gold" scale for colour. The lateral and vertical deflection traces are the result of the interaction between the cantilever tip and the sample surface.

Imaging with Scanning Transmission Electron Microscopy (STEM)

Magellania venosa shell fibers were imaged with a STEM detector attached to a Hitachi SU5000 field emission SEM. 40–100 nm thin sections were cut from fresh shells using a Reichert Ultracut S and an Ultra-type diamond knife (Diatome). Sections were mounted on copper EM grids and imaged with a HAADF Annular SEM STEM detector (Deben).

Geochemical analyes

Oxygen isotope analysis by Ion Microprobe

Oxygen isotope compositions of two specimens of the Recent brachiopod *P. atlantica* and one specimen of the Recent brachiopod *M. venosa* was analysed by ion microprobe. We investigated primarily the ventral valves for both species. To assess the variability in oxygen isotope composition, transects through the shells were performed from outermost to innermost shell portions; 20 µm spots were shot with a step size between spots of 50 µm. Prior to analyses, the valves were cut from anterior to posterior shell regions into halves. One half was embedded in epoxy resin and polished with diamond paste down to 1 µm. Measurements were carried out at CRPG (Centre de Recherches Pétrographiques et Géochimiques, Nancy, France) and closely followed the technique described by Rollion-Bard et al. (2007). A Cameca IMS 1280-HR2 was used for measurements. Instrumental mass fractionation (IMF) was corrected for by normalizing the results gained on the samples with two in-house calcite reference materials, BRET ($\delta^{18}O = -10.87‰$ V-PDB, Rollion-Bard and Marin-Carbonne 2011) and CCciAg ($\delta^{18}O = -11.61‰$ V-PDB). IMF was also corrected for the effect Mg content with the correction of $-0.3 \times MgO$ wt% (Rollion-Bard and Marin-Carbonne 2011). The internal $2\sigma_n$ error was less than $\pm 0.1‰$. External reproducibility (1σ), based on replicates of the calcite in-house reference materials, was ± 0.13 and $0.28‰$, depending on the analytical session. The total error for each $\delta^{18}O$ value takes into account the external reproducibility and the internal error. All $\delta^{18}O$ values are reported in‰ and are given relative to V-PDB (Vienna Pee Dee Belemnite) international standard.

Trace and minor element compositions by Laser Ablation Coupled to an ICP-MS (Inductively Coupled Plasma Mass Spectrometer)

The method described in Rollion-Bard et al. (2019) was applied for measuring the trace and minor element compositions. An Analyte G2 Excimer laser ablation system (193 nm), coupled to a quadruple Agilent 7900 series

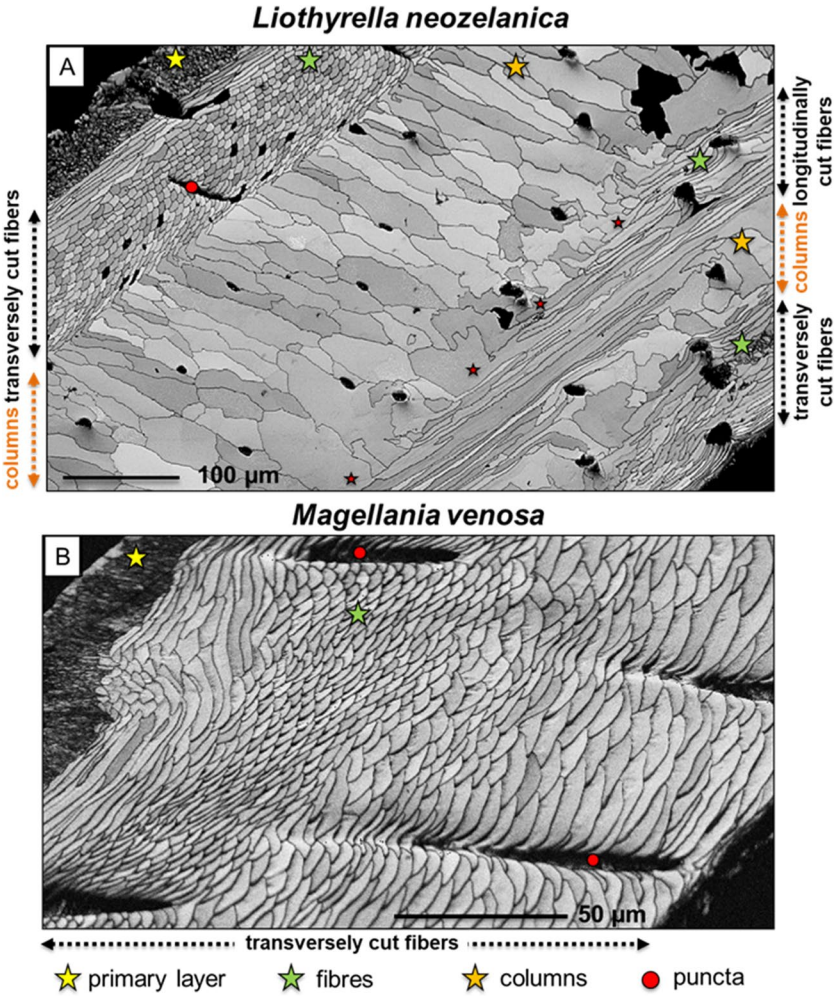

Fig. 1 EBSD band contrast measurement images depicting the shell microstructures that we find for both valves of *Liothyrella neozelanica* (**A**) and *Magellania venosa* (**B**). Note (1) the difference in microstructure between the primary (yellow star in **A** and **B**) and the other mineralized shell layers; (2) for the shell of *L. neozelanica* the distinctness in the mineral unit (biocrystal) size and morphology. Note further the alternation of fibers (green stars in **A**) and columns (large orange stars in **A**) within the innermost mineralized layer of *L. neozelanica* (see also Goetz et al. 2009; Ye et al. 2018a, b). Red dots in **A** and **B** indicate endopunctae. The transition from columns to fibers is sharp. A delineating organic membrane is absent between fibrous and columnar shell layers (red stars in **A**)

(LA-Q-ICP-MS) was operated at a repetition rate of 5 Hz and an energy fluence of 3.7 mJ/cm^2. Samples were analyzed using a laser spot of 40 µm diameter. The isotopes ^{7}Li, ^{23}Na, ^{24} Mg, ^{25} Mg, ^{27}Al, ^{44}Ca, and ^{88}Sr were monitored. Measurements of NIST glass standard 610 and 612 were acquired before and after each run of 10 to 20 analyses, depending on the shell thickness. The overall precision (relative standard deviation, RSD) of the element ratios, calculated adding the errors in quadrature, are based on repeated measurements of NIST 612 glass. RSD was 10% for Li/Ca in *M. venosa*, 20% for Li/Ca in *P. atlantica* and 2% for Na/Ca, 4% for Mg/Ca and 2% for Sr/Ca in both species.

Section 1: Diversity of Recent brachiopod shell microstructures

EBSD band-contrast images highlight the distinctness and diversity of biocrystal shapes, sizes and microstructures that we observe in Recent rhynchonellide and terebratulide (Fig. 1), thecideide (Fig. 2A), and craniide (Fig. 2B) brachiopod shells.

Depending on the species, Recent rhynchonellide and terebratulide valves consist of up to four layers: an outer organic layer, the periostracum and, at most, three mineralized layers, the primary, fibrous (secondary) and columnar (tertiary) shell layers. Although the three mineralized layers have distinctly different microstructures (Fig. 1), the calcite of rhynchonellide and terebratulide shells exhibits a systematic pattern of crystallographic preferred orientation and, accordingly, a well-ordered structure (this study and Schmahl et al. 2004; Griesshaber et al. 2007, 2009; Cusack et al. 2008; Goetz et al. 2009; Ye et al. 2018a, b).

This well-ordered structure in terebratulide and rhynchonellide shells contrasts profoundly with the degree of mineral unit and calcite crystallite arrangement and ordering in thecideide and craniide shells (Fig. 2). The degree of crystal co-alignment in the shells of thecideide and craniide taxa is low, close to random (Sect. 5 and Simonet Roda et al. 2021). Modern thecideides secrete mineral units, biocrystals, which have a multitude of sizes and shapes (Fig. 2A);

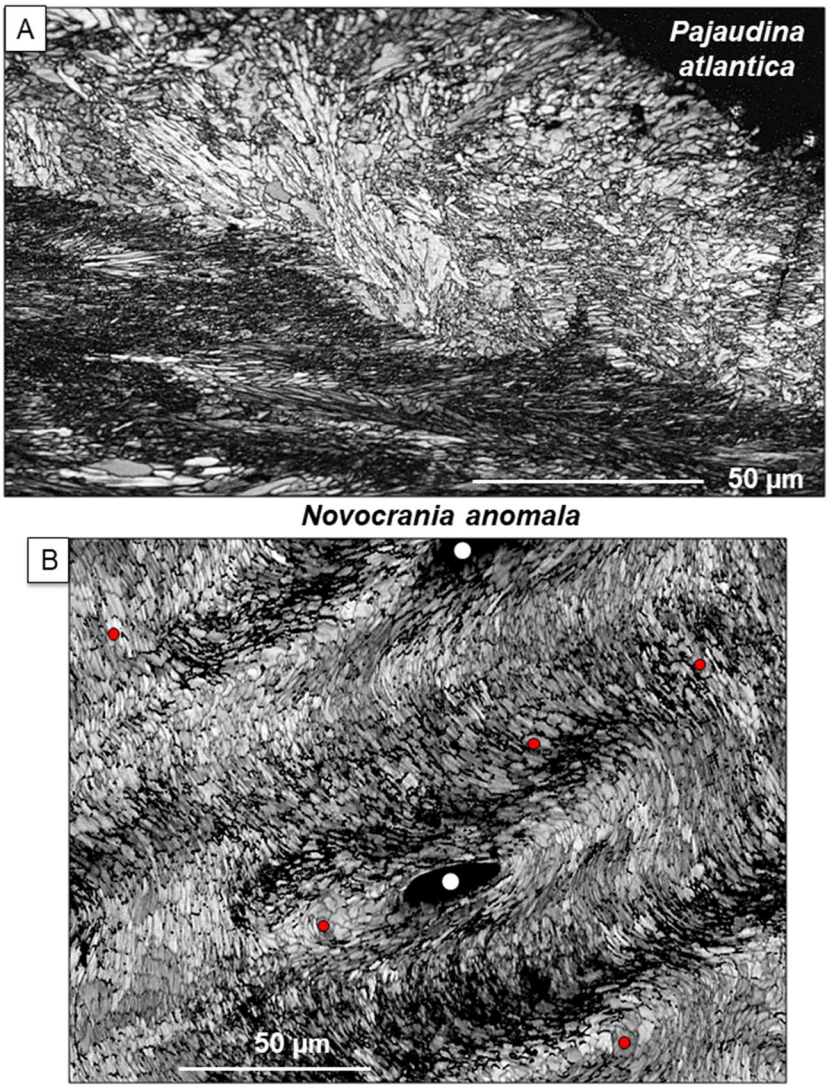

Fig. 2 EBSD band contrast measurement images depicting the shell microstructure that we find for both valves of *Pajaudina atlantica* (**A**) and *Novocrania anomala* (**B**). The shell of *P. atlantica* consists of a multitude of differently shaped and sized calcite crystals without any systematic assemblage pattern. Most of the calcite in *N. anomala* consists of a multitude of small crystal entities (red dots in **B**) that comprise few (on average three to six) small tablet-shaped crystals (see also Figs. 29, S16). The crystals form arrays of parallel layers that are curved and undulate within the shell (**B**). Yellow dots in **B** indicate punctae. **A** Modified after Simonet Roda et al. (2021)

these comprise the shell without any obvious arrangement pattern. Modern craniides form most of their shell of (1) a myriad of small crystals (red dots in Fig. 2B) and (2) of interlinked laminae (discussed further in Sect. 5.1, e.g. Figs. 24A, 25, S15). The small crystals consist of few tablets and are arranged in arrays of thin, generally curved, layers (Fig. 2B). Being tablet-shaped, the tabular mineral units in craniide shells were previously categorized as 'semi-nacre' structures (Williams and Wright 1970; England et al. 2007; Pérez-Huerta et al. 2007), because they resembled the nacre of bivalve shells. However, in accordance with Checa et al. (2009), our study shows that the microstructure and texture of craniide shells are mineralogically and crystallographically dissimilar to any nacreous or foliated crystal assemblies observed in bivalve shells.

In summary, the shells of Recent rhynchonellide, terebratulide, thecideide and craniide taxa exhibit a wide range of mineral unit/biocrystal morphologies, arrangements and architectures. We will show in this review that craniide shells have the weakest texture as calcite crystals in these shells are the least co-oriented. Relative to Craniida, the calcite in thecideides has a slightly higher preferred co-orientation. The highest crystallographic preferred co-orientation is observed for the columnar shell layer of Terebratulida. Relative to the columns, slightly reduced in co-orientation strength, is the primary shell layer of Rhynchonellida and Terebratulida. The fibrous shell layer of Rhynchonellida and Terebratulida always has a lower preferred co-orientation, when compared to that of the primary and columnar shell layers. Accordingly, not only structural characteristics of mineral units and their microstructural arrangement but also the textures vary widely for rhynchonellide, terebratulide, thecideide and craniide shells.

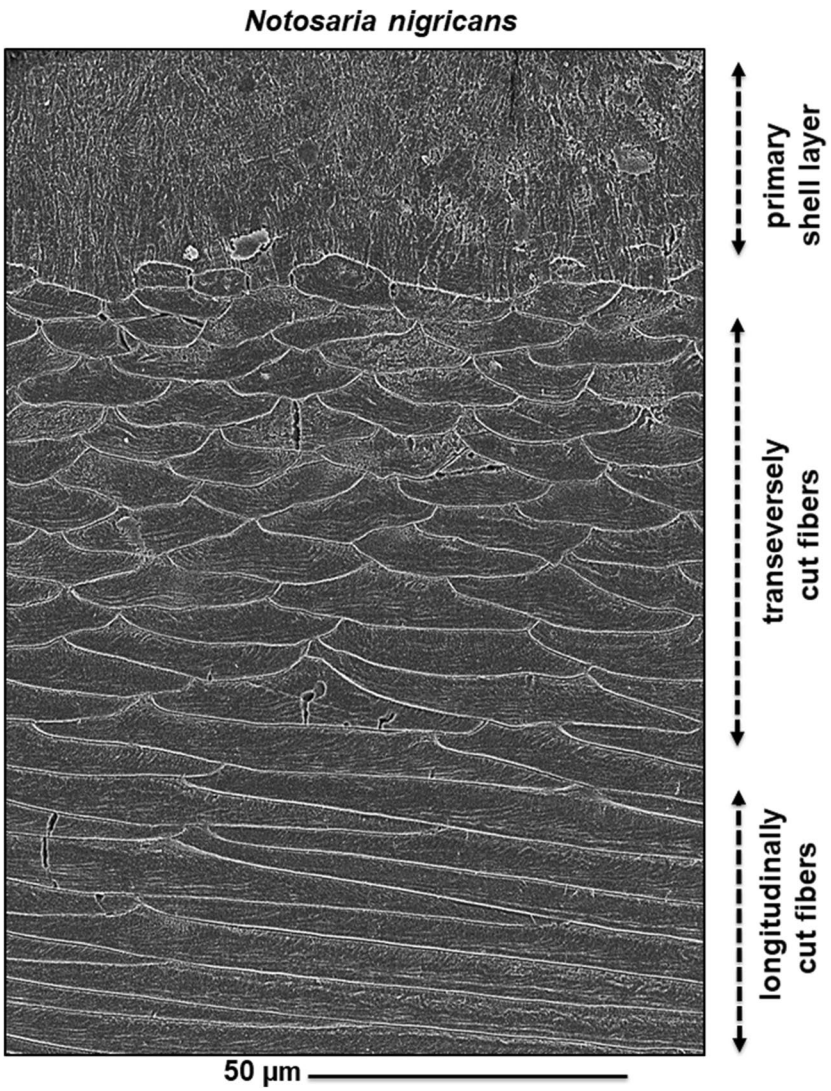

Fig. 3 The primary and fibrous shell layers of *Notosaria nigricans*. SE image of a microtome knife polished, etched and critical-point dried cross-section through the shell. Well visible is the lack of an organic matrix in the primary shell layer, but its presence in the fibrous shell layer portion, respectively. Note the stacks of transversely and longitudinally arranged fibers. Well visible in most fibers is a striation, indicative of the mode of calcite secretion: deposition of thin layers, increments, of calcite; described in great detail in Simonet Roda et al. (2019a)

Section 2: Diversity of brachiopod shell biocrystal morphologies

Figures 3, 4, 5, 6, 7, 8, 9, 10 and S2, S3 visualize morphological differences of biocrystals in rhynchonellide, terebratulide, thecideide and craniide shells. We show characteristics on the micrometer and submicrometer scale levels. Nanometer scale characteristics of calcite fibers will be discussed in Sect. 4.

Modern brachiopod shell valves consist of two or three mineralized layers formed of distinct material microstructures: (1) the outermost primary (Fig. 3), (2) the adjacent fibrous, secondary (Fig. 3), and (3) the innermost, columnar, tertiary (Fig. 6B), layer, respectively. The primary shell layer of rhynchonellides and terebratulides (Figs. 4A, B, 5B, 6, S2) consists of interdigitating mineral units. These are often larger-sized at the base of the primary layer, next to the fibers (yellow star in Figs. 4A, 5B), and decrease in size towards the outer primary layer region (Fig. 4A). Even though, we observe often that the outermost primary shell layer section is seamed by a row of large crystals (yellow arrows in Fig. 6). The anterior margin of both valves of rhynchonellide and terebratulide brachiopods is always formed of primary-shell layer-type calcite material (white arrows in Fig. 6).

The primary layer of rhynchonellide and terebratulide brachiopod shells is not nanogranular as described by Williams (1973). This shell layer has a specific microstructure and is devoid of intercalations of organic material (Griesshaber et al. 2009). TEM and EBSD measurements (Figs. 19A–C, 20A; Griesshaber et al. 2009; Goetz et al. 2011) show that large fractal-like, dendritic and differently oriented mineral units interdigitate in three dimension. An assembly of these strongly interdigitated crystals forms the primary shell layer; the specific mode of interlinkeage of the irregularly shaped, dendritic mineral units creates the impression that this part of the shell is nanogranular (Goetz et al. 2011). The transition from the primary to the fibrous

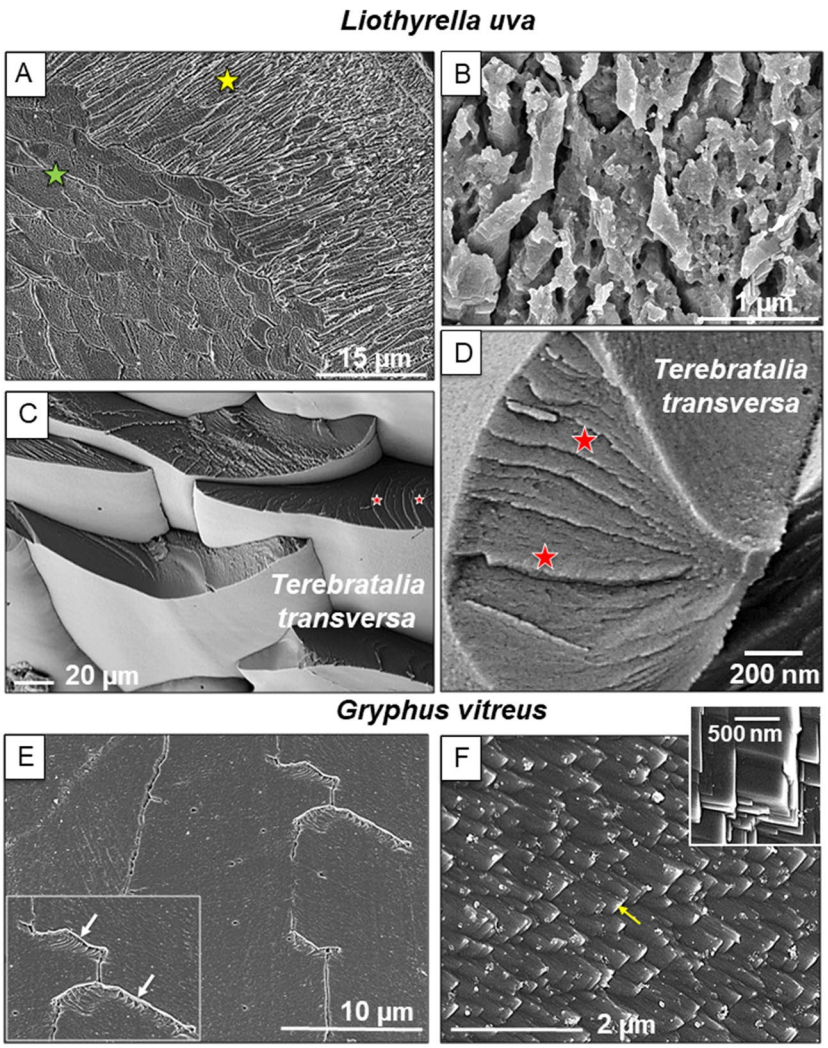

Fig. 4 SE images of microtome knife polished, etched and critical-dried (**A**, **B, E, F**) and of fractured surfaces (**C, D**) of the different shell layers of *Liothyrella uva* (**A, B**), *Terebratalia transversa* (**C, D**) and *Gryphus vitreus* (**E, F**). **A, B** Primary shell layer **C, D** fibrous shell layer, **E, F** columnar shell layer. Even though the etching procedure was similar for all shell layers, we see, for the calcite of the different layers, structural differences at the submicron scale: **B** irregularly shaped units comprise the primary layer, **D** sequences of layers with nano-sized calcite entities form the fibers, **F** calcite crystals with rhombohedral morphologies (yellow arrow in **F**) constitute columns. Insert in **F**: SE image of non-biological calcite; note the similarity in crystal morphology between columnar layer calcite (**F**) and that of inorganic calcite, calcite crystals precipitated from solution (insert in **F**). Yellow star in **A**: primary shell layer; green star in **A**: fibrous shell layer. Red stars in **C** and **D**: sequences of nano-scale layers within a calcite fiber. White arrows in **E** point to organic membranes between adjacent columns

shell layer is sharp (Figs. 5B, 6), and an organic membrane delineating the two shell layers is absent.

In all rhynchonellides and terrebratulides, the layer next to the primary shell layer is formed by stacks of fibers (Figs. 3, 4C, D, 5, 6), the latter being within a network of organic membranes, the extracellular biopolymer matrix (Sect. 3, and Fig. A5B in Simonet Roda et al. 2019b). The membranes are about 100–120 nm thick (see Sects. 3 and 4). However, individual fibers are not fully encased by the organic substance, only one surface of the fiber is covered by an organic lining (see Sect. 3 and Simonet Roda et al. 2019b).

Within the fibrous shell layer, the fibers form stacks consisting of, more or less, parallel arrays of fibers (Figs. 3, 5, 6, and Griesshaber et al. 2007, 2009; Goetz et al. 2011). Usually, the stacks change their orientation within the layer by a few tens of degrees, occasionally by up to almost 90°. Accordingly, in two-dimensions, we find diagonally, transversely and longitudinally arranged fibers (Figs. 3, 5B, 6). This arrangement pattern of the stacks of fibers is comparable to fiber organization in a twisted plywood structure. When cut in cross-section, the convex-concave (keel and saddle) morphology of the fibers and their staggered arrangement is a unique characteristic of terebratulide and rhynchonellide brachiopod shells (Figs. 3, 4C, 6A, E, and Simonet Roda et al. 2019a, b), which differs significantly from fibrous assemblies of other biological hard tissues, such as calcite fibers in *Mytilus edulis* shells. It has been shown by Ye et al. (2018a, b) that brachiopod fiber length, roundness and convexity of Recent rhynchonellides and terebratulides can be related to ontogenetic development and environmental conditions. Calcite fibers in brachiopod shells are curved, unlike those calcite fibers noted in *Mytilus edulis* shells, especially at endopunctae (insert in Fig. 5A, Checa et al. 2019). In cross-section, the calcite within an individual fiber is arranged in thin, 80–100 nm-sized, layers (Figs. 4D, 5C, 18).

When present in a shell, the columnar shell layer is formed of large, prism-shaped entities, called columns (Figs. 4E, 6B). The columns are delineated from each other by organic membranes (white arrows in insert in Fig. 4E),

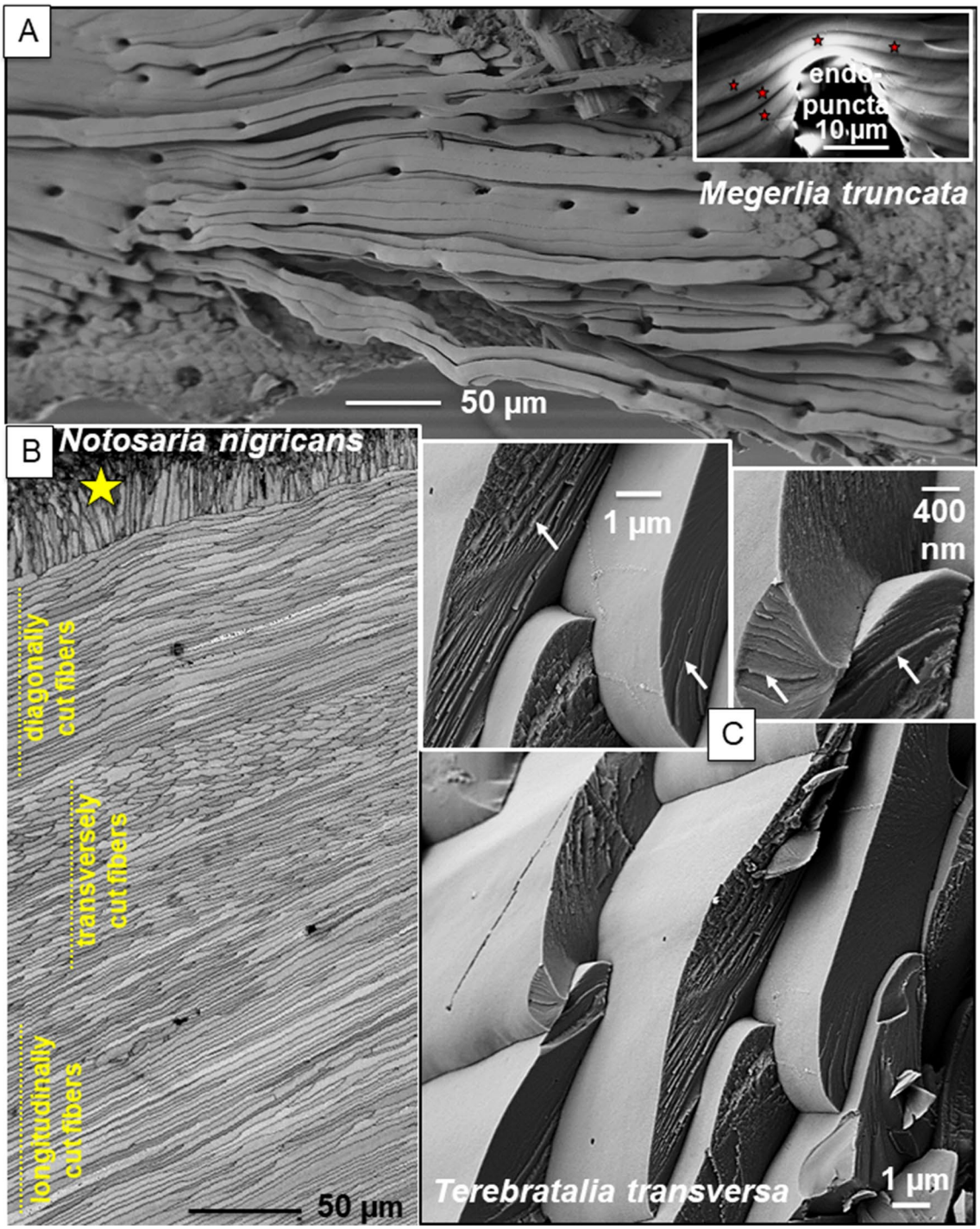

Fig. 5 The fibrous shell layer of *Megerlia truncata* (**A**), *Notosaria nigricans* (**B**) and *Terebratalia transversa* (**C**). **A, C** SE images of fractured surfaces. **B** EBSD band contrast measurement on a cross-section through the primary and the fibrous shell layer. Well visible are in **B**: (1) the differently oriented stacks of, more or less, parallel fibers and (2) a row of large, primary layer, crystals (yellow star in **B**) at the transition from the fibrous to the primary shell layer. **C** Staggered arrangement of fibers in a stack of fibers; sequence of thin calcite layers within individual fibers (white arrows in **C**). Insert in **A**: note the bending of fibers around an enodpuncta (red stars) and Griesshaber et al. (2005). It is remarkable that with the bending of a fiber the calcite lattice remains coherent, even though, due to bending, the morphological axis of the fiber changes direction

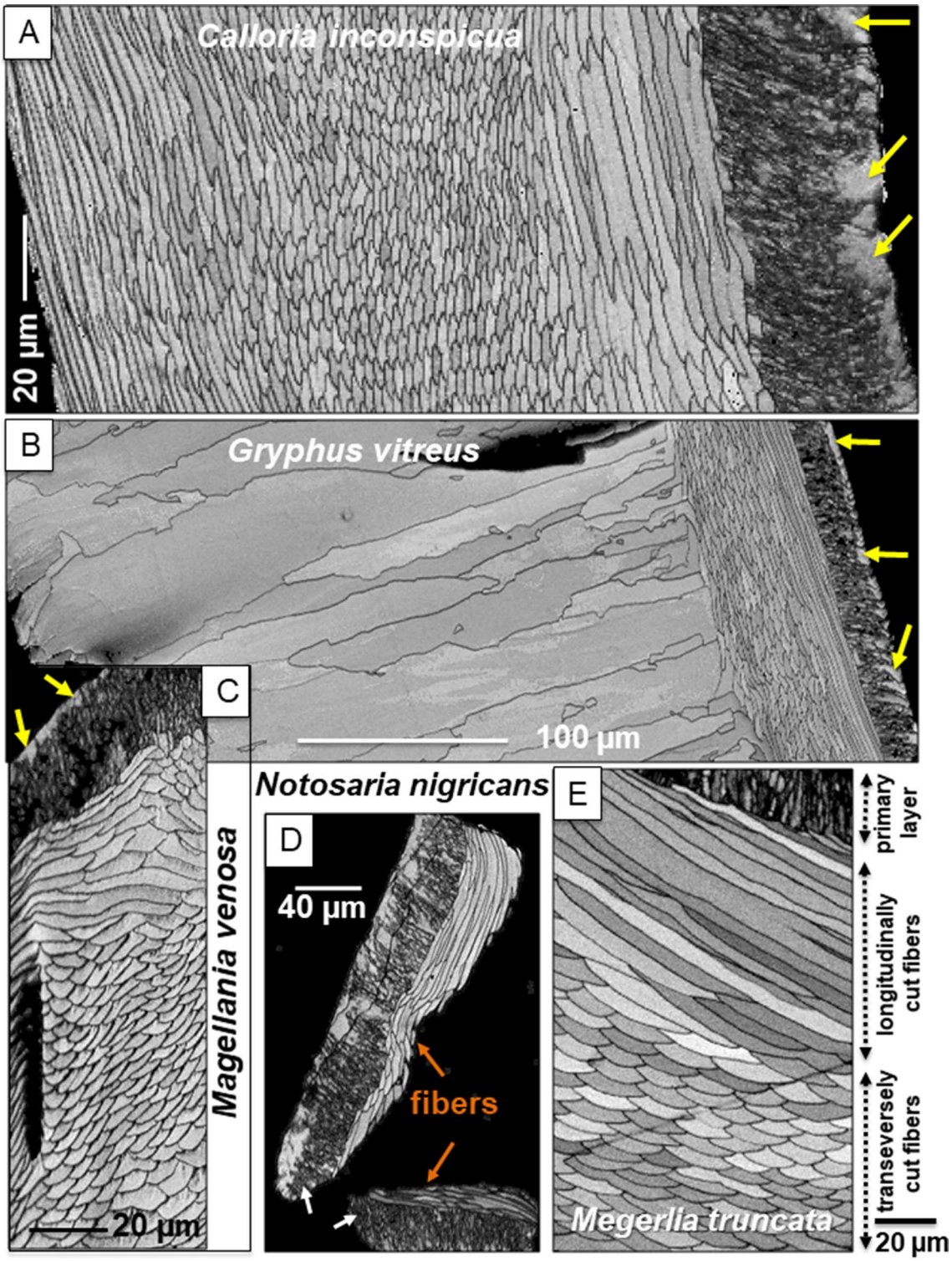

Fig. 6 EBSD band contrast measurement images through cross-sections of terebratulid brachiopod shells. Note: (1) the cut through differently oriented stacks of fibers and (2) the string of large/larger crystallites (yellow arrows) that seam outermost primary layer surfaces. The anterior margin of the valves (white arrows) consists always of primary layer type material with its characteristic microstructure and texture. Arrays of parallel fibers form stacks. These stacks are misoriented to each other, often by about 90°; when cut in two dimensions, we observe stacks of longitudinally and transversely arranged fibers, respectively (well visible in *Calloria inconspicua* and M*egerlia truncata*)

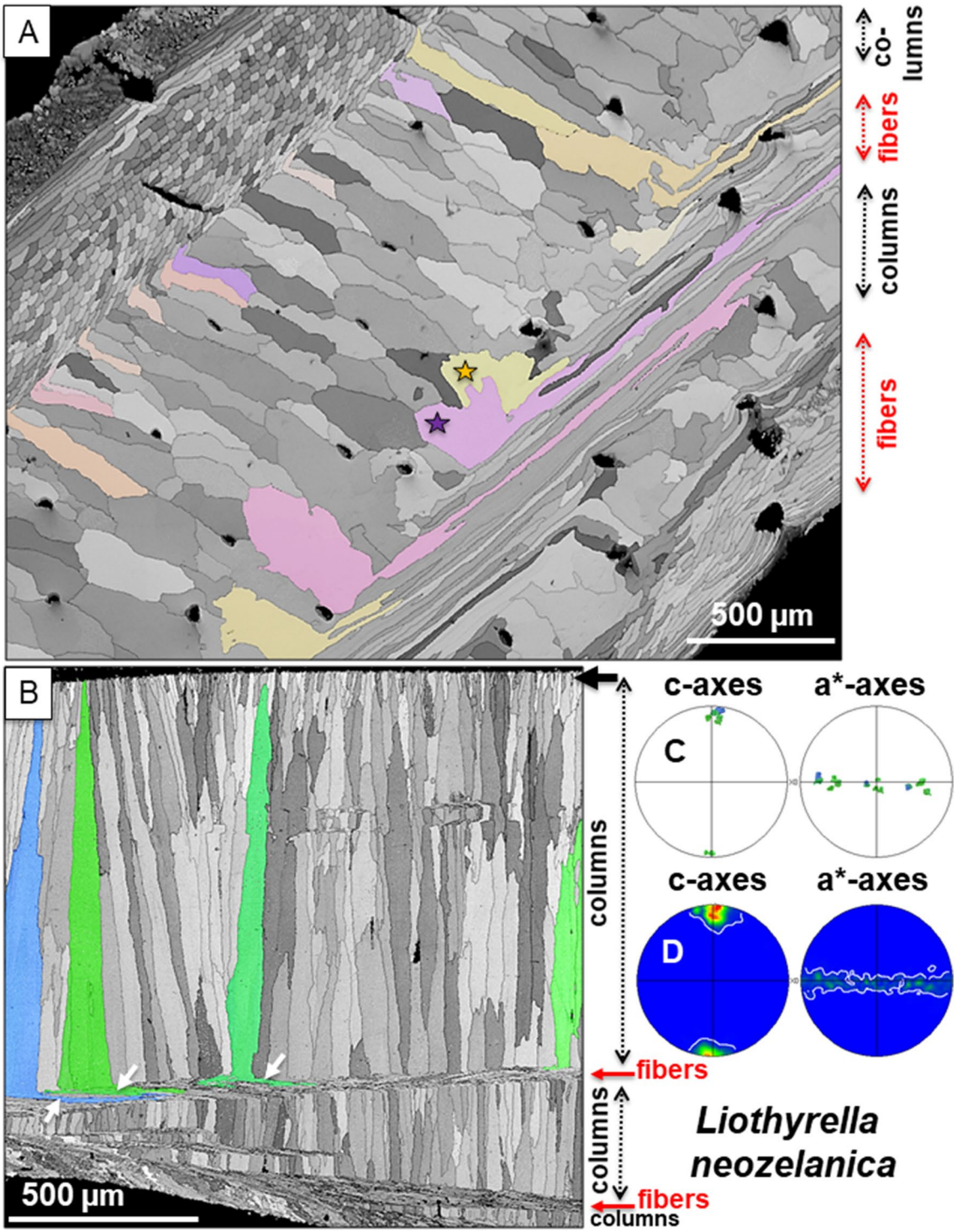

Fig. 7 EBSD band contrast (grey) measurement images **A, B** of a cross-section through the shell of *Liothyrella neozelanica*. Figs. **A** and **B** show two different cuts through the shell for: (1) a better visualization of column morphology and (2) the change-over from the columnar to the fibrous microstructure. In colour in **A** and **B** we show for selected columns calcite orientation. Columns have irregular morphologies and might interdigitate (e. g. the two columns marked with a yellow and magenta star in **A**). The transition from columns to fibers is smooth (**A** and white arrows in **B**). In both cuts through the shell there is an alternation between columnar and fibrous shell layers. It is well visible in **B** that columns form through competitive growth; see the first-formed small-sized columns (black arrow in **B**) that develop with increasing distance away from the nucleation front to large columnar units; see also Goetz et al. 2009; Schmahl et al. 2012. The pole figure in **C** shows calcite co-orientation for the selected columns given coloured in **B**. The pole figure in **D** gives calcite orientation for all measurements shown in **B**. The colour-code is given in Fig. S13

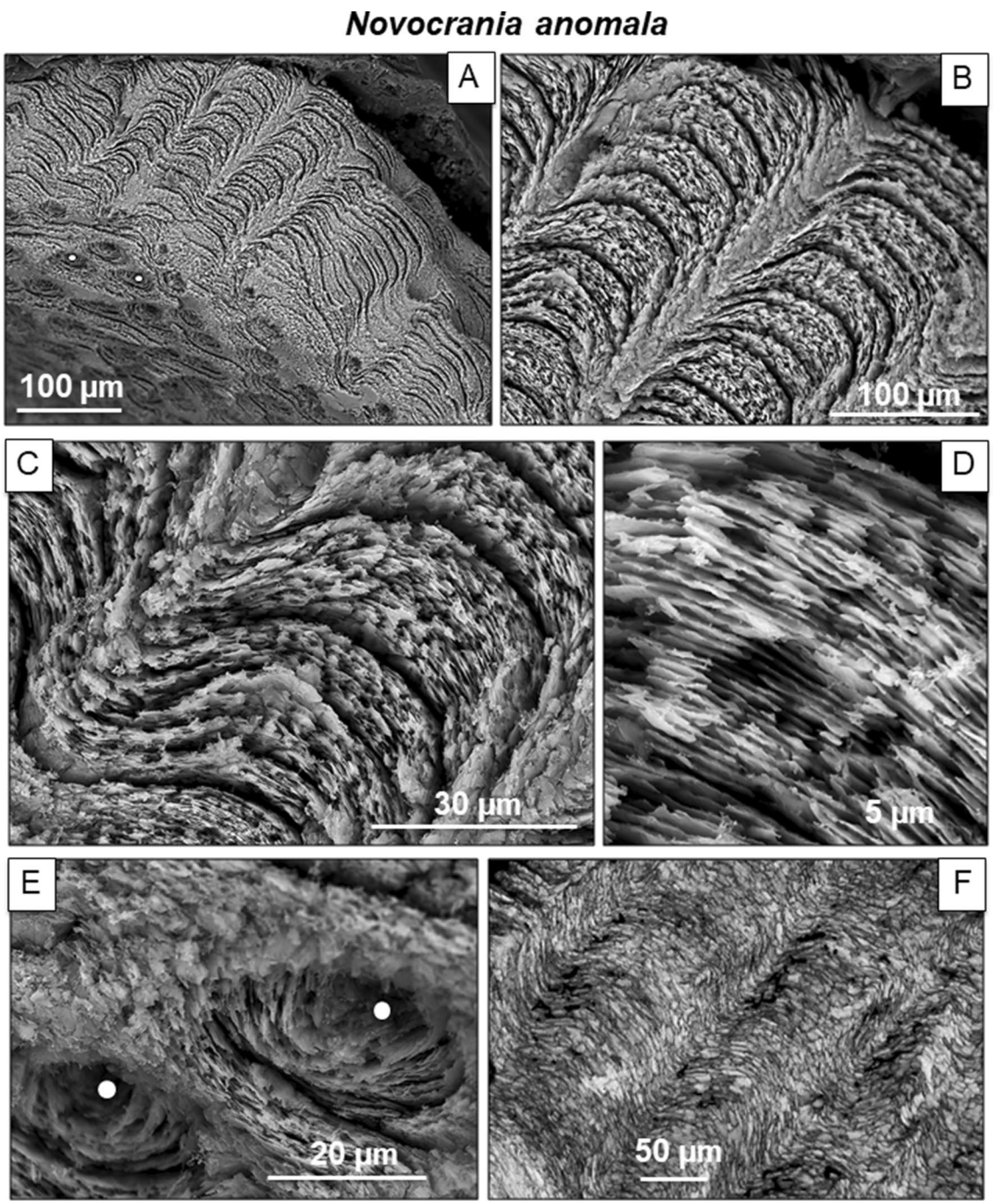

Fig. 8 SE images of fractured surfaces (**A–E**) and EBSD band contrast measurement image (**F**) of the shell structure and microstructure of *Novocrania anomala*. Most of the shell (ventral valve, see also Fig. S3), consists of a sequence of 300–400 nm thin and curved calcite layers (**A–D, F**), the latter formed of strings of platelet-shaped calcite crystallites (**F**). The shell is interspersed by many punctae (white dots in **A, E**); the calcite layers curve around the punctae (**E**)

have irregular morphologies (Fig. 6B) and interdigitate slightly (yellow/magenta stars in Fig. 7A). For *L. neozelanica* we see an alternation between columns and fibers (Fig. 7A, B). The transition from columns to fibers is sharp, especially between columns and longitudinally arranged fibers (Fig. 7A, B). When etched, calcite crystallites within the columns have rhombohedral morphologies similar to that of the non-biological calcite analogue (Fig. 4F). Goetz et al. (2009) and Schmahl et al. (2012) described brachiopod column growth in detail and found that columns form through a competitive growth process (Fig. 7B). Competitive growth in calcite is based on the fact that the *c*-axis is the fastest

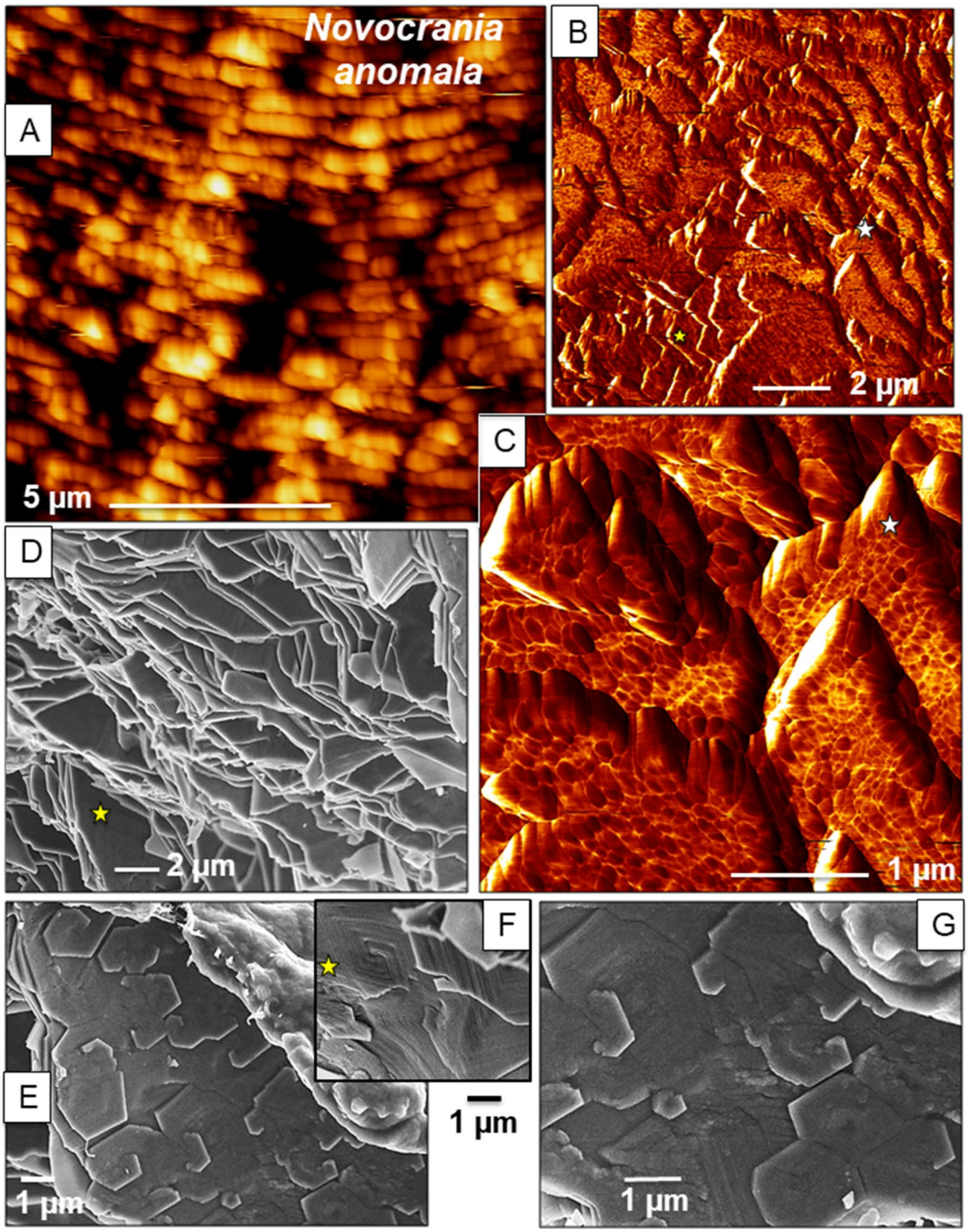

Fig. 9 AFM and SE images depicting characteristics of *Novocrania anomala* shell calcite. **A** AFM height; **B, C** AFM lateral deflection, **D–G** SE images of fractured surfaces. Curved arrays of 300–400 nm-thick layers of calcite **A, D** that constitute the largest part of the ventral valve. Individual layers are formed of crystals that exhibit morphologies similar to those of non-biological calcite (**E**) and (**G**). Individual layers consist of calcite crystals that exhibit crystallographically regular growth edges (**E, G**, white star in **B, C**). In side view, individual crystals appear to be curved tablets (**D**). In top view, these crystals/tablets show a spiral structure (**E–G**). Note: the spiral features are on the 1 µm scale level while classical growth spirals on inorganic crystals are on the ångstrøm scale level. The microscale growth spirals are confined to individual or/and their immediate neighbouring crystals; the spirals do not extend over several adjacent crystals. The curved platelets show an internal nanostructure (**B, C**)

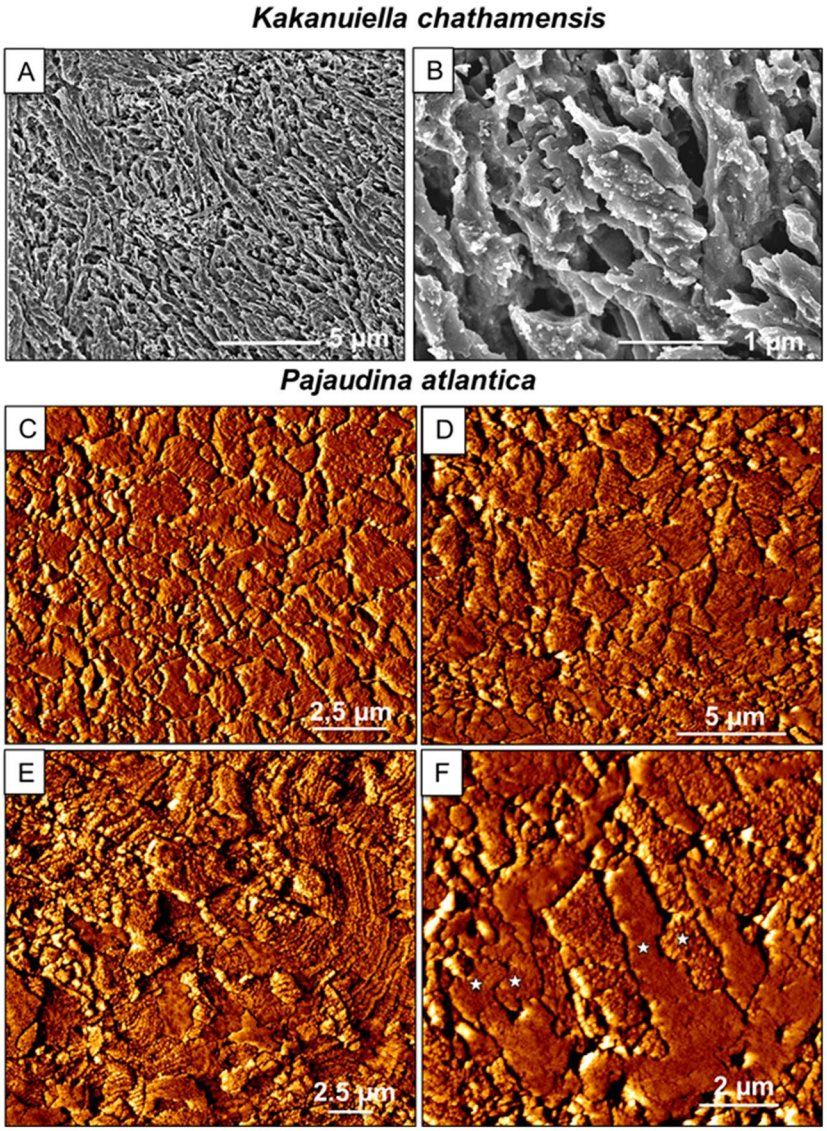

Fig. 10 SE images, **A** and **B**, of microtome knife polished and etched shell surfaces of the thecideide brachiopod species *Kakanuiella chathamensis*. The shell of *K. chathamensis* consists of an assembly of interdigitating, dendritic calcite units that are highly irregular in size and morphology. **C–F** Vertical deflection AFM images depicting the mineral units that comprise both valves of the shell of the thecideide brachiopod *Pajaudina atlantica*. In the shell of this species as well there is no regularity in crystal morphology or crystal size. Adjacent crystals interdigitate (white stars in **F**). **C–F** Modified after Simonet Roda et al. (2021)

growth direction, and that only crystals with their *c*-axis parallel to the main growth direction of the shell extend in size. Crystals that have their *c*-axis inclined to the plane of nucleation are hindered in growth since they abut with their neighbors. Brachiopod column generation will be addressed in greater detail in Sect. 7.3.

Modern craniide and thecideide species form their shell with different structural design concepts (Figs. 8, 9, 10). Most of the calcite in *craniide shells* is assembled into two microstructures: (1) an arrangement of laminae forming predominantly the dorsal valve (discussed in detail in Sect. 5.1) and (2) sequences of 300–400 nm thin layers consisting of crystallites comprising tabular calcite (Figs. 9, S3). The layers are curved and are formed of platelet-shaped crystallites that do not interdigitate and are only slightly misoriented to each other. In surface view, individual tabular crystals vary in size and often exhibit a spiral aspect (Figs. 9, S3).

Modern *thecideides form their shell* of a multitude of differently sized and shaped mineral units (Fig. 10) without any obvious and regular assembly pattern (Fig. 2A). We note the occasional interlinking of mineral units (white stars in Fig. 10F).

Section 3: Organic matrices within shell calcite

The distribution pattern of organic substance is not only distinct for representatives of the four calcite shelled brachiopod orders, it varies also for the different shell layers of terebratulide and rhynchonellide species. Figures 11, 12, 13, 14, 15 and 16 and supplementary Figs. S4–S11 highlight the mode of distribution of organic biopolymers within shells. Figures 11, 12 and 13 show extracellular matrices;

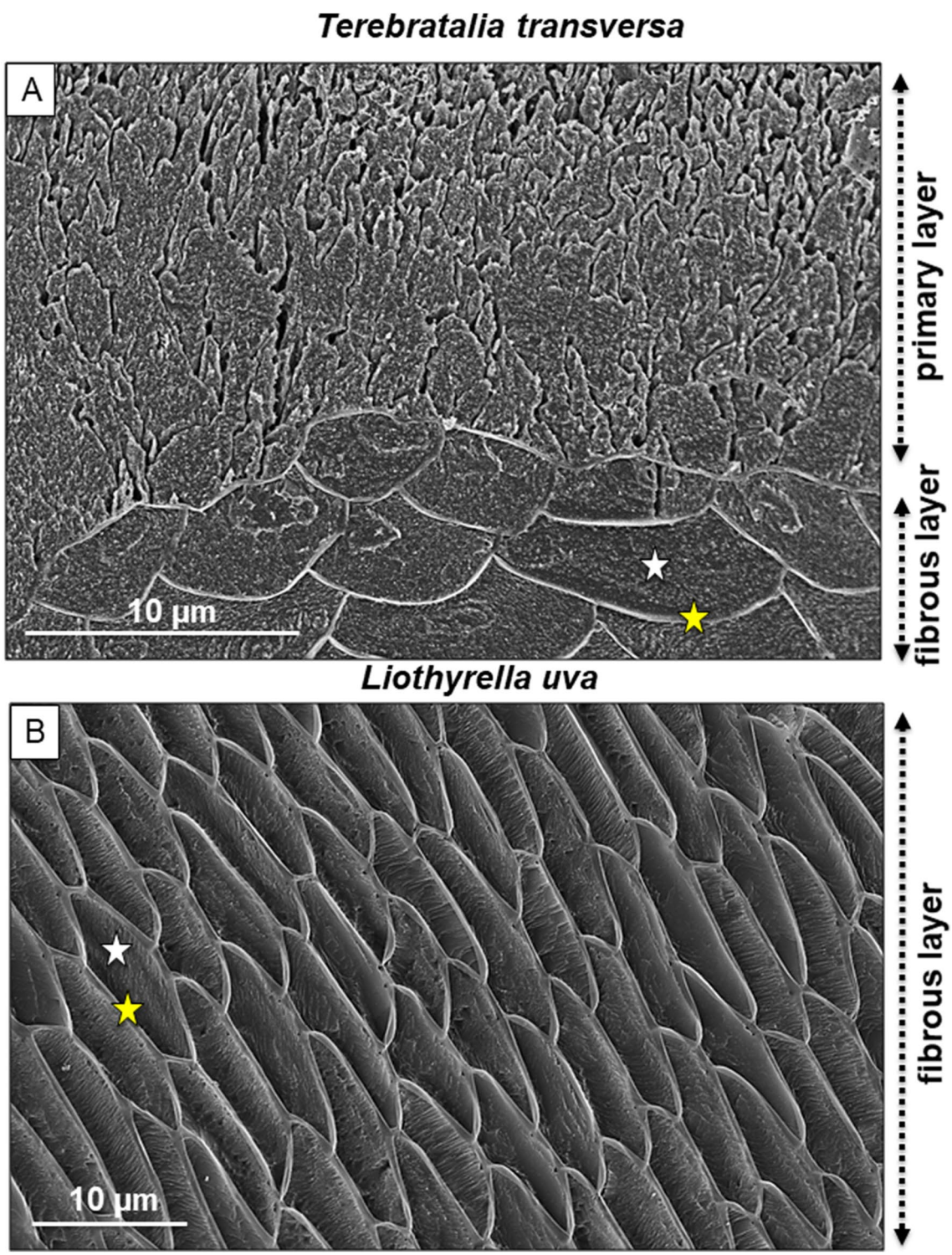

Fig. 11 SE images of microtome knife polished and etched surfaces of the primary and fibrous shell layer of *Terebratalia transversa* (**A**) and the fibrous layer of *Liothyrella uva* (**B**). The primary layer **A** does not contain any organic substance (this study; observations by TEM in Griesshaber et al. 2009). In contrast, an extracellular matrix is present within the fibrous shell layer formed of an assembly of organic membranes. Yellow star in (**A**) and (**B**): organic membranes of the extracellular matrix separating adjacent fibers; white star in **A** and **B**: the calcite of the fibers

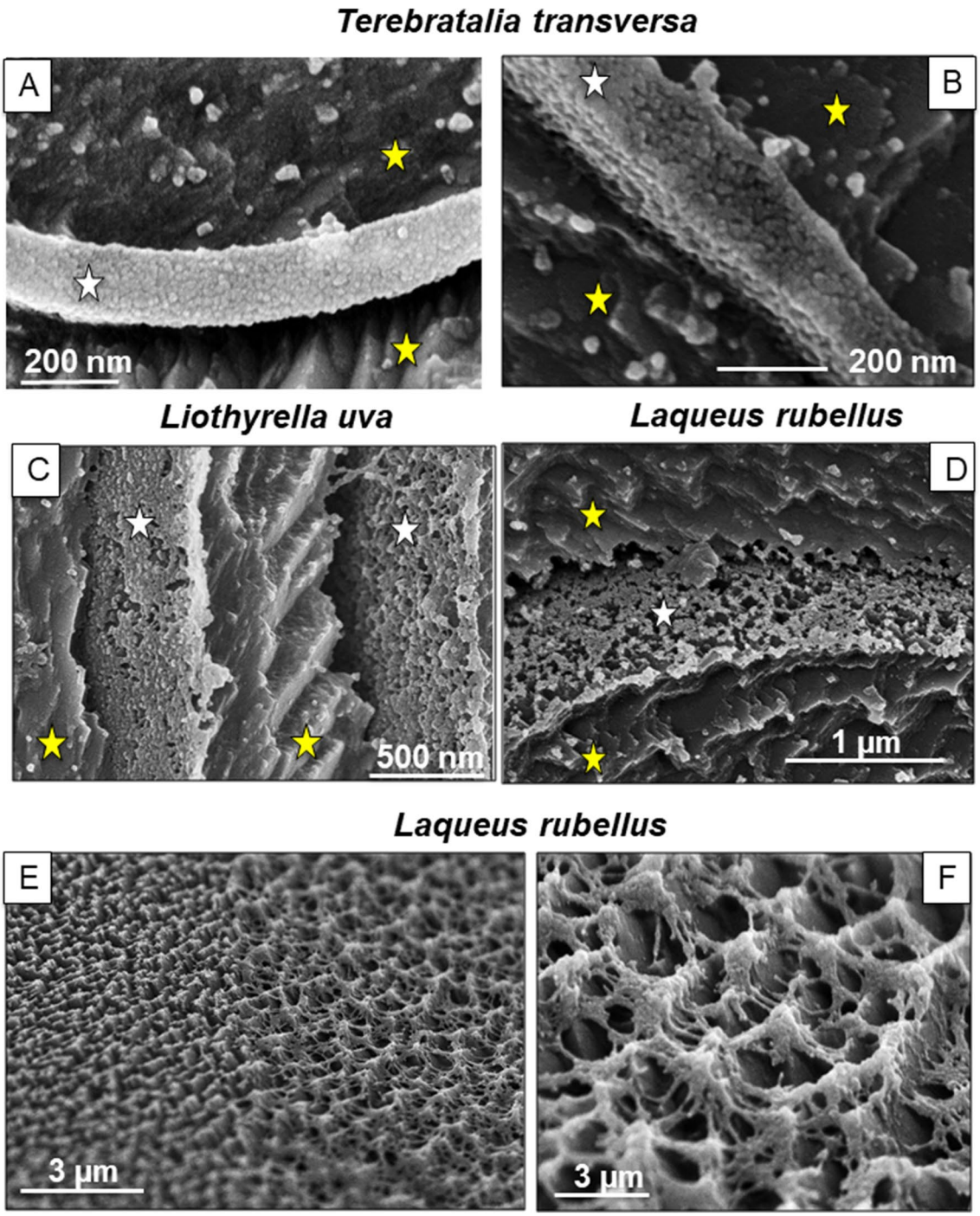

Fig. 12 SE images taken on microtome knife polished, etched and critical-point dried shell cross-sections visualizing the presence and fabric **C–F** of biopolymer membranes of the extracellular organic matrix (white stars in **A**–**D**) delineating adjacent fibers (yellow stars in **A**–**D**). Figure 8C modified after Griesshaber et al. (2017). **E**, **F** Surface view of the organic membrane covering a calcite fiber

Figs. 15F, S9B depict the thin network of organic fibrils that is occluded within the calcite of the fibers.

Organic material content is high in the fibrous shell layer of terebratulide and rhynchonellide brachiopods as well as throughout the shell of *N. anomala* (Craniida). In the shell of these taxa the organic substance is developed as an extracellular biopolymer matrix (Figs. 11, 12, 13C–F, S5B, C) that delineates neighboring fibers in terebratulides and rhynchonellides and neighboring layers in craniides.

No organic material has been observed in the primary shell layer of terebratulides and rhynchonellides (Figs. 11A, S4A, Griesshaber et al. 2009), even though it was searched

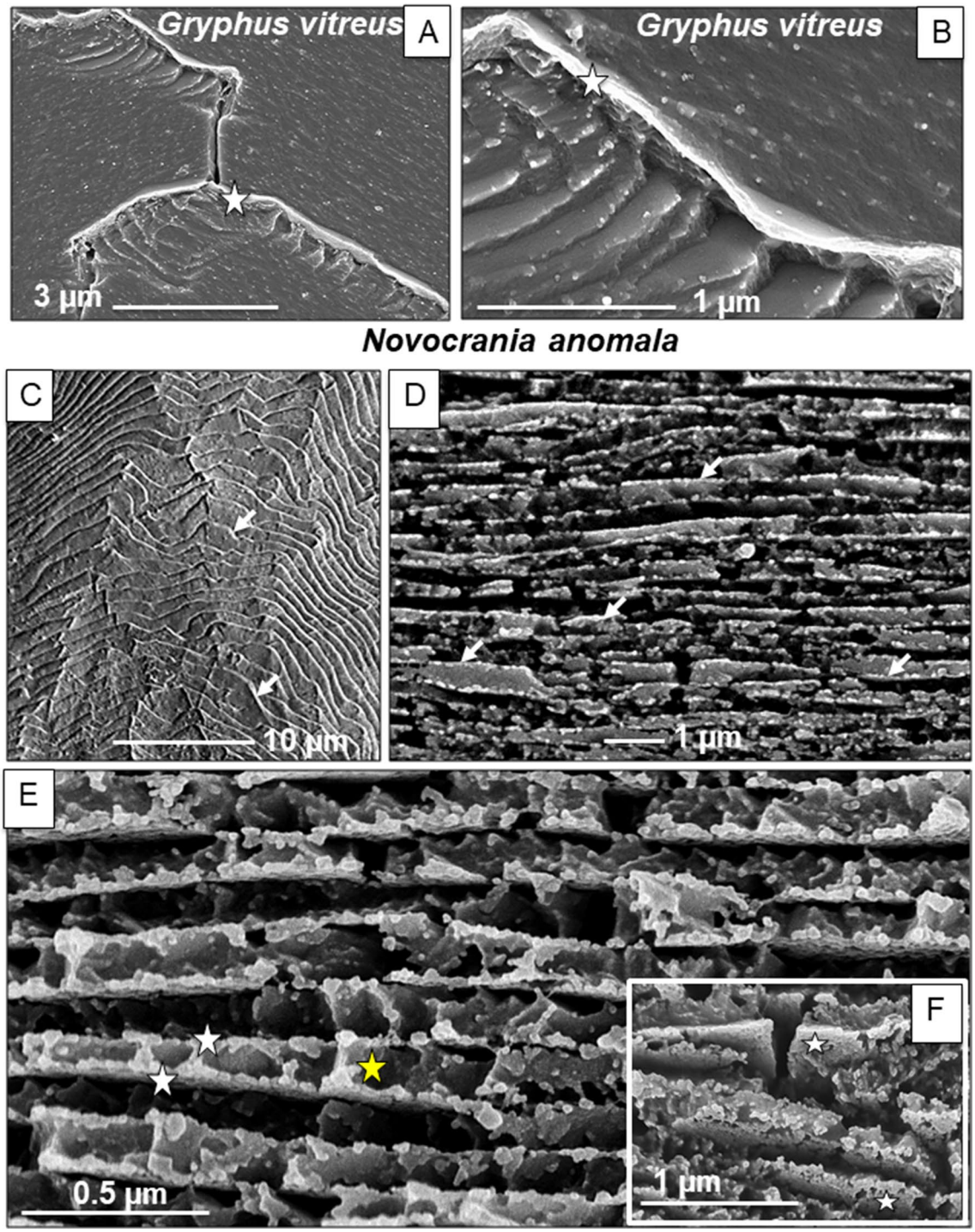

Fig. 13 SE images of microtome knife polished, etched and critical-point dried shell cross-sections depicting membranes between columns (**A, B**) in *G. vitreus* and calcite layers (**C**–**F**) in *Novocrania anomala*. White stars and white arrows in **A–C, E, F** point to organic membranes incorporated into the shells; the yellow star in **E** shows calcite sandwiched between organic membranes

for with various biochemical preparation as well as SEM and TEM imaging techniques (Griesshaber et al. 2009; Simonet Roda et al. 2019a). However, we do find biopolymers within the fibrous and columnar shell layers. Applicable to both fibrous and columnar shell layers, organic material is developed as membranes and delineates neighboring columns from each other (Fig. 13A, B). In cross-section (Figs. 12A, B, S4B–S4D) the organic membrane varies in thickness between 50 and 150 nm and appears to be compact. However, in surface view (Fig. 12) it becomes

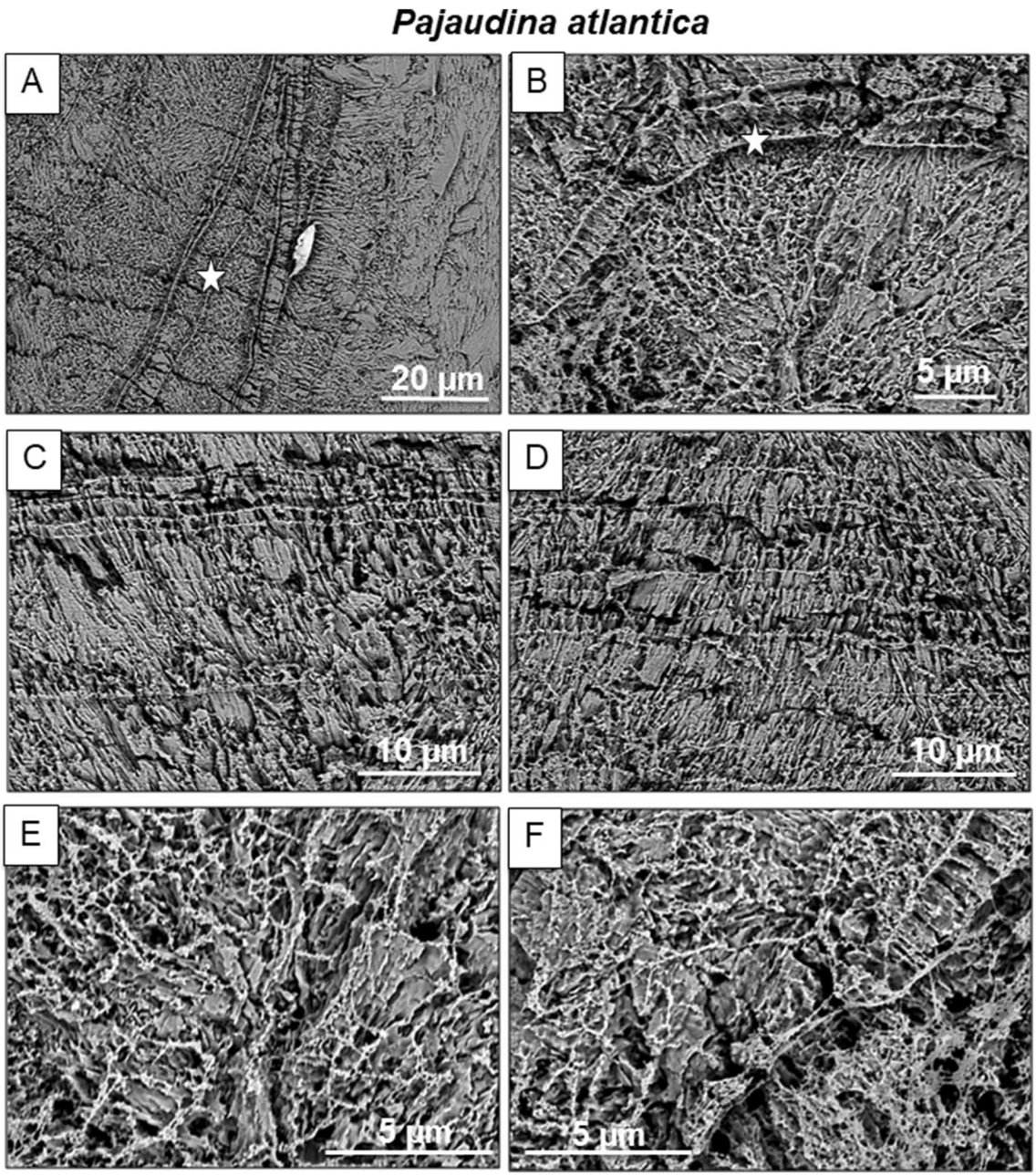

Fig. 14 SE images taken on microtome knife polished, etched and critical-point dried shell cross-sections visualizing the distribution pattern of organic substance in the two valves of the thecideide brachiopod *Pajaudina atlantica*. Thecideides incorporate much organic substance into shell calcite. The organic component is developed as thin membranes (white star in **A** and **B**) and as networks of fibrils (**E, F**). Note: both membranes and fibrils are irregularly distributed within the shell

quite apparent that the organic membranes consist of a rather porous fabric.

Organic membranes delineate calcite layers in the shell of *N. anomala* (Figs. 13C–F, S5B, C). Membrane thickness in craniide shells is well below 100 nm, and it varies between 20 and 40 nm. In the shell of terebratulides, rhynchonellides and craniides the distribution of organic matter is patterned, as it is an extracellular matrix. In contrast, in Recent thecideides there is no obvious regularity in the distribution of the organic substance within the shells (Figs. 14, S6–S8). Organic material in the latter is developed predominantly as a network of fibrils (e.g. Figs. 14B, E, F) and, to a lesser extent, as thin membranes (Figs. 14A–D, S6, S7). The mode of biopolymer occlusion into and distribution within thecideide shells is, more or less, random (white arrows in Figs. 14, S6–S8).

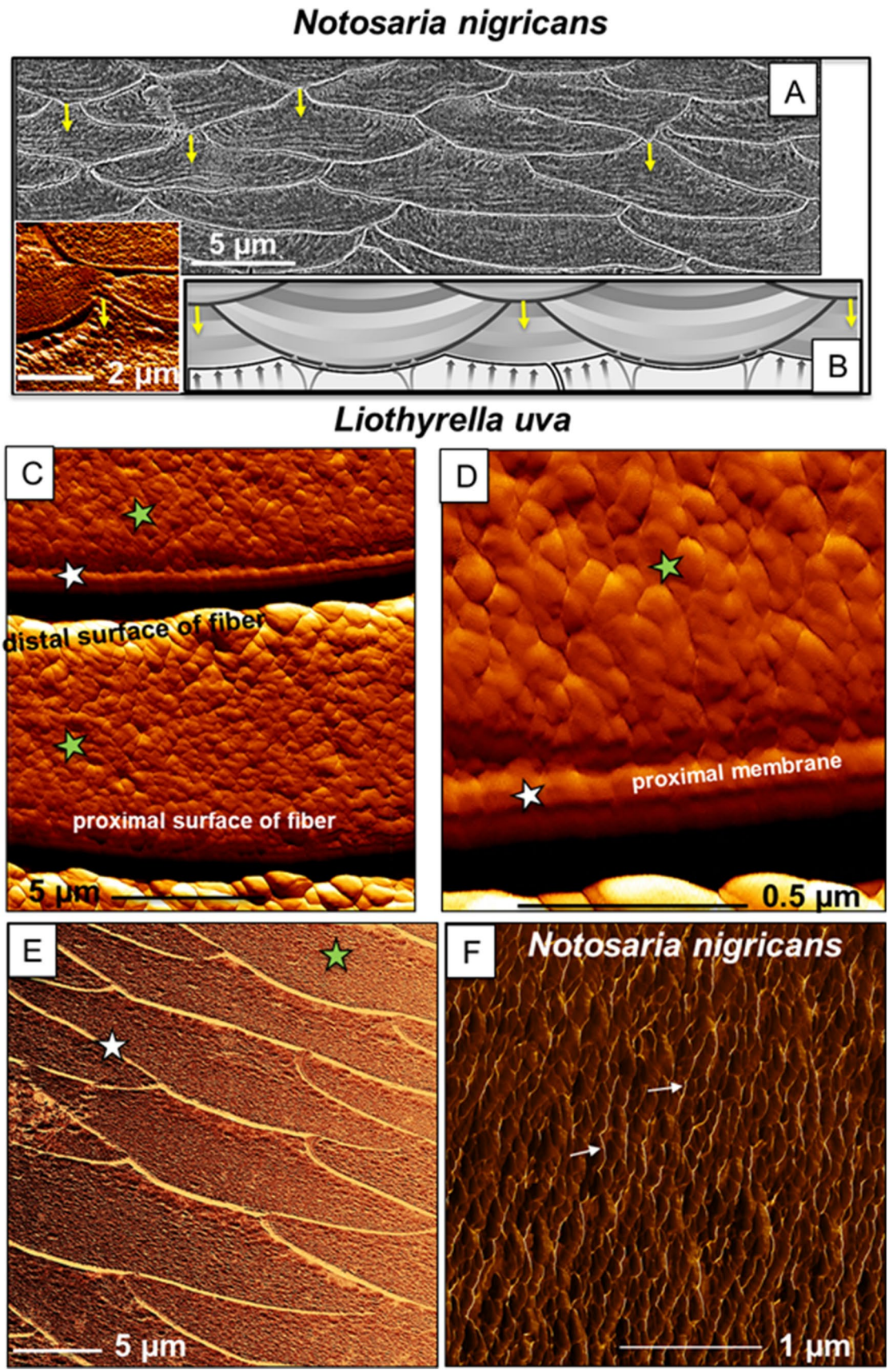
Notosaria nigricans
A
5 µm
2 µm
B
Liothyrella uva
C
distal surface of fiber
proximal surface of fiber
5 µm
D
proximal membrane
0.5 µm
E
5 µm
F
Notosaria nigricans
1 µm

◂**Fig. 15** Transverse cut through calcite fibers of *Notosaria nigricans* (**A, F**) and *Liothyrella uva* (**C–E**). Insert in **A** depicts the shell of *L. uva*; the full image is shown in Fig. 12D. **A** SE image taken on a microtome polished, etched and critical-point dried shell cross-section surface. Insert in **A** vertical deflection AFM image indicating the start of fiber calcite nucleation and growth (yellow arrow). **B** Sketch depicting successive growth of the fibers by addition of thin calcite layer increments (see striation within individual fibers). **B** Modified after Simonet Roda et al. (2019a). **C, D** Lateral deflection AFM images depicting in high-resolution neighboring fibers; the calcite of the fiber (green star in **C, D**) and the fiber growth terminating membrane (white star in **C, D**) on the proximal surface of a fiber. **C, D** Visualize that the distal surface of a fiber is not covered by an organic membrane, only its basal, proximal, surface (white star in **C** and **D**). **E** Vertical deflection AFM image showing the extracellular matrix (white star in **E**) within the fibrous shell layer. **F** Lateral deflection AFM image demonstrating the presence of a thin organic network within the fibers (white arrows in **F**; and Fig. S9). White stars in **C–E** point to organic membranes, green stars in **C–E** mark calcite

Section 4: Nanometer and sub-micrometer organization of fiber calcite (rhynchonellides and terebratulides)

Understanding how diagenetic overprinting influences microstructural archival data is of fundamental importance in palaeoecological and palaeoclimatological studies (e.g. Immenhauser et al. 2015). Of particular interest is the identification of low degrees of diagenetic overprint, as a severe overprint is easily recognized due to the, more or less, complete destruction of the hard tissue's microstructure and texture during shell recrystallization (e.g. Figs. 10C, 11E in Casella et al. 2018). Studies have shown that the identification of altered nanostructure is of immense importance in identifying low degrees of diagenetic overprinting. It has been shown that, even though original structural characteristics and features may be preserved at the micrometer scale, the nanostructure of the hard tissue might be completely reset by diagenesis (Fig. 4C in Casella et al. 2018).

Since the fibrous shell layer of rhynchonellide and terebratulide brachiopods is regarded an appropriate archival material for environmental reconstruction, it is important that we focus on the nano- and submicrometer scale characterization of the fibers (Figs. 15, 16, 17, 18, S9–S11). Modern brachiopod fibers are hierarchical composites where biopolymers and calcite are interlinked on at least five levels: (1) the rotated plywood structure of stacks of fibers, (2) a stack of fibers, (3) the individual fiber, (4) calcite sublayers within a fiber, and (5) nanoscaled internal structure and composite nature of a sublayer within a fiber. Simonet Roda et al. (2019a, b, 2021) investigated in great detail fiber secretion and fiber organization of the Recent terebratulide *M. venosa* and showed that individual fibers are not fully sheathed by an organic membrane. In contrast to the observations of Williams (Williams 1966, 1997), who suggest that individual fibers are fully encased by organic substance, Simonet Roda et al. (2019a, b) demonstrated that only the convex surface of a fiber is covered by an organic lining or membrane, specifically the proximal surface of the fiber (white stars in Fig. 15C–E). The concave, distal sides of each fiber are juxtaposed to the proximal membrane of neighboring fibres. Accordingly, solely the mode of fiber stacking, that is specific for brachiopod fibers, creates the impression that an individual fiber is fully sheathed by organic substance.

Simonet Roda et al. (2019a) demonstrated that mantle epithelial cells are in direct contact with the calcite of a forming fiber. Calcite deposition of a new fiber starts at the proximal surface of the proximal membrane of a previously secreted fiber (yellow arrows in Fig. 15A, B). Ongoing fiber growth is achieved by the successive addition of thin calcite-layer increments to previous layered increments within the fiber (see the striation, indicating growth lines, of all fibers in Fig. 15A, sketch shown in Figs. 3, 15B). Fiber growth is terminated by the addition of a membrane (white star in Fig. 15C–E) along the proximal surface of the fiber. In addition to the extracellular organic matrix, modern rhynchonellide and terebratulide fiber calcite contains organic matter as well. As the AFM image in Fig. 15F and the enlargement in Fig. S9B highlight, calcite fibers contain a thin/sparse network of organic fibrils (see white arrows in Figs. 15F, S9). However, the latter is almost negligible, and as we will discuss below, does not influence crystal organization within brachiopod fiber.

When etched with a HEPES solution (pH of 6.5 and 0.1 M) we find for many terebratulide and rhynchonellide species a structural sub-division of fibers into porous/spongy material in the distal region (white dots in Figs. 16A, C–G, S10 white arrows in Fig. 16B) and dense material in the proximal region (red dots in Figs. 16A, C–E, S10), respectively. Accordingly, material that etches easily is readily removed, such as ACC or remains of specific biopolymers. We find that easily etched areas are concentrated in distal parts of a fiber; the first secreted fiber portions.

The calcite of fibers is further substructured (Fig. 17A, B and STEM images of Fig. 17D–F). STEM images made on 60–100 nm thick microtome cuts of shell calcite (Fig. 17C) show that fibers have an internal nano-scale structure (see the patchiness within individual fibers). Furthermore, STEM images visualize that the calcite of a fiber consists of 80–100 nm-thick layers (yellow star and black arrows in Fig. 18A, yellow stars in Fig. 18B, C). In turn, these layers consist of 50–100 nm-sized calcite crystallites (yellow arrows in Fig. 18A–C). It is important to note that the SE images in Fig. 18A, B, and the STEM images, are not made on etched surfaces, thus, sample surfaces are not etched or modified by any chemical processes.

Imaging results presented in this section show that individual fibres, with their single crystallinity documented on the micrometer scale with EBSD measurements, have an

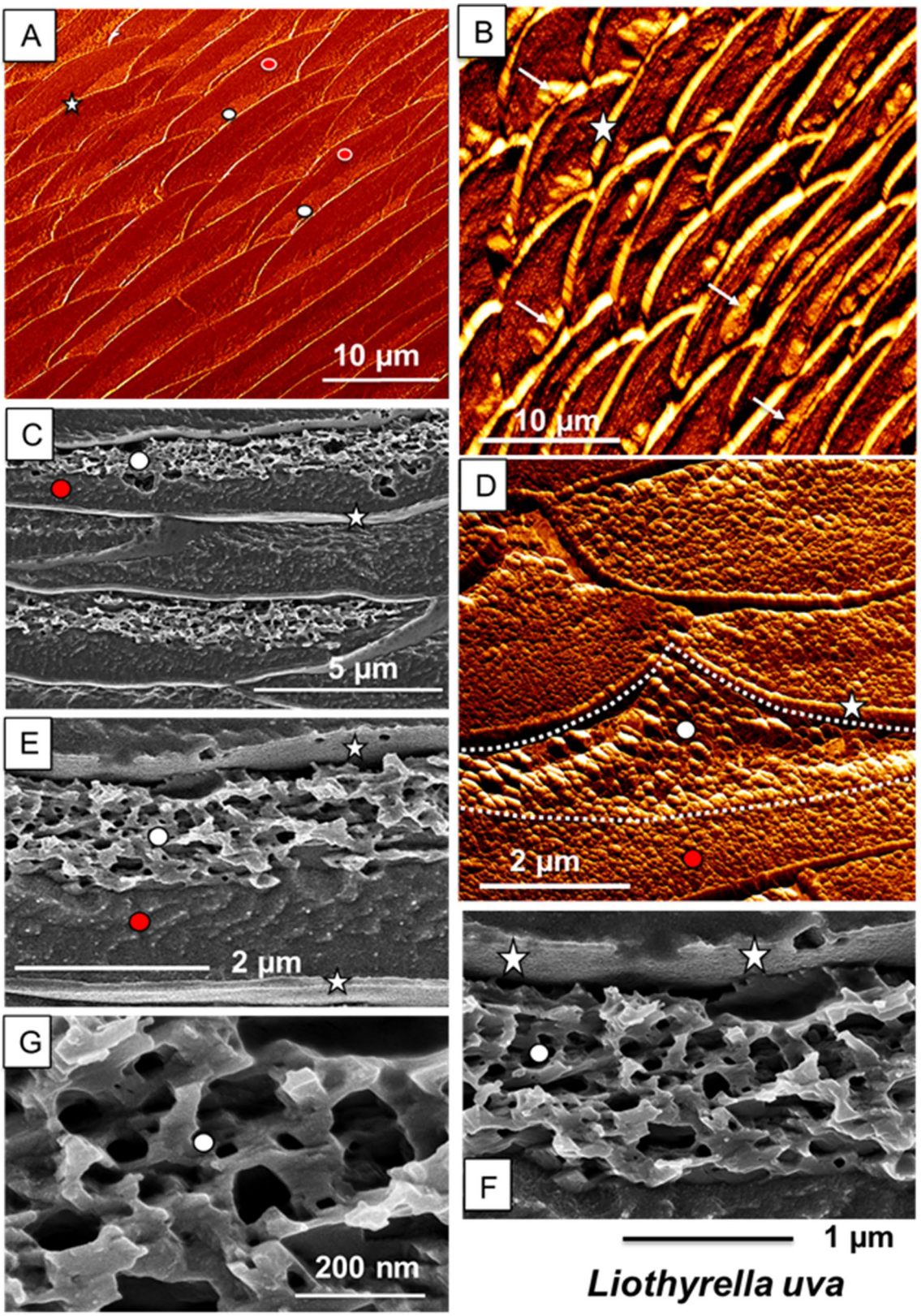

Fig. 16 AFM and SE images of fibers in *Liothyrella uva*. When etched with HEPES solution, the calcite in distal regions has a porous, spongy fabric, and in proximal sections (white dots in **A**, **C**–**G**, white arrows in **B**) a dense appearance (red dots in **A, C–E**). **A** Lateral deflection, **B**, **D** Vertical deflection AFM images. **C–G** SE images of microtome knife polished, etched and critical-point dried surfaces. White stars in **A–F** point to the organic membrane lining at the proximal surface of a fiber

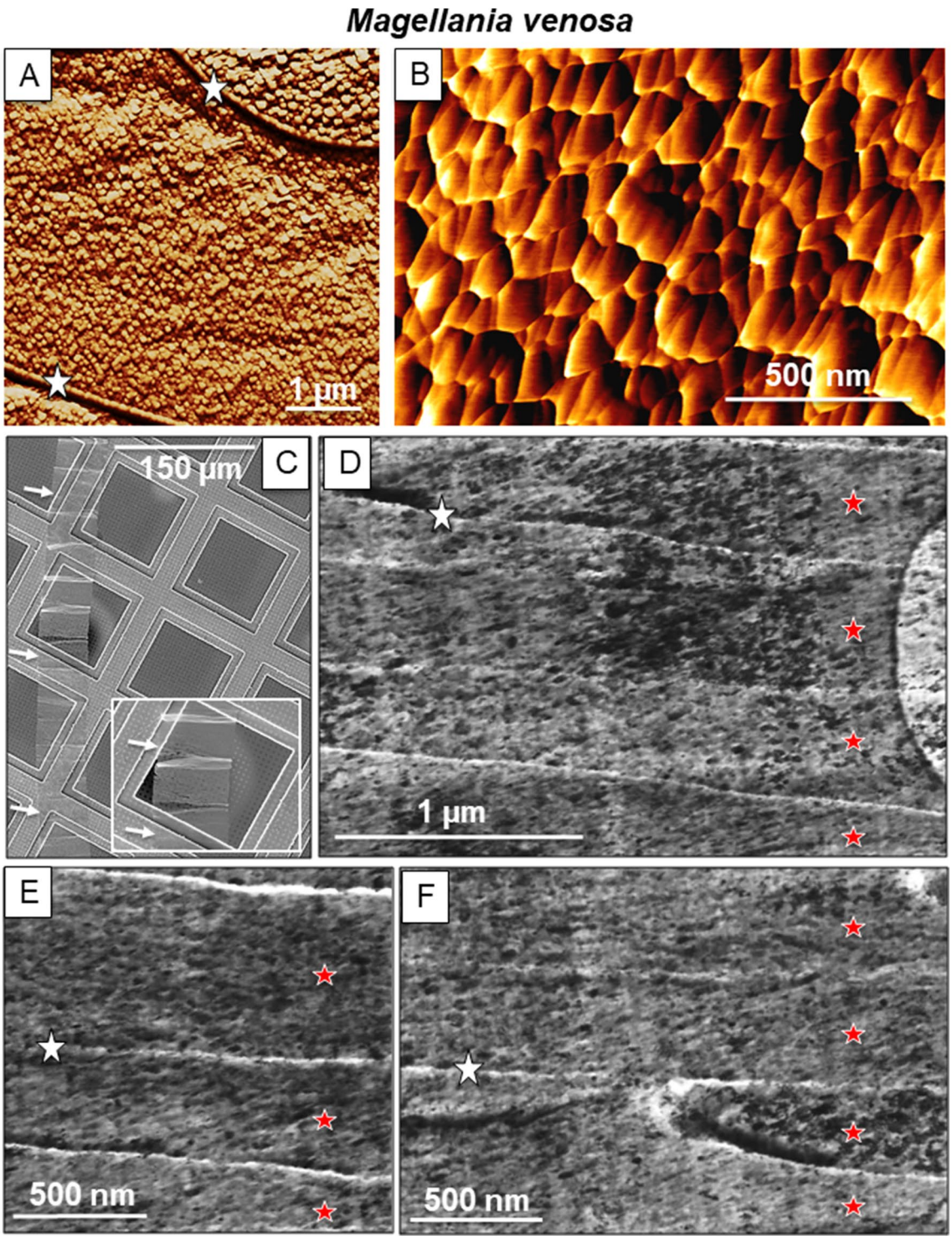

Fig. 17 Submicrometer to nanomete-scale structuring of calcite fibers in *M. venosa*. The features are visualized with AFM vertical deflection (**A**), AFM lateral deflection (**B**) and STEM (**D–F**) images. STEM images are taken on 80–100 nm thin layers **C** cut from the calcite of the fibers (white arrows in **C**); the obtained calcite ribbon rests on a TEM grid. The white star in **A, D–F** points to the organic membrane between adjacent fibers. The patchiness visualized with STEM imaging **D–F** indicates that the calcite of brachiopod fibers consists of about 50–100 nm-sized, crystallographically perfectly aligned, crystallites. Red stars in **D–F** indicate individual fibers

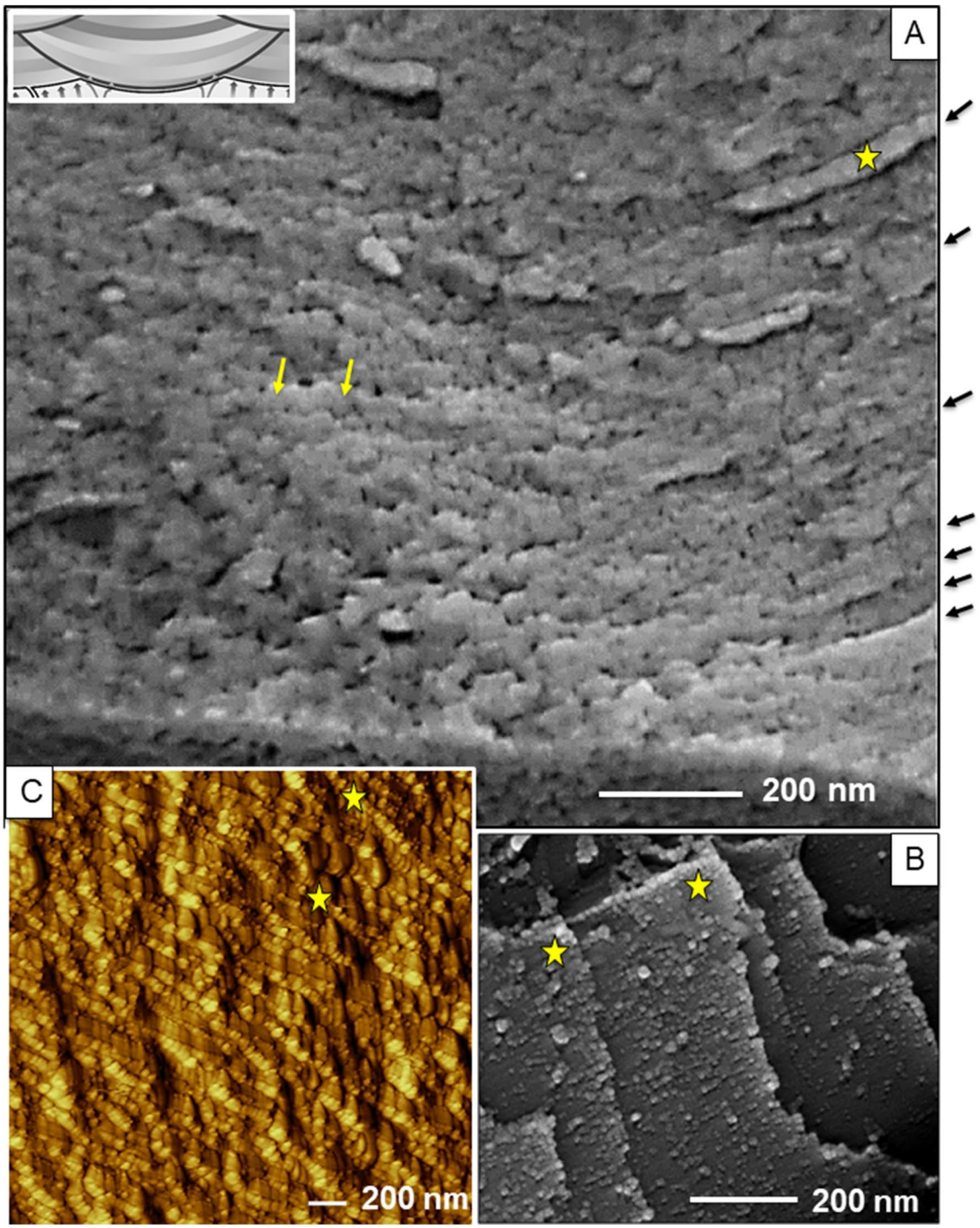

Fig. 18 The internal nanoscale structure of calcite fibers in *Notosaria nigricans*. These are visualized with SE images of fractured surfaces (**A, B**) and a vertical deflection AFM image (**C**). Well visible are the thin sublayers (black arrows in **A**, yellow stars in **B, C**) that comprise a fiber and the 50–100 nm-sized highly co-oriented crystallites (yellow arrows in **A**) that constitute a calcite sublayer (yellow stars in **B** and **C**). A sequence of these sublayers forms a fiber (Figs. 4C, D, 15A, B). Important to note: images in Figs. 18A, B were taken on fractured surfaces, the surface of the fiber was not modified by etching or other chemical means during sample preparation

internal nanometric structure (Figs. 17D–F, 18A). These consist of (1) thin sublayers within the fibers, (2) each sublayer consists of smaller nanometric units. The calcite of these nanometric units as well as the thin sublayers that constitute the fibers are highly co-oriented (Sect. 5 and Schmahl et al., 2008, Fig. A8C in Simonet Roda et al. 2019a). The

nanometric units should not be regarded as individual nanoparticles but rather part of the crystal which has grown consecutively in separate compartments of the pre-existing organic matrix. The sparse organic network occluded into a fiber does not cause much misorientation between crystallites within a fiber, at least misorientation that can be resolved within our 1.5° experimental orientational-resolution capacity.

In summary, modern thecideides, craniides and rhynchonellides/terebratulides differ significantly in the mineral unit, biocrystal, morphology, presence of extracellular matrix and microstructure. Even though, at the submicrometer scale the structure of crystallites in the mineral units/biocrystals is similar for the aforementioned groups of species (S11).

Section 5: Recent brachiopod shell microstructures and textures

The different modes of calcite assembly in shells

Assembly patterns of shell calcite for representatives of the four extant calcite-secreting brachiopod orders are given in Figs. 19, 20, 21, 22, 23, 24, 25, 26, 27, 28, 29, S12–S16. Modern rhynchonellides and terebratulides produce three calcite material fabrics with similar textures, but with distinct crystal morphologies (Figs. 19, 20, 21, S12, S13) and calcite co-orientation strength (Figs. 31, 32).

Previous studies demonstrated (Goetz et al. 2011; Schmahl et al. 2012) that the primary shell layer of Recent rhynchonellides and terebratulides is not nanogranular (Figs. 19A–C, 20A). Instead, primary layers of Recent brachiopod shells consist of an array of large calcite grains with concave/convex outer surfaces (yellow stars in Fig. 19A, B, and Goetz et al. 2011) and dendritic morphologies (Fig. 4B). These calcite grains, termed dendrites, interdigitate strongly with-one-another (Fig. 19C). Recesses and protrusions of abutting crystals occur without any cavities in or between the dendrites. The interface between the primary shell layer grains ranges from a few tens of nanometers to a few tens of micrometers. Dendrites show a range of several degrees in their crystallographic orientation, and can be referred to as mesocrystals. Individual mesocrystals range in size from 20 or more micrometers (Figs. 19C, 20A) and are, accordingly, not nanometer-sized grains, as described, on the basis of SE images, in previous studies. The preferred crystallographic orientation of the primary shell layer is similar to that of the adjacent fibrous shell layer (Fig. 20), although these two layers consist of biocrystals with totally different crystal morphologies and grain boundary topologies.

The primary shell layer is well developed in all Recent rhynchonellide and terebratulide brachiopod shells. Hence, irrespective of differences in environments this outer shell-margin structure is of major importance to Recent rhynchonellide and terebratulide brachiopods. The primary shell layer together with the periostracum forms a 'protective cap' against external mechanical impacts for the inner shell layers and for the internal soft tissue. The interlocked nature of the dendrites affects the hardness (Vickers hardness) of the primary shell layer; it is about twice as hard as that of non-biological calcite (Griesshaber et al. 2007; Schmahl et al. 2008). The overall hardness of the adjacent fibrous shell layer is significantly lower and is similar to calcite precipitated directly from solution (Tretsch 1950). Primary shell layer material with its specific microstructure and hardness forms also the anterior margin of both valves, as shown for *N. nigricans* in Fig. 6D.

The fibrous layer of Recent rhynchonellide and terebratulide shells is pliant and tough. These properties are obtained by virtue of the composite nature of the fibers, their hierarchy and their mode of layer organization. Individual fibers are hierarchical mesocrystal composites that vary in length, in 3-D dimension and fiber morphology (Ye et al. 2018a, b). Fibers of all Recent terebratulide and rhynchonellide shells have one convex proximal and three concave distal surfaces. The specific morphology of fibers allows their staggered arrangement and facilitates their interlocked packing (Figs. 3, 4C, 6A, C, E). The internal organization of calcite within a fiber (Figs. 4D, 18B) evokes their conchoidal mode of fracture.

Another unique feature of brachiopod fibers is that they have curved outer surfaces, while the calcite within the entire length of the fiber has a coherent crystallographic lattice orientation (Figs. 19D, insert in 5A). Thus, while the morphological orientation of a fiber can change, its calcite lattice orientation remains always the same, a material property feature that is specific to biologically secreted materials. Analogous non-biologic calcite or aragonite breaks with the slightest deformation. For Recent calcite-shelled brachiopods, morphological fiber axis direction and the orientation of calcite *c*-axes are generally perpendicular to each other.

Neighboring fibers are often co-oriented due to stacking formation (e.g. see the similarity in colour in Fig. 19D: mainly green colours on the left and mainly blue colours on the right-hand side of the image, respectively). However, even though differing in crystal morphology and microstructural arrangement relative to that of the primary shell layer, the fibrous shell layer as well has a strong fiber or axial texture (the terminology for the latter is explained in the methods section; compare EBSD maps and pole figures of the different shell layers in Figs. 20, S12A). In contrast to the valves, the texture of the fibers at the hinge, within the tooth and the socket, is not axial, but is bi- or even multi-modal (Figs. S12B–S12D, and Griesshaber et al. 2007). We observe at the hinge two different calcite crystal arrangements, one

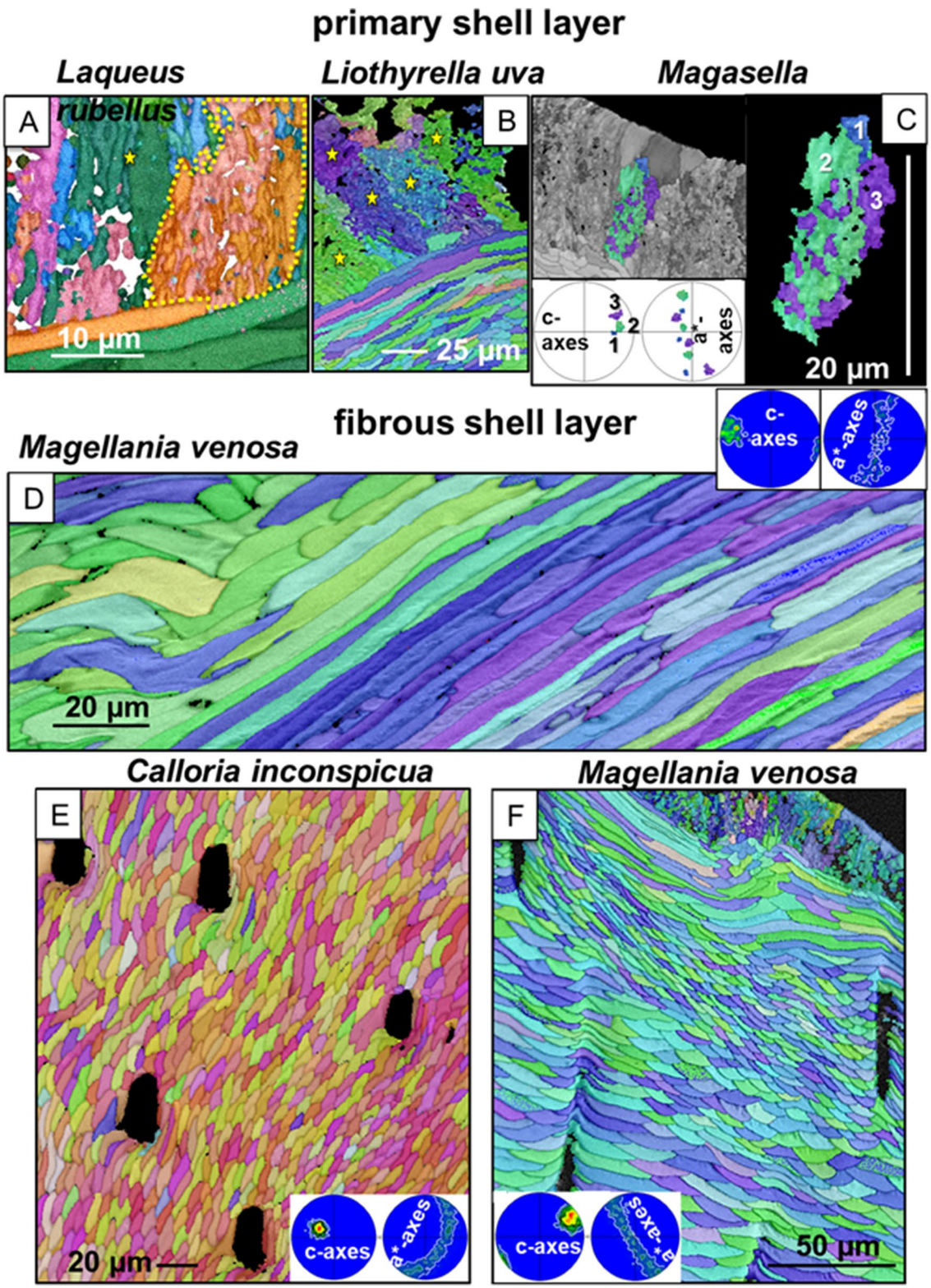

within the tooth (Fig. S12D) and one within the socket (Fig. S12C).

The columnar shell layer was investigated for *G. vitreus* and *L. neozelanica* (Figs. 7, 21, S13). Similar to the primary and the fibrous shell layers, the columnar shell layer has a strong axial or fiber texture (see the pole figures in Figs. 21, S13), even though the morphology of the columns is distinctly different to that of fibers and to the primary shell

◂**Fig. 19** The microstructure (EBSD maps) and texture (pole figures) of the primary and fibrous shell layer of terebratulide and rhynchonellide brachiopods. The primary layer of these brachiopods is not nanocrystalline; it consists of large, several micrometer sized, units (yellow stars in **A, B**) that are highly interdigitated (**A–C**). The primary shell layer has a dendritic, microstructure. **C** Three interweaved dendritic crystals with slightly diferent orientations; see the three clusters of *c*- and *a**-axes data points in the pole figure given in **C**. The fibrous shell layer (**D–F**) consists of parallel arrays of fibers. These arrays change orientation; accordingly, in 2D views stacks of fibers are longitudinally or transversely arranged (see also Figs. 3, 5B, 6). Brachiopod fibers can be curved (**D**), often around endopunctae (Fig. 5A). The used colour-code for (**A**) and (**E**) is given in Fig. S12, for (**B–D**, **F**) in Fig. S13

layer dendrites. Calcite within individual columns is highly co-oriented, it is almost single crystalline, as indicated by MUD values that range from 650 to 720 (Fig. 21). Although similar in general microstructure and texture, we find one difference between the columnar layers of *G. vitreus* and that of *L. neozelanica*. In *L. neozelanica* columnar-layers there is always an alternation between columns and fibers, generally, longitudinally oriented fibers (Figs. 7, 21C; Griesshaber et al. 2009; Goetz et al. 2009). This is never observed in *G. vitreus* (Fig. 21A). Instead, the thickness of the fibrous and columnar shell layers can vary significantly in *G. vitreus*, even within the same specimen (Figs. S13A, B). Sometimes, the fibrous layer dominates the shell cross-section while the columns are minor (Fig. S13); even though, the opposite arrangement has also been observed in *G. vitreus* shells. The transition between fibers and columns is sharp in both *L. neozelanica* (Fig. 21C) as well as in *G. vitreus* (Fig. 21A, B). The calcite of the columns starts adjacent to the organic membrane lining the proximal surface of a fiber. Calcite orientation within a fiber and within the adjacent column is continuous; as documented by their similarity in colour in EBSD maps (Fig. 21B).

The support or brachidium of the lophophore of articulated brachiopods consists of calcite. We investigated the microstructure and texture of the brachidium of *M. venosa*. The brachidium structure of this species is laminated (Fig. 22A) and comprises, at least, two subregions (white and yellow stars in 22A). One region has a honeycomb structure (white star in Fig. 22A), while the other region has a smooth surface without any internal structure pattern (yellow star in Fig. 22A). MUD values of the primary and the fibrous shell layers of *M. venosa* range from 90 to 100 (Fig. 32), whereas the calcite in the brachidium is highly co-oriented as documented by its higher MUD value of 175 (Fig. 22C, D). Based on calcite orientation one can distinguish between individual units within the brachidium (Fig. 22E, F). Calcite co-orientation strength in these is high with MUD values of 470 and 517, which approach those of a single crystal.

The microstructure and texture of representatives of extant calcite-shelled brachiopod orders that live in less open marine habitats and are cemented to substrate (Thecideida, Figs. 23, S14; Craniida, Figs. 24, 25, 26, 27, S15, S16) is distinct from what we find in shells of extant Terebratulida and Rhynchonellida. Structural order for the shells of cemented species is low to almost absent, especially for the ventral valves of Craniida. There is, however, one difference between the shell microstructure of the investigated cementing taxa. While Recent thecideides form shells with a large diversity in crystal shape and size (Figs. 23, S14), craniides build their shells of mainly two biocrystal/mineral unit types: (1) thin calcite crystals consisting of platelets (Figs. 2B, 8, 25A, S15), and (2) irregularly shaped, interlinked, laminar units (Fig. 25B). The platelet strings form thin calcite layers, and arrays of layers form the largest part of the shell, especially most of the ventral valve. Structural order in individual layers or for arrays of layers was not observed for the shell of Craniida (e.g. Figs. 24, S15).

Williams and Wright (1970), England et al. (2007), Pérez-Huerta et al. (2007) addressed structural features of Recent and fossil craniide shells. Crystallographic characterization of craniide calcite crystals and microstructures was given by Checa et al. (2009). When based on calcite orientation and sectioned in different directions (sagittally: Figs. 24, 25, S15; tangentially: Figs. 26, 27, S16) we find the following four microstructures in *N. anomala* shells: (1) an assembly of laminae; these form the entire dorsal valve and the outermost shell part of the ventral valve (Figs. 24B, 25A, B), occasionally addressed as primary shell layer (2) an assembly of small mineral units/biocrystals (Figs. 24A, 25A, S15), with each of these consisting of very few (less than 10) calcite tablets (Figs. 29, S16), (3) an assembly of irregularly shaped, substructured and interdigitated large crystals, that are occluded in the central portions of the ventral valve (Fig. 26C–F), and (4) a honey-comb structure intercalated into the innermost layers of the ventral valve consisting of dense calcite walls encasing a multitude of minute calcite crystallites (Fig. 26B, G, H). The latter structures form lenses (white arrows in Fig. 26B) and are also, as the rest of the ventral valve, permeated by punctae (Fig. 22B). We observe two to four lenses per ventral valve. These lenses, consisting of calcite with this specific microstructure, are the muscle attachment sites.

Another, specific structure in craniide shells are concentric centers between adjacent puncta (yellow arrows in Fig. 27B, C, G), best observed in surface views of the shells (Fig. 27). We consider these as being target patterns and morphological traits. We find within these concentric centers a spiral arrangement of the organic membrane that delineates adjacent calcite layers (Fig. 27D). However, there is no trace of any systematic spiral arrangement of calcite that would extend over many calcite crystals (Fig. 29). Even though, as shown in Figs. 9, S3, in surface views individual platelets have a spiral surface structure. The linear structures

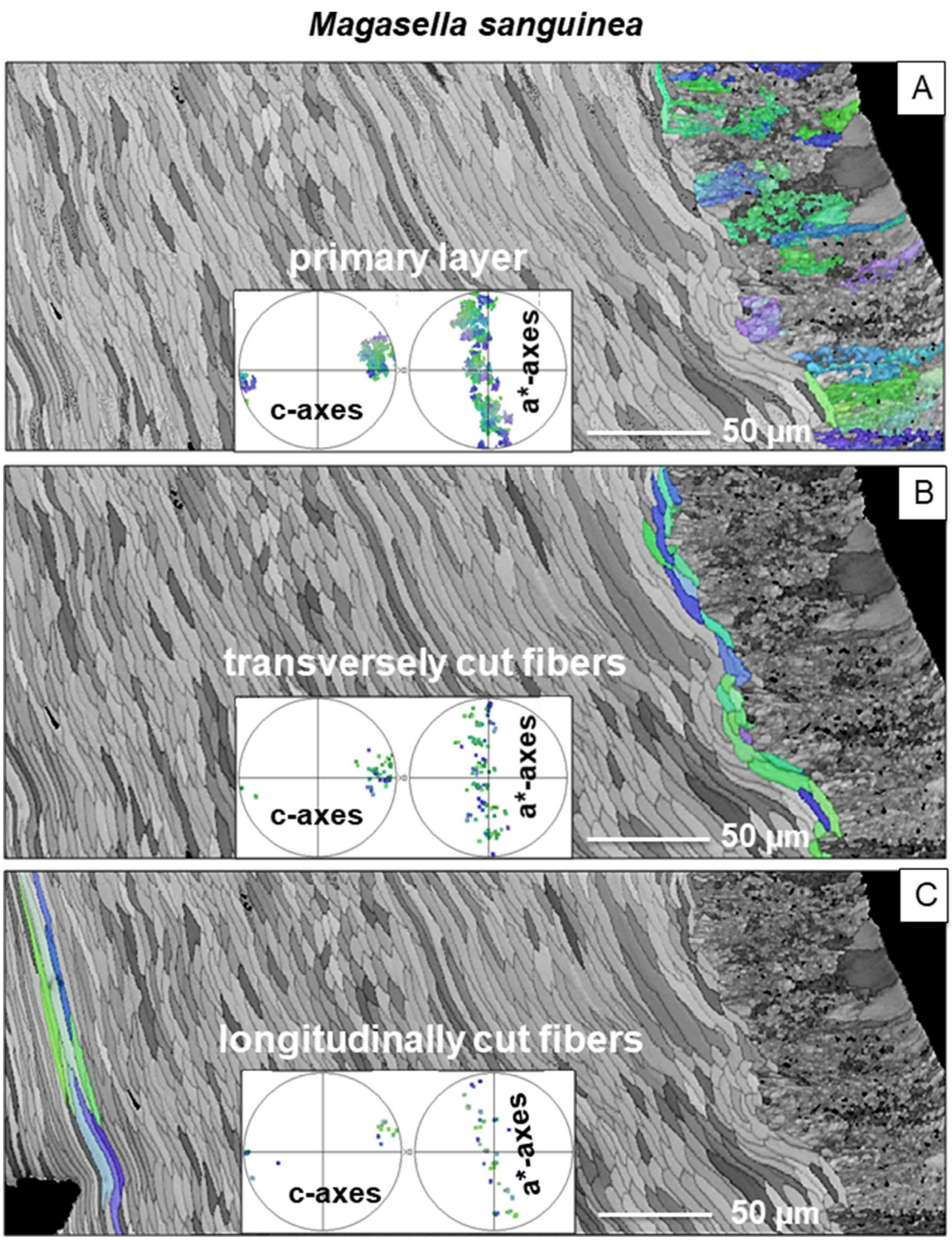

Fig. 20 EBSD band contrast and colour-coded orientation measurement images taken on a cross-section through a valve of *Magasella sanguinea*. **A** Shown in colour are selected dendrites of the primary shell layer and their orientation; **B** shown in colour is the orientation of adjacent fibers; **C** shown in colour is the orientation of fibers close to the inner shell margin. Pole figures in **A–C** give the orientation of only those shell portions that are highlighted in colour. Note that there is no difference in crystallographic orientation and texture between the primary and fibrous shell layers even though crystal morphologies (dendrites, fibers) comprising the two layers are distinct. Colour-code as in S13

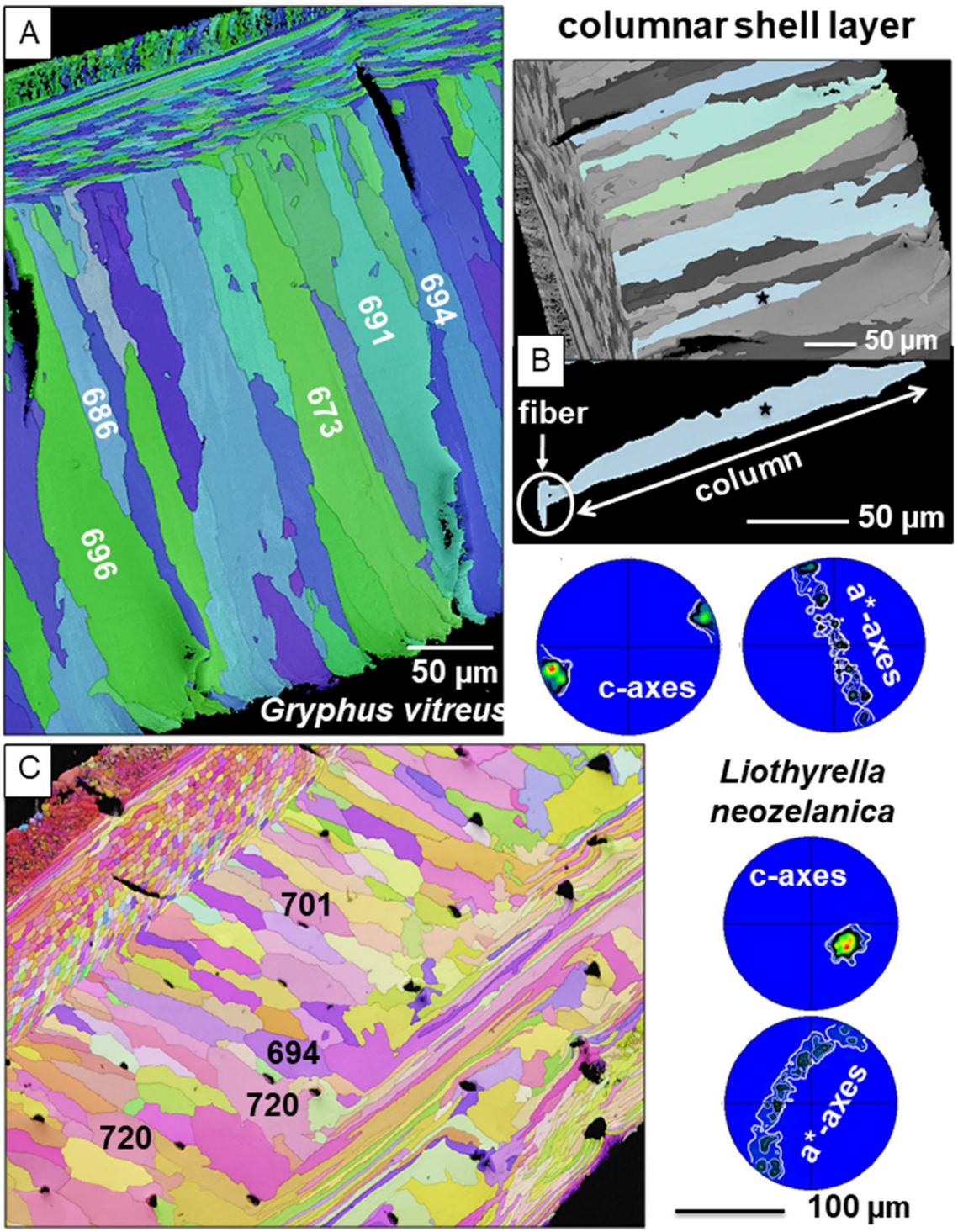

Fig. 21 Columnar shell-layer microstructure (EBSD maps) and texture (pole figures) deduced from EBSD measurements. *Gryphus vitreus* (**A, B**) and *Liothyrella neozelanica* (**C**) develop a columnar shell layer consisting of large irregularly shaped, prism-resembling calcite units. The calcite of the columns is coherently attached onto the proximal membrane covering the basal surface of a fiber (white circle in **B**); accordingly, there is full crystallographic continuity between fibers and columns. In *L. neozelanica* we find an alternation between columns and fibers (**C**), a feature not observed in shells of *G. vitreus* (**A**) (see also Goetz et al. 2009; Ye et al. 2018a). For both taxa, calcite crystallites in the columns are highly co-oriented (see the pole figures and the high MUD values in **A** and **C**). For the columns an axial texture prevails: all *c*-axes in the pole figure point in one direction, while *a**-axes co-orientations scatter on a great circle. Numbers given in black in the columns are MUD values; the latter are very high and are almost similar to those of crystalline calcite grown from solution (Yin et al. 2019). Colour-codes as in S13 for **A** and **B** and S12 for **C**

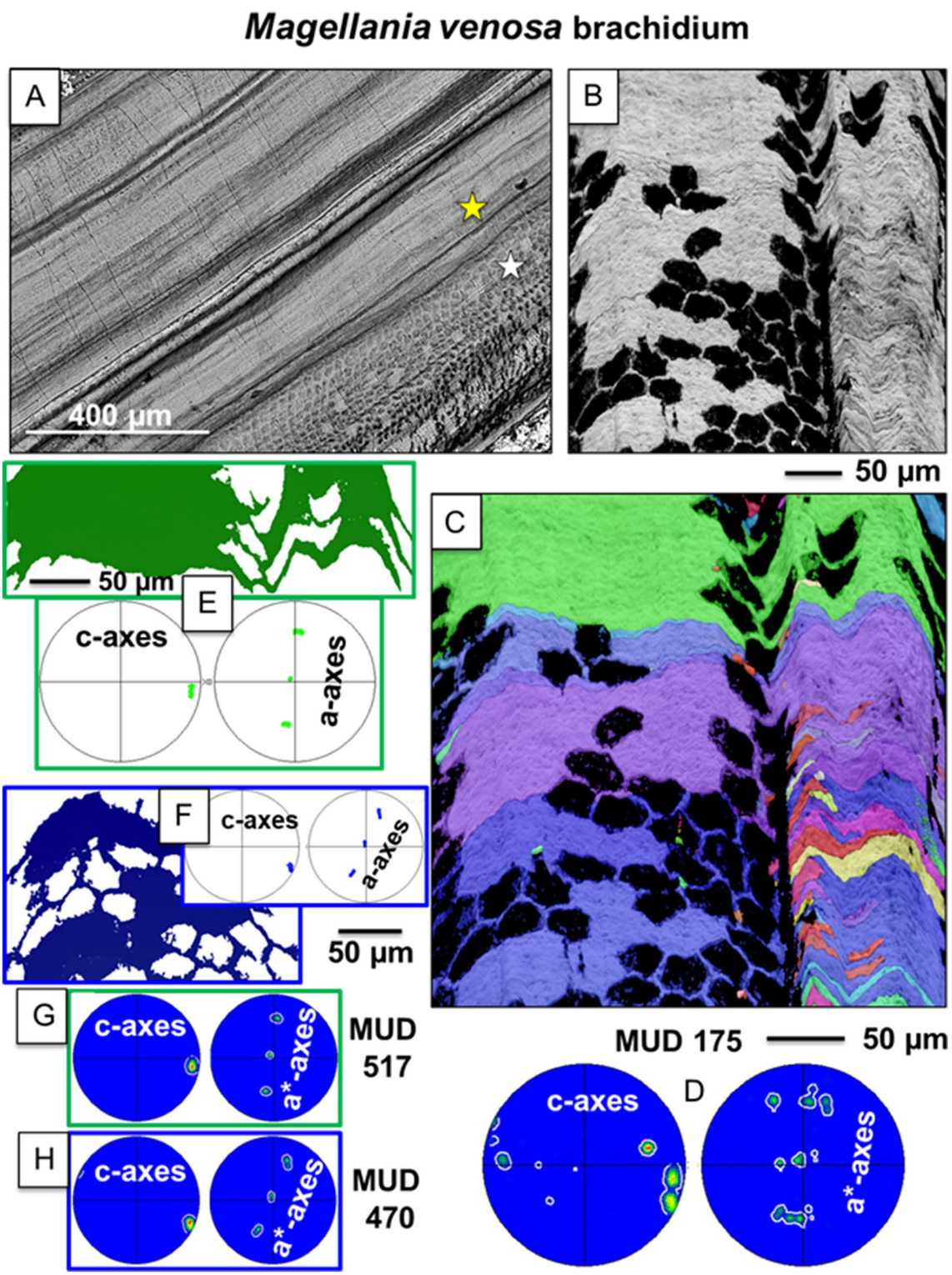

Fig. 22 Structure (**A**, BSE image), microstructure (**B**, EBSD band contrast measurement image) and texture (**C–H**) of the brachidium of *Magellania venosa*. Since the brachidium is thin and flat, it was not possible to prepare it with conventional preparation techniques for EBSD measurements. However, the flat surface of the brachidium allowed EBSD measurements on the pristine, unprepared surface. The brachidium of *M. venosa* has laminated and honey-comb portions (**A**) and (**B**). In both brachidium portions, calcite crystallites are well co-aligned (e.g. MUD value of 175 for the measurement shown in **C**). The brachidium consists of large mineral units (**E–H**). The pole figures in **E–H** show that these mineral units consist of calcite with well co-aligned single-crystal in 3-dimensional co-orientation. The colour-code is in S13

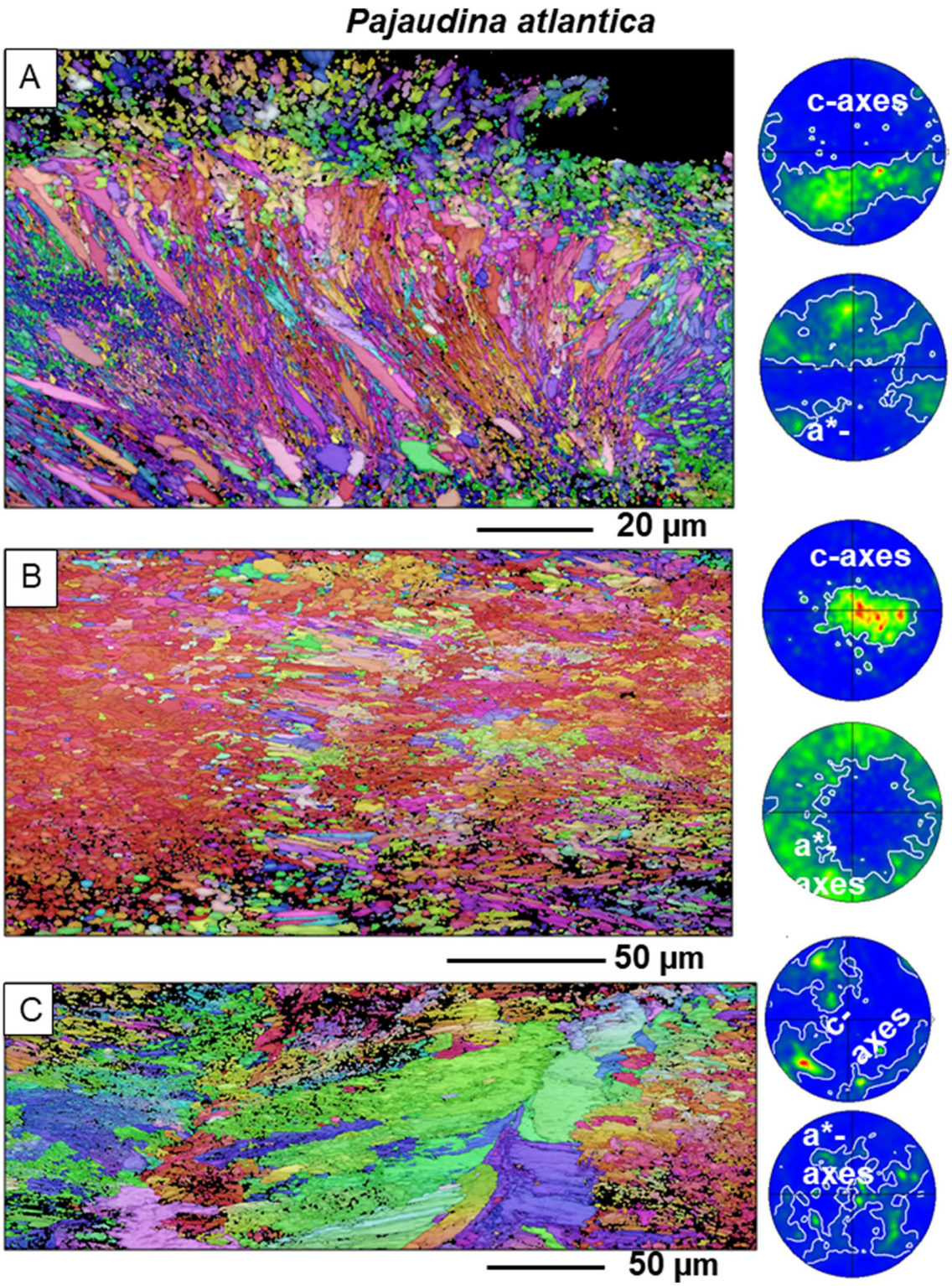

Fig. 23 Microstructure and texture of shell calcite of two valves of the thecideide brachiopod *Pajaudina atlantica* deduced from EBSD measurements. The shell of this thecideide species consists of a multitude of irregularly shaped, sized and co-oriented calcite crystals (**A–C**). These show weak co-orientation strength and texture (see pole figures). The colour-code for **A** and **C** is given in S13, for **B** in S12

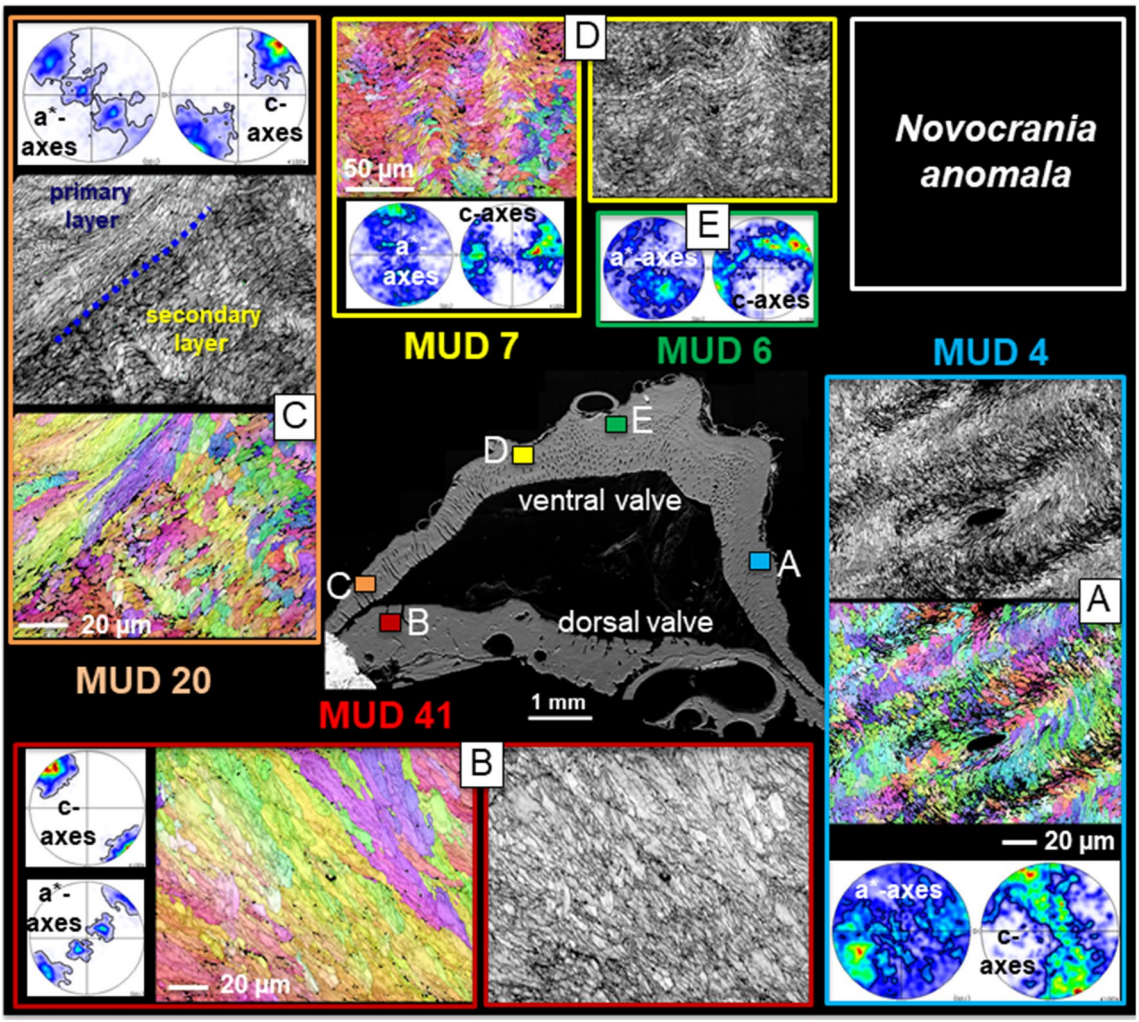

Fig. 24 Microstructure and texture patterns in *Novocrania anomala* shells deduced from EBSD band contrast (grey-scaled) and orientation (in color) maps and corresponding pole figures. The shell (SE image in the center of the figure) is sectioned sagittally. We show measurements from different sites of the ventral and the dorsal valve (**A–E**). For the largest part of the shell two main microstructures are observed: (1) an arrangement of calcite laminae in the dorsal valve and **B** in the outermost, the primary shell layer part, of the ventral valve, and (2) a sequence of calcite layers consisting of calcite tablets that form the secondary layer of the ventral valve (**A**, **C–E**). For a better visualization of the structure we show enlargements of EBSD maps given in this figure in Figs. 25 and S15. The dashed blue line in **C** delineates the primary from the secondary shell layer. Crystallite co-orientation strength is weak for *N. anomala* calcite; see the low MUD values, in particular for shell portions consisting of calcite tablets (**A, D**). Calcite crystallites that form the laminae of the dorsal valve have higher co-orientation strength, with corresponding higher MUD values (**B**); see also Fig. 25. Colour-code for calcite orientation is given in Fig. S12

following regular crystallographic edges in Figs. 9E–G and S3G are the projections of the actual growth surfaces which are (sub)perpendicular to the face. These growth surfaces have heights in the 100 nm range (or slightly larger). It should be kept in mind that the micrometer-scale spiral growth patterns observed in *N. anomala* are not at all related to atomistic spiral growth. For the latter, steps would be in the 1 ångstrøm range and one would expect the steps on growth faces perpendicular to the face we are looking at in Figs. 9E, G, and S3G. Figure 27C, D show clearly that there are organic membranes penetrating perpendicular into the surface of observation, the surface shown in Figs. 9E, G, and S3G. Coherent crystal lattice growth spans across a few, three to five, of these perpendicular membranes but does not follow in complete helical circles around the concentric structure (e.g. Fig. 27D, also Fig. 27C). Again, indicating that the observed micrometer-scale growth helices are not related to any atomistic spiral growth pattern. The texture pattern of concentric growth centers, as shown in Fig. 27F, is rather multiaxial (see pole figures in Fig. 23H, I) with the *c*-axes clustering parallel to the shell surface having a spread of 30°–40°. The texture strength at concentric growth

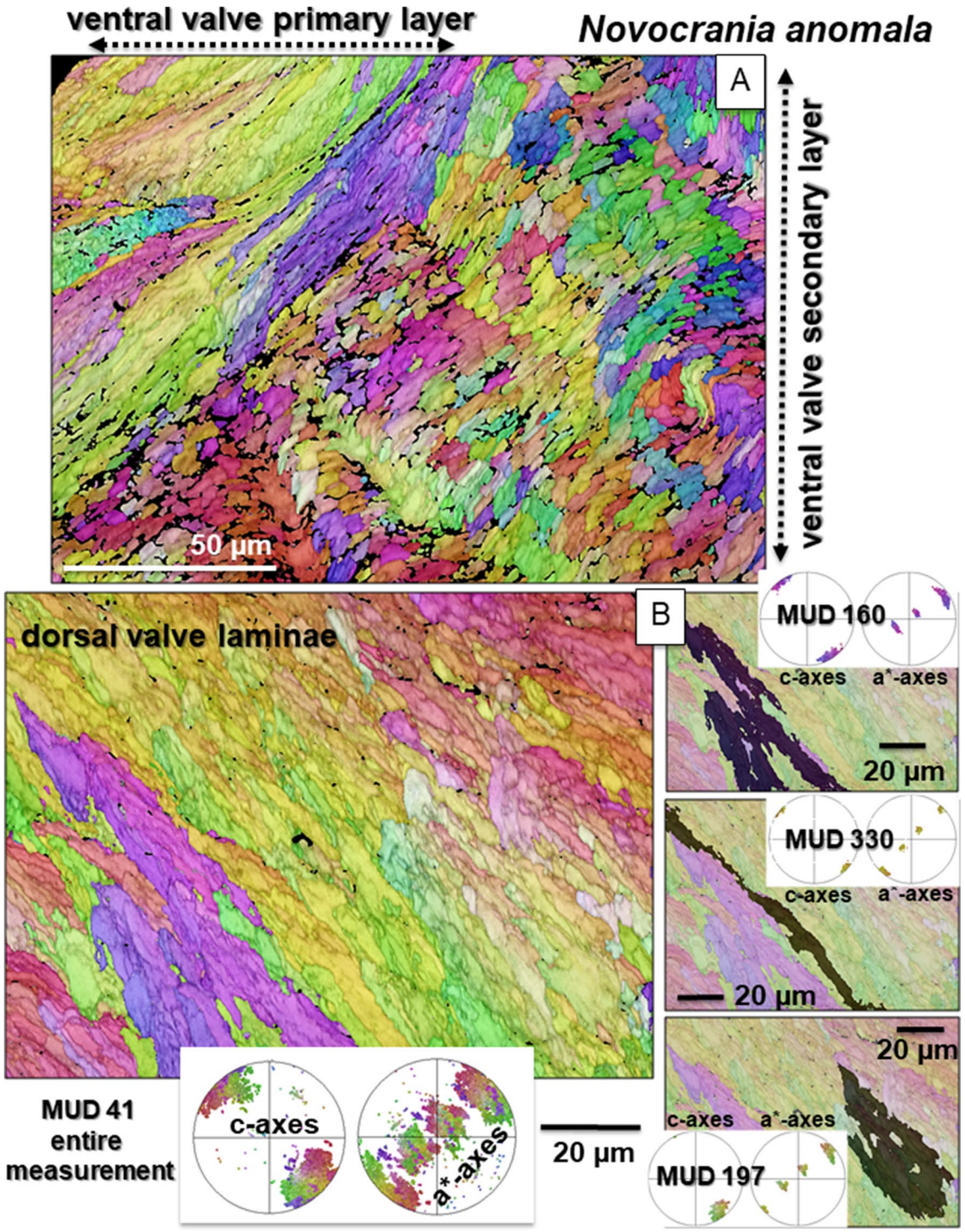

Fig. 25 Assemblage of laminae forming the dorsal valve (**B**) and the outermost shell region of the ventral valve (**A**). Colour-code for calcite co-orientation is given in Fig. S12. The transition from laminae to layers of tablets is smooth (**A**); the two microstructures grade into each other. The dorsal valve is formed of large, interlinked laminae; the latter with irregular morphologies (**B**). Calcite within individual laminae is well co-aligned, MUD values for selected laminae are 160, 330, 197. MUD value of the entire measurement shown in **B** is 41. It is significantly lower, relative to MUD values of individual laminae, however, it is increased relative to MUD values that we find for the secondary layer of the ventral valve consisting of calcite layers formed of calcite tablets (see also Fig. 5D, E)

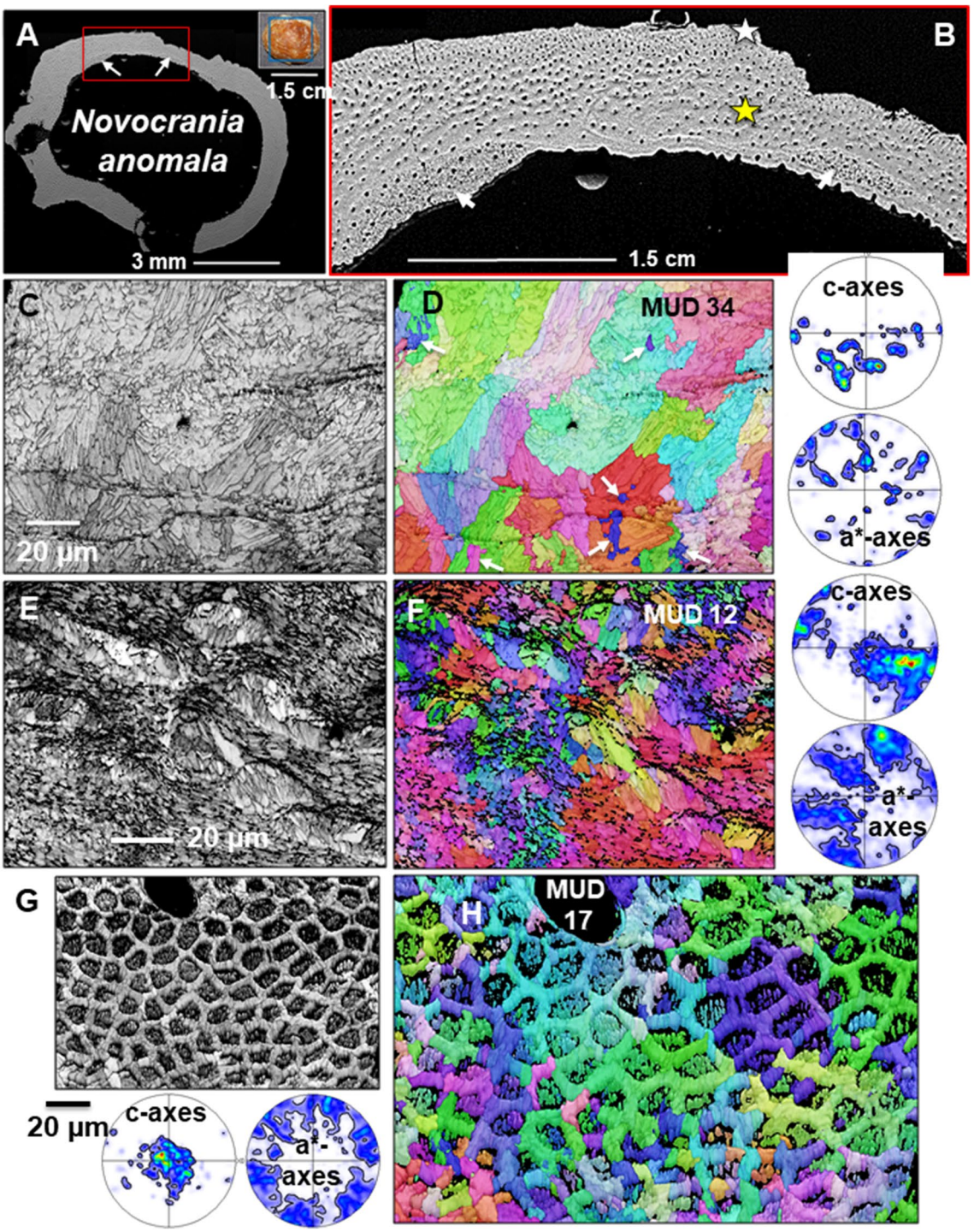

Fig. 26 Additional microstructures in *Novocrania anomala* shells detected with EBSD band contrast and crystal orientation measurements. The colour-code is given in Fig. S12. These structures are observed only in the ventral valve, when the latter is sectioned tangentially (**A**). In certain shell portions (white arrows in **B**) we find a honeycomb structure (**G**, **H**) consisting of dense calcite walls and an assembly of small to minute crystals between the walls, the sites of muscle attachment to the shell. In addition, we find assemblies of large, substructured crystals (**C–F**). These are irregular in shape, size and are interlinked in 3D (white arrows in **D**). Puncta branch in the primary shell layer and appear to be smaller in outer shell sections (white star in **B**), relative to puncta in the secondary layer (yellow star in **B**). This may be because puncta terminate in the primary layer as finely divided branches (Williams and Wright 1970)

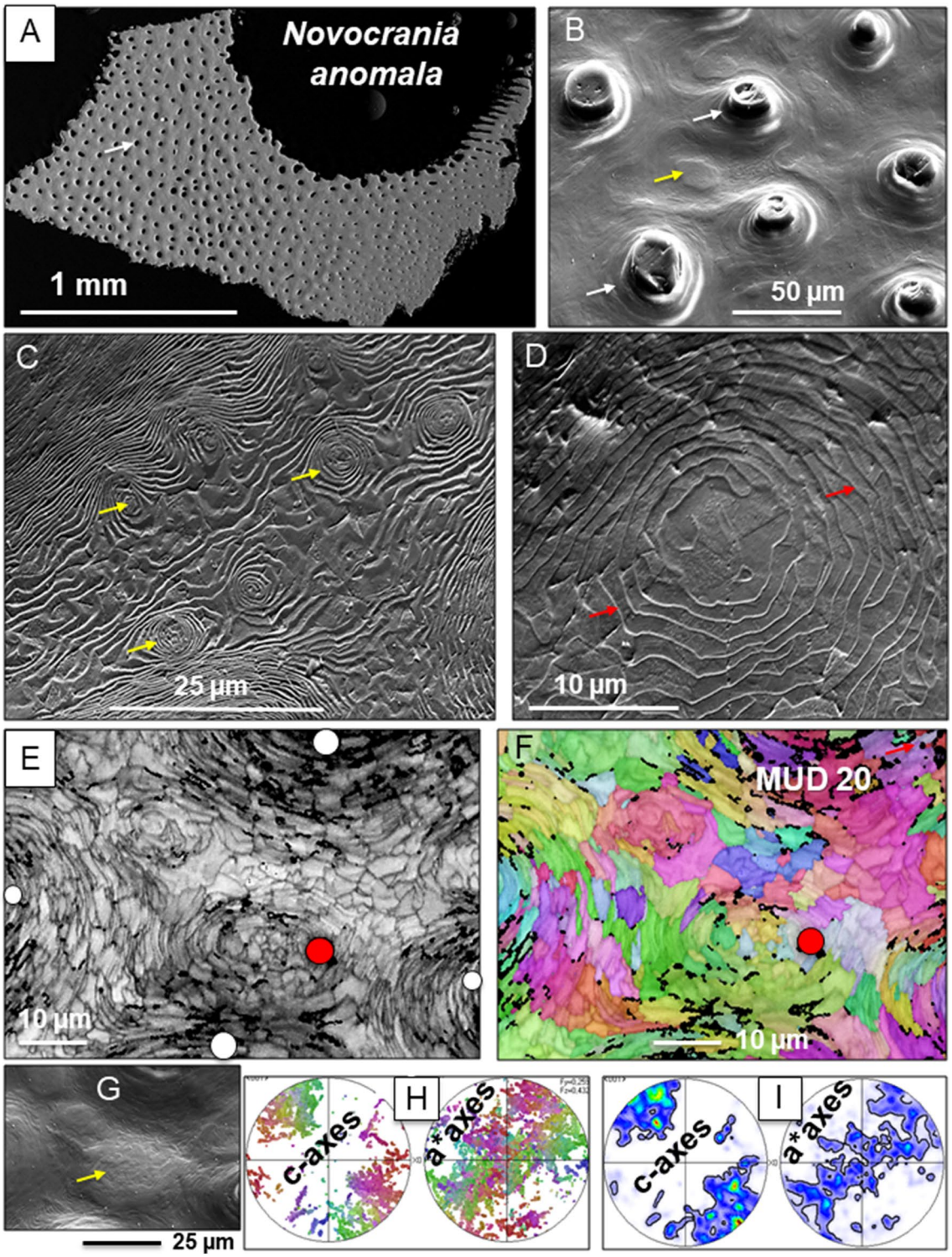

Fig. 27 Surface view of a shell of *Novocrania anomala*. **A**, **B** Depict a large number of puncta that pervade the shell (white arrows in **B**). **A–D**, **G** BSE images; **E, F** EBSD band contrast and orientation images, respectively. Between puncta (white arrows in **A** and **B**) entities with concentric features are developed (yellow arrows in **B, C, G**) consisting of, more or less, parallel arrays of calcite layers demarcated from each other by organic membranes (red arrows in **D**). We consider these concentric entities (yellow arrow in **B, G**) as morphological traits. The microstructure of these concentric structures (**E, F**) is formed of calcite crystallites consisting of few calcite tablets. The crystals have a weak axial fiber texture (pole figures in **H** and **I**) and show low crystal co-orientation strength (MUD of 20). White dots in **E** indicate the position of puncta, red dot in **E** points to a concentric structure between the puncta

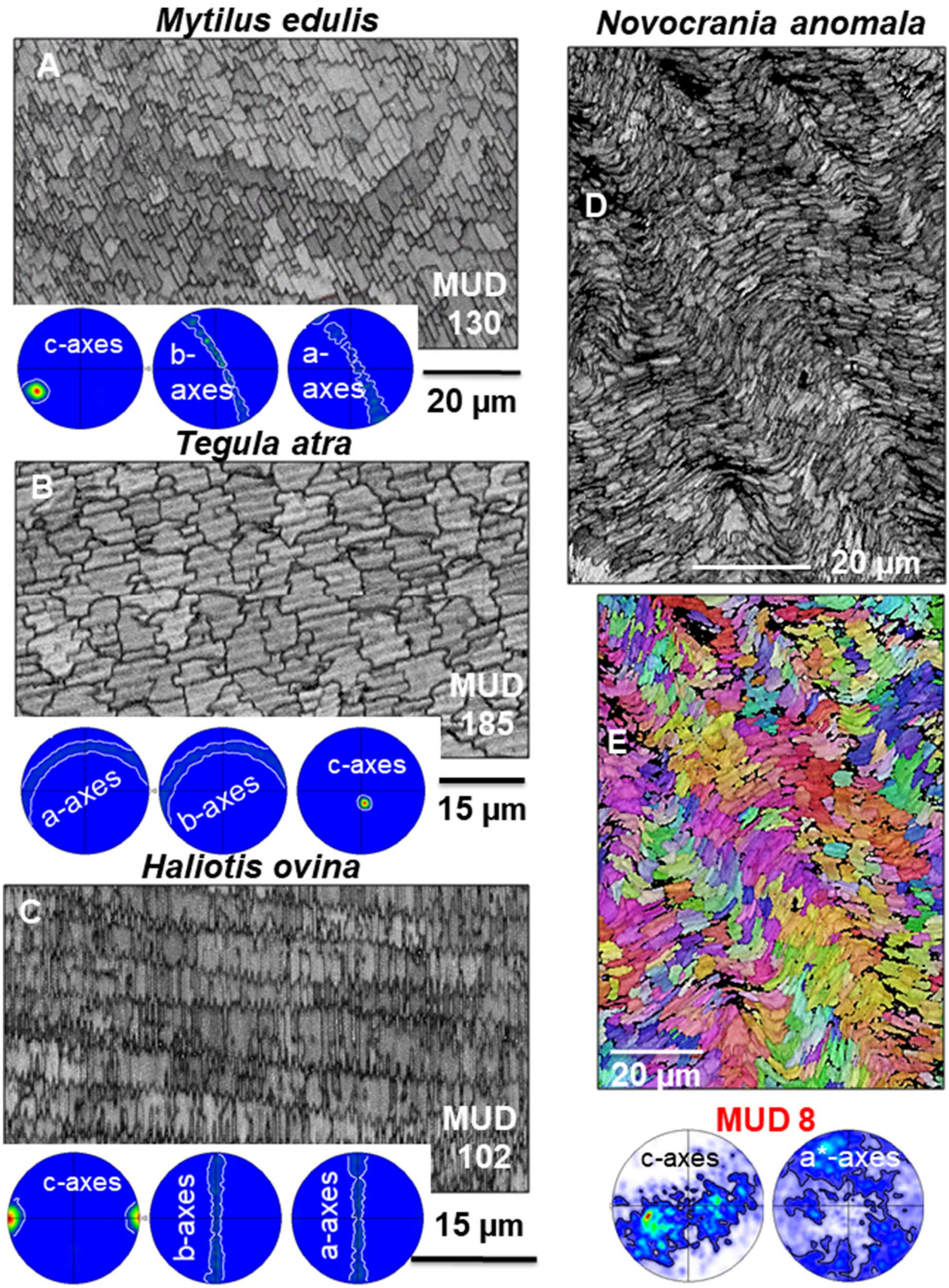
Mytilus edulis
A
MUD 130
c-axes
b-axes
a-axes
20 µm
Tegula atra
B
MUD 185
a-axes
b-axes
c-axes
15 µm
Haliotis ovina
C
MUD 102
c-axes
b-axes
a-axes
15 µm
Novocrania anomala
D
20 µm
E
20 µm
MUD 8
c-axes
a*-axes

◂**Fig. 28** Carbonate shell material formed of tablet/platelet-shaped crystals: *Mytilus edulis* (**A**), *Tegula atra* (**B**), *Haliotis ovina* (**C**) aragonite, *Novocrania anomala* calcite (**D, E**). Even though all four shell structures are formed of tabular crystals, there is significant difference between the aragonitic (**A–C**) and the calcitic (**D, E**) platelet arrangements in: mineralogical phase, microstructure, texture and crystal co-orientation strength (see the difference in MUD values). Accordingly, there is no structural relationship between the structure of aragonitic nacre in bivalves, gastropods, cephalopods and the calcite tablets in *N. anomala*. Williams and Wright (1970; England et al. (2007); Perez-Huerta et al. (2007) described the tabular arrangement of *N. anomala* shells as a 'semi-nacreous' microstructure, a term that (1) should not be used for the shells of *N. anomala* (this study and Checa et al. 2009). Figures **A–D** are EBSD band contrast measurement images; Fig. 28E shows calcite orientation. The colour-code is given in S13

centers is weak, as indicated by the low MUD value of 20 (Fig. 27F).

Figure 25B depicts the structure of the laminated microstructure for the dorsal valve of *N. anomala*. If based on co-orientation, we can discern large, interlinked and substructured laminar units (Fig. 25B). These laminar units are strongly mineralized, the calcite shows a graded arrangement and has high co-orientation (see the high MUD values in Fig. 25B).

The tabular morphology of Craniida calcite initiated the term 'semi-nacre' for the calcite of craniide shells (Williams and Wright 1970; England et al. 2007; Perez-Huerta et al. 2007). Nacre and nacreous assemblies refer to and define columnar and sheeted aragonite tablet arrangements (Bevelander and Nakahara 1969; Nakahara 1991; Cartwright and Checa 2007) with a spiral growth pattern that covers a large sequence of tablets (see the 'tower grain' in Fig. 2 in Griesshaber et al. 2013) and not only one (e.g. as described in Checa et al. 2009) or very few (this study) tablets, as it is the case for craniide shells. Accordingly, even though being tablet shaped, *N. anomala* platelets should not be compared to nacre tablets. Tablet arrangements that we find in *N. anomala* shells are unlike the nacreous microstructures that we find for mollusc shells. Neither the carbonate phase, nor the size of the platelets, nor crystal co-orientation strength, nor the microstructure nor the texture of craniide shells can be compared to the nacre secreted by bivalves, gastropods, and cephalopods (Fig. 28, and Checa et al. 2009). The nacre of mollusc shells is formed of aragonite, tablet assemblages are sheeted or columnar, have high aragonite crystal co-orientation strength (e.g. MUD values of 185, 130, 102 compared to an MUD around or/and below 10 in *N. anomala*) and a strong fiber texture (Griesshaber et al. 2013; Peter et al. 2021). For *N. anomala* shells a weak fiber texture is observed only for the interlinking laminae in the dorsal valve (see pole figure in Fig. 24B for the entire measurement). For most EBSD scans made on the ventral valve of *N. anomala* (Fig. 24) calcite co-orientation strength is exceptionally low and a clear-cut fiber texture cannot be deduced from the diffraction data. The use of platelets for craniide and mollusc shell construction should rather be regarded as analoguous fabrics resulting from convergent evolution, as it is the case, for example, with the use of fibers for shell formation in brachiopod and bivalve shells. Microstructures and textures are unique in the later-evolved craniids.

In Rhynchonellida, Terebratulida and Craniida, the preferred crystallographic orientation is passed from one shell layer to the other (Terebratulida: primary to fibrous to columnar; Rhynchonellida: primary to fibrous; Craniida: primary to fibrous). Neighboring layers smoothly grade into each other (also noted for Craniida by Checa et al. 2009). Thus, the calcite in adjacent shell layers has a similar preferred crystallographic orientation, even though crystal morphologies and grain boundary topologies in neighboring shell layers are distinct (this study, and Goetz et al. 2011). This observation holds for taxa of different brachiopod orders.

Characteristics of the different textures

This review is based on more than one hundred EBSD measurements (Table S1) and has allowed us to deduce textural patterns for shell calcite of the investigated terebratulide, rhynchonellide, thecideide and craniide taxa (Figs. 30, 31, 32).

EBSD links the molecular with the macro-scale (Fig. 30), as it connects the orientation of planes formed by ions in a crystal structure (Fig. 30B) with the macro-scale architecture of the skeleton, or skeletal elements (Fig. 30, and Schmahl et al. 2004; Griesshaber et al. 2007). This characteristic holds for the valves of the layered shells of Terebratulida and Rhynchonellida where we find a sharp, axial texture, irrespective of how an EBSD measurement was scanned, such as (1) different, several or (2) just one layer in the shell. In shells of rhynchonellides and terebratulides, calcite *c*-axes are more or less perpendicular to the surface of the valves and rotate with their curvature (Fig. 30). This important characteristic was shown first for the Recent brachiopod *M. truncata* (Schmahl et al. 2004) and is recognized as an intrinsic feature of biologically secreted carbonate hard tissues (e.g. brachiopods, molluscs, benthic and planktonic foraminifera shells and sea urchin teeth (Schmahl et al. 2004; Griesshaber et al. 2007; Goetz et al. 2014; Yin et al. 2021). The valves of rhynchonellide and terebratulide brachiopods have a uniaxial fiber texture, while the hinge shows a bimodal, occasionally even a multimodal, distribution pattern of calcite *c*-axes (Figs. 30C, S12B–S12D, Griesshaber et al. 2007).

Comparing the texture of terebratulide species with three mineralized layers (*L. neozelanica, G. vitreus*) to each other (Fig. 31A–C), we find the following characteristics: (1)

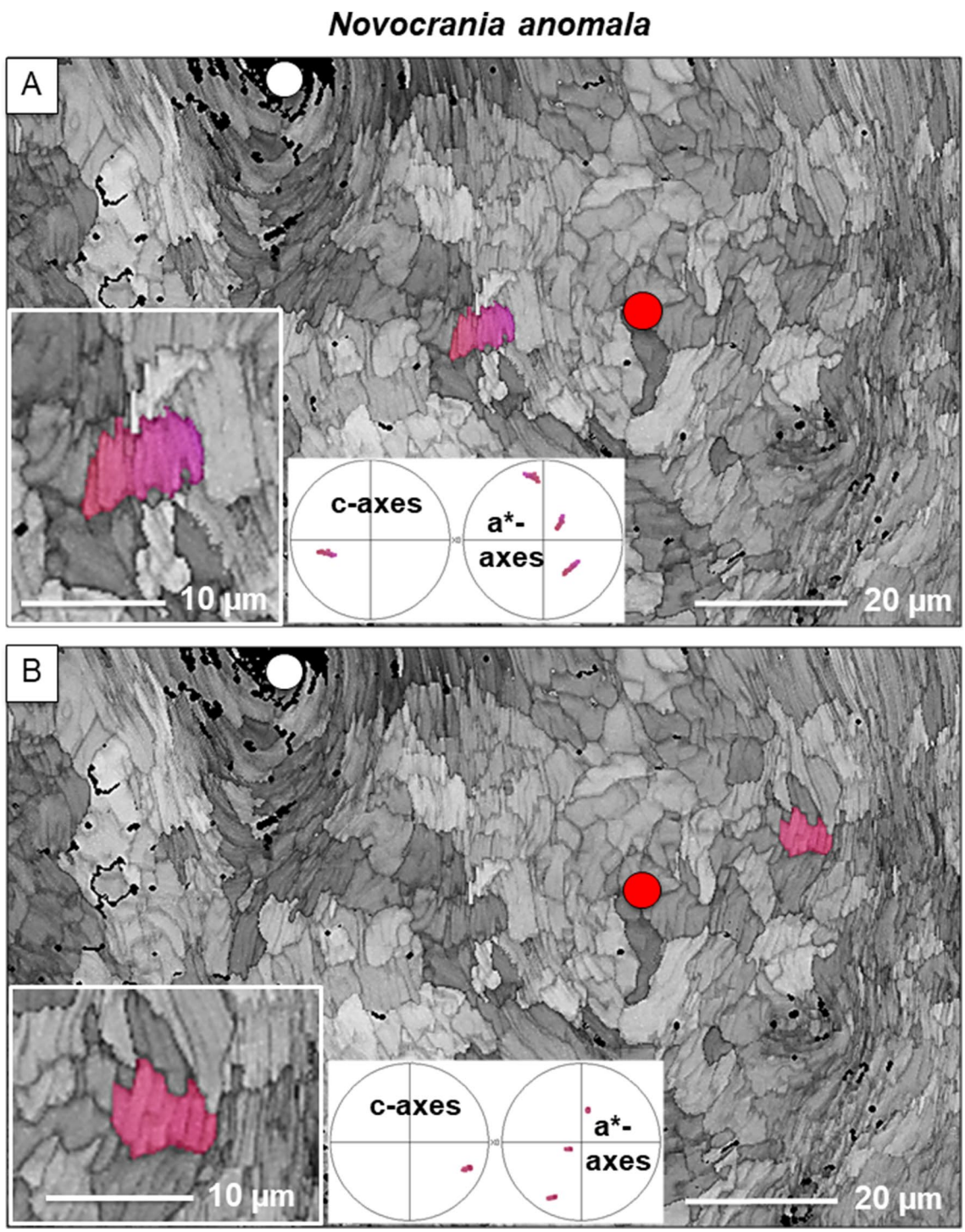

Fig. 29 Tablet arrangement, microstructure and texture of mineral units, biocrystals, of *Novocrania anomala*. Further information is shown in Fig. S16. White and red dots in **A** and **B** indicate a punctum and a concentric center between adjacent puncta, respectively. Colour-code is given in S12

the columnar layer has the strongest calcite co-orientation strength, thus the strongest texture and is followed (2) in calcite co-orientation strength by the primary shell layer. The fibrous shell portion (3) has the weakest texture and lowest co-orientation strength of calcite crystallites compared to those of the columnar and primary shell layers. For both, *G. vitreus* and *L. neozelanica,* we investigated six specimens each and show in Fig. 31 pole figures and MUD values for

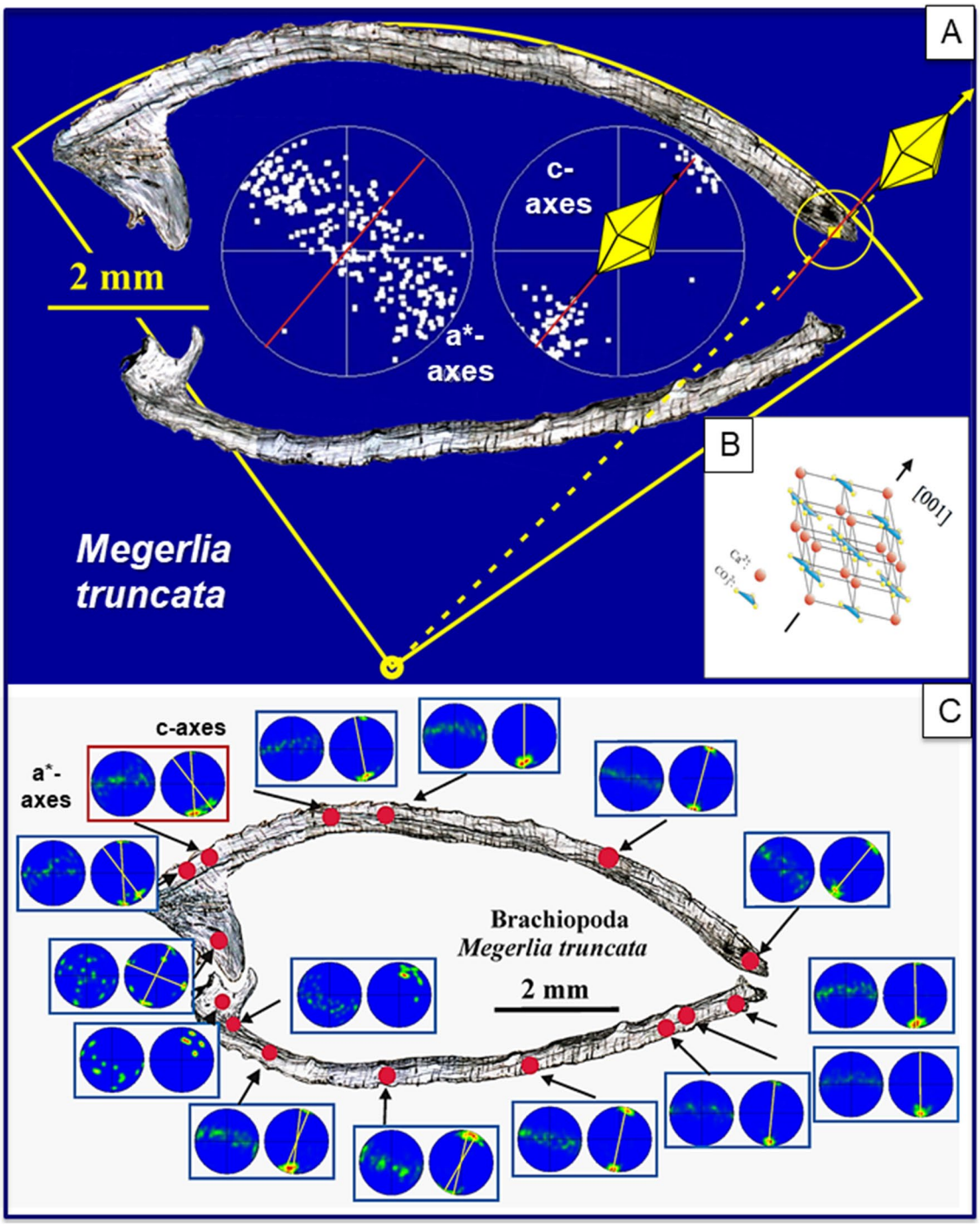

Fig. 30 Pattern of calcite *c*- and *a**-axes orientation measured on a cross-section through the median plane of both valves of the terebratulide species *Megerlia truncata*. Calcite *c*-axes are parallel to the radius of the curvature of the shell, are perpendicular to the shell surface (A and Schmahl et al. 2004) and rotate with the curvature of the shell vault (B and Griesshaber et al. 2007). The valves have a sharp axial fiber texture, while at the hinge a bimodal or even multimodal distribution of *c*-axes prevails (B and Griesshaber et al. 2007). *C*-axes pole data are always on the right, *a**-axes pole data are on the left of the pole figure

two specimens per taxon. We observed a stronger texture for shell calcite of *G. vitreus* (for all shell layers higher MUD values, Fig. 31A–C) compared to the texture strength of *L. neozelanica* shells (lower MUD values for all shell layers, Fig. 31A–C).

For the shells of craniides and thecideides, textural strength is significantly lower than for Rhynchonelliformea

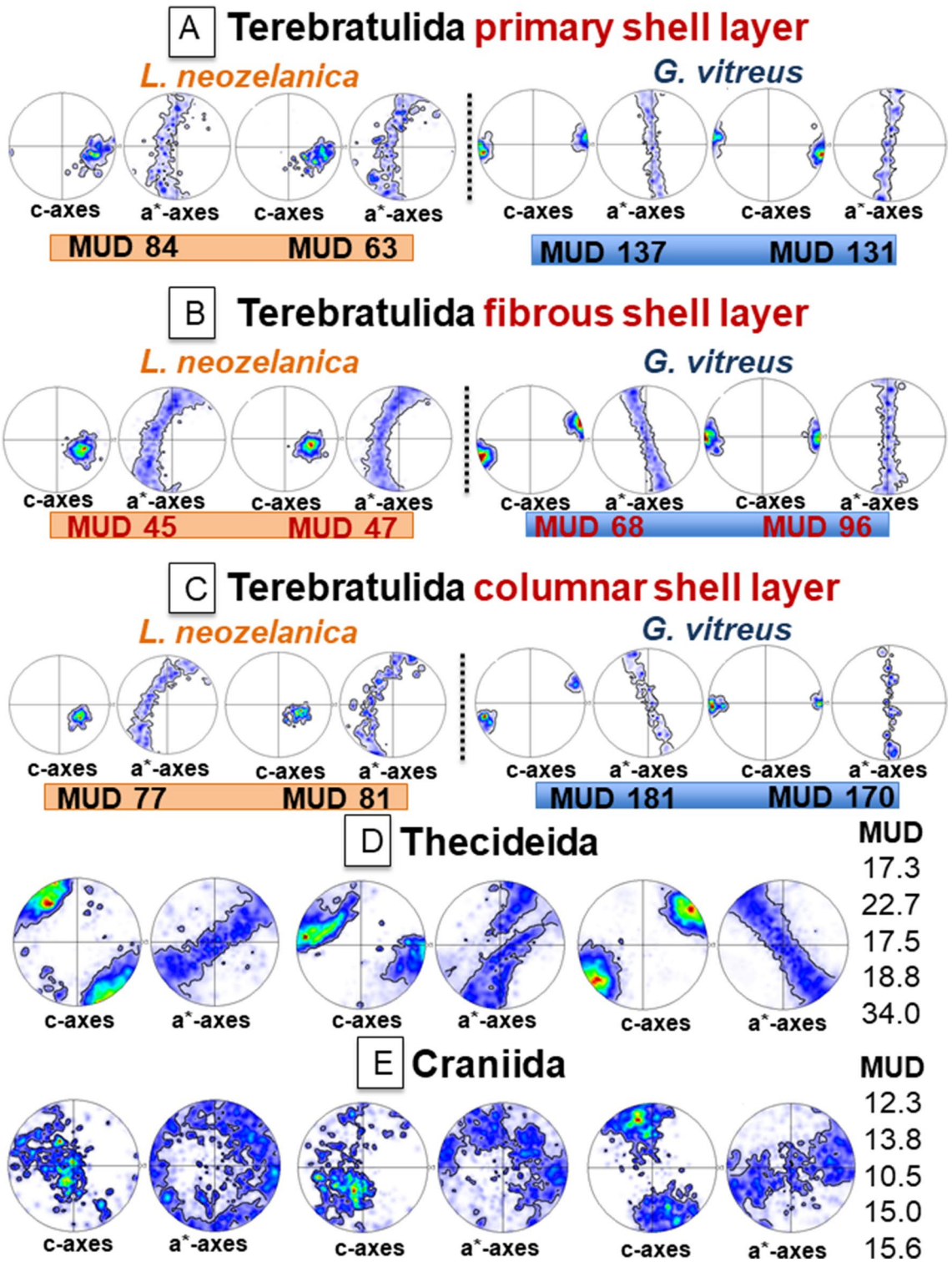

Fig. 31 Comparison of orientation between terebratulide, thecideide and craniide shells. MUD values give calcite co-orientation strengths. With a half width of 5 and a cluster size of 3 an MUD value of 1 indicates random crystal orientation, while an MUD above 700 indicates single crystallinity. For *Gryphus vitreus* and *Liothyrella neozelanica* we show the texture of two specimens, and for the Thecideida and Craniida three specimens each. We deduce the following: (1) relative to the terebratulide species, calcite crystals in thecideide and craniide shells are significantly less co-aligned, (2) the least co-aligned is the calcite in craniid shells, (3) there is a huge difference in calcite co-orientation strength between *L. neozelanica* and *G. vitreus*. (4) for the latter two species the fibrous layer has the lowest calcite co-orientation strength (see MUD values given in red), while, (5) co-orientation is highest for the columnar layer, (6) it is, however, also high for the primary shell layer

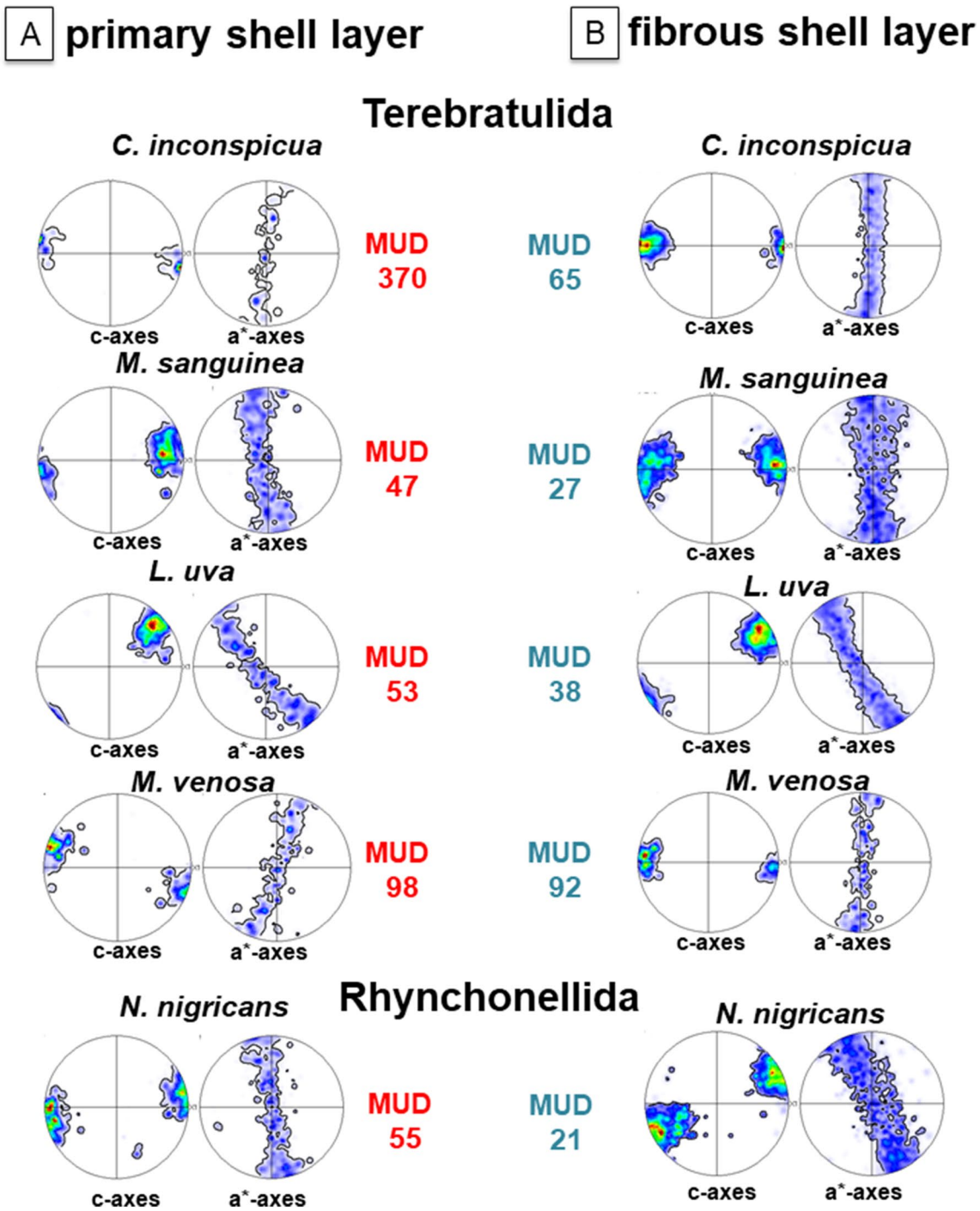

Fig. 32 Comparison in crystal co-orientation strength between species with a primary and a fibrous shell layer. We see the following: (1) calcite co-orientation in the primary shell layer is always higher relative to that in the fibrous layer and (2) there is a significant difference in calcite co-orientation strength for the different Recent terebratulide and rhynchonellide taxa

(Fig. 31D, E); for both taxa we investigated several specimens but show two examples per taxon. The pole figures show that thecideide shells have an axial, cylindrical, texture as well, similar to the texture of terebratulide and rhynchonellide taxa. However, calcite co-orientation strength in thecideide shells is low (see MUD values in Fig. 31D), thus the shell has a weak texture (compare pole figures and MUD values of Fig. 31A–D). The craniide species *N. anomala* forms its shell with little textured calcite (Fig. 31E, see MUD values). Even though the calcite achieves almost

complete random distribution, there is still some pattern of calcite organization, especially in the laminated arrangement of the dorsal valve, as described in Sect. 5.

Figure 32 compares the texture strength of the primary and fibrous shell layers for taxa that form their shell of only two mineralized layers. We observe that: (1) for the same specimen, calcite in the primary shell layer is always more co-oriented; it has always the stronger texture, relative to the fibrous shell layer, (2) texture strength differs for the different species, for both the primary and the fibrous shell layers. The largest difference can be observed for *C. inconspicua* (MUD 370 and 65) and *M. sanguinea* (MUD 47 and 27) (Fig. 32). Interestingly, both species live in comparable environments, in Doubtful Sound, New Zealand.

Are thecideide shells reliable archives for environmental reconstruction?

Palaeoclimate and paleoenvironmental reconstructions are based on analyses of geochemical proxies performed on archives such as biogenic hard tissues and cements (e.g. Brand et al. 2011). Shells of the Terebratulida and Rhynchonellida are one of the most used biogenic structural materials for paleoenvironment reconstruction as they cover almost the entire geologic record, are wide-spread in marine habitats and, most of them, secrete low-Mg calcite shells (Al-Aasm and Veizer 1982; Veizer et al. 1999; Brand et al. 2003, 2011; Auclair et al. 2003; Parkinson et al. 2005; Angiolini et al. 2009; von Allmen et al. 2010; Payne and Clapham, 2012; Garbelli et al., 2012, 2014; Cross et al. 2015; Immenhauser et al. 2015; Rollion-Bard et al. 2016; Ye et al. 2019; Jurikova et al. 2020).

Thecideide brachiopods are the last brachiopod order to appear in the fossil record (early Triassic; Carlson 2016). In contrast to the rhynchonellides and terebratulides, thecideides are small-bodied, relatively thick-shelled animals that live in tropical and warm seas, in cryptic habitats and are cemented to the hard substrate (e.g. Rudwick 1970; Baker 1990; Richardson 1997a, b; Lüter 2005; Carlson 1995, 2007; Nebelsick et al. 2011; Simonet Roda et al. 2021). Thecideide shell microstructure was proposed to be similar to the primary layer microstructure of rhynchonellides and terebratulides (Williams 1973, 1997; Baker 2006; Williams and Carlson 2007). However, Simonet Roda et al. (2021) showed that the microstructure and texture of modern Thecideida is specific and unique to that order.

If thecideide shell microstructure were similar to the primary shell layer of Rhynchonellida and Terebratulida, then, thecideide shells could not be considered a reliable paleoenvironmental archive, since geochemical studies have demonstrated that the primary layer of rhynchonellide and terebratulide shells is not precipitated in isotopic equilibrium with ambient seawater (Carpenter et al. 1991; Carpenter and Lohmann 1995; Parkinson et al. 2005; Brand et al. 2011; Rollion-Bard et al. 2019). Subsequently, we focus on this issue and complement our microstructural work (chapters 1–5) with geochemical analyses obtained on a terebratulide (*M. venosa*) and a thecideide (*P. atlantica*) specimen (Figs. 33, 34 and Milner Garcia 2018).

For the terebratulide *M. venosa*, the $\delta^{18}O$ signature of the primary shell layer is strongly depleted in ^{18}O, relative to the isotopic equilibrium field (Fig. 33B), a feature attributed to kinetic and physiological effects (Auclair et al. 2003). Towards the inner shell surface, $\delta^{18}O$ values become heavier: at the innermost shell sections, formed of fibers, $\delta^{18}O$ values are close or within the equilibrium field (Fig. 33B). Water temperature variation at the sampling location of *M. venosa* is 3.5 °C and accounts for a $\delta^{18}O$ variation of about 1‰. Accordingly, the observed variation of about 3‰ in $\delta^{18}O$ values for the fibrous layer of *M. venosa* is due to physiological and kinetic effects (see also discussions in Yamamoto et al. 2010, 2013; Takayanagi et al. 2013; Bajnai et al. 2018; Brand et al. 2019; Rollion-Bard et al. 2019; Ye et al. 2019).

For the thecideide *P. atlantica,* $\delta^{18}O$ results diverge from what we find for *M. venosa* (Fig. 33A). Furthermore, for *P. atlantica* there are differences in $\delta^{18}O$ values between ventral and dorsal valves (Fig. 33A). In the ventral valve $\delta^{18}O$ values fluctuate close to the field of isotopic equilibrium with seawater, while $\delta^{18}O$ values of the dorsal valve scatter fully within the range of values that span the equilibrium field (Fig. 33A). Water temperature variation at sampling of *P. atlantica* was 3.7 °C and accounts for a variability in $\delta^{18}O$ values from 58 to 77% of the overall shell $\delta^{18}O$ value. The remaining can be attributed to kinetic effects. For transects through the ventral valve we find that outer shell layers of *P. atlantica* are depleted in ^{18}O relative to equilibrium values, while the inner shell portions are secreted in equilibrium with ambient seawater (Fig. 33A). As the overall variability across the transect through the valve is not in agreement with the temperature variation of 3.7 °C, we can assume that kinetic effects affect mainly outer and to a lesser degree inner shell sections; a result that is in concert with $\delta^{18}O$ measurements of Brand et al. (2003). Hence, inner shell calcite of *P. atlantica* incorporates oxygen isotopes, more or less, in equilibrium with ambient seawater.

Magnesium concentration across shell transects of the terebratulide *M. venosa* follows a characteristic trend: high Mg-contents in the primary shell layer that decrease in the fibrous layer, however, increase again at innermost shell surfaces (Fig. 34); a previously described well-known trend (e.g. Griesshaber et al. 2007; Romanin et al. 2018; Rollion-Bard et al. 2019). Mg content in the thecideide *P. atlantica* (Fig. 34) is also structured and its concentration is distinct from what we observe for *M. venosa* shells: (1) the Mg/Ca ratio in *P. atlantica* is significantly higher relative to values that we observe for *M. venosa* (Fig. 34), (2) within the outer

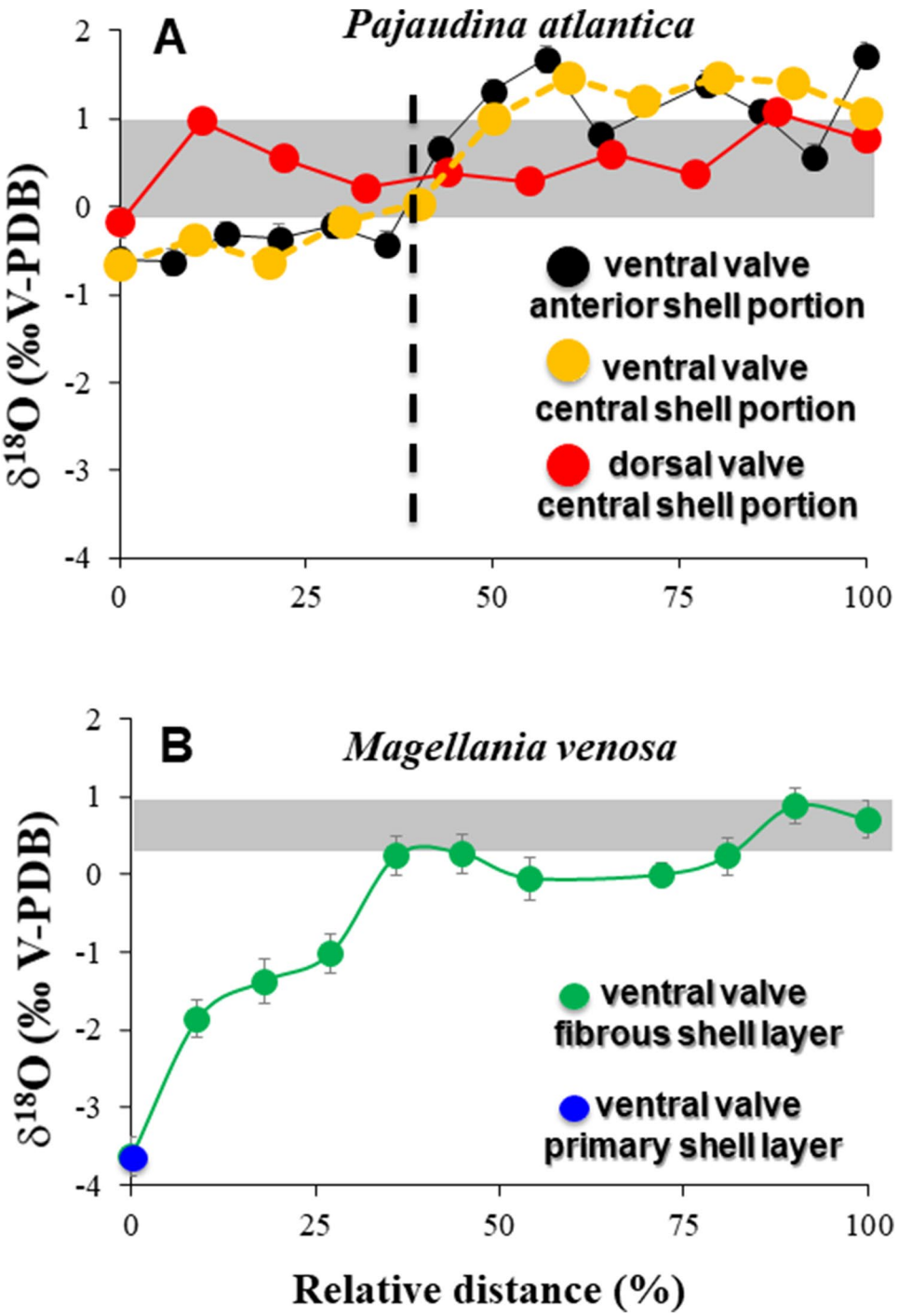

Fig. 33 Oxygen isotope composition along cross-sections through the shells of *Pajaudina atlantica* and *Magellania venosa*. Error bars represent the standard deviation. The grey field in the figures indicates the region of $\delta^{18}O$ where inorganic calcite precipitates in equilibrium with seawater. The calculation of the latter is based on the equation given by Watkins et al. (2013), and for the brachiopod sample localities. The relative distance along the shell cross-section is that 0% corresponds to outermost, and 100% to innermost layers, respectively. For further information see Milner Garcia 2018

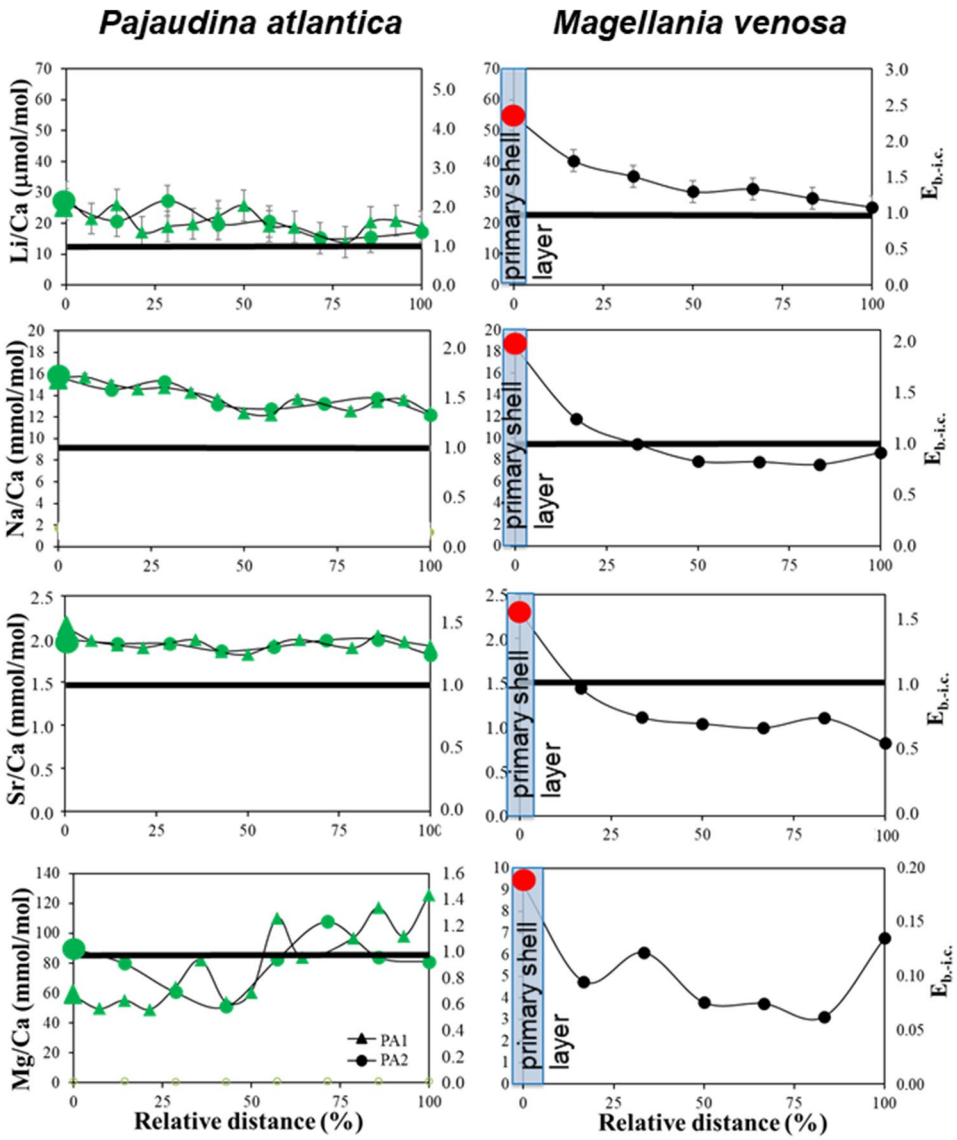

Fig. 34 Li/Ca, Na/Ca, Mg/Ca and Sr/Ca variations along shell cross-sections comprising outermost and innermost shell portions of the ventral valve of *Pajaudina atlantica* and *Magellania venosa*, respectively. Further information is given in Milner Garcia 2018. The black line in the diagrams marks the equilibrium value (see also Okumura and Kitano 1986; Oomori 1987; Marriott et al. 2004; Gabitov and Watson 2006). Error bars represent the standard deviation. The relative distance along the shell cross-section is 0% for the outermost and 100% for the innermost part of the shell. The blue rectangle indicates the extent of the primary layer in *M. venosa*. Eb-i.c. is the ratio of the measured concentration and the value which is expected for equilibrium with sea water

half of the shell (in cross-section) Mg/Ca ratios fluctuate between 50 and 90 mmol/mol, while Mg contents increase within the inner half of the shell and vary between 80 and 120 mmol/mol (Fig. 34).

Strontium distribution in *M. venosa* shells resembles that of magnesium (Fig. 34). As Sr/Ca values are negatively correlated with oxygen isotope compositions, an influence of precipitation rate can be suggested (this study, cf. Ullman et al. 2017; Romanin et al., 2018; Rollion-Bard et al. 2019). Indeed, kinetic effects tend to decrease the value of $\delta^{18}O$ in carbonate (McConnaughey 1989; Zeebe and Wolf-Gladrow 2001; Beck et al. 2005; Rollion-Bard et al. 2011), while an increase in precipitation rate increases the incorporation of Sr into the calcite lattice (Lorens, 1981; Morse et al. 1990). In *P. atlantica*, Sr is homogenous within the shell, Sr/Ca ratios scatter between 1.9 and 2.1 mmol/mol across the cross-section through the shell (Fig. 34 and for other thecideides Lowenstam 1961; Delaney et al. 1989; Carpenter et al. 1991; Carpenter and Lohmann 1995; Brand et al. 2003).

The lithium distribution in the shell of *M. venosa* (Fig. 34) is comparable to that of Sr. The primary layer has some of the highest and most variable values, which is followed by a drop in Li contents in the fibrous shell layer (this study, and Rollion-Bard et al. 2019). In *P. atlantica* as well, Li contents are higher in the outer, relative to the inner portions. However, the decrease in *P. atlantica* is less marked compared to the trend in Li contents in *M. venosa*.

Sodium concentration distribution in *M. venosa* cross-sections through the valve follows closely the trend of Li and Sr (Fig. 34). The primary shell layer is enriched in Na, relative to inner shell regions. Such a trend is observable for Na contents along cross-sections through *P. atlantica* valves as well (Fig. 34), however, less pronounced.

Finally, even though much of the literature invokes precipitation rate effects to explain the deviations from equilibrium with sea water, the simplest explanation, however, is that brachiopod calcite does not precipitate directly from seawater but from the liquid hydrous phase in the extracellular polymeric substance in the well-controlled narrow (maximum some tens of nanometers) space between the epithelial cells and the growing calcite (Simonet Roda et al. 2019a, b). Thus, perhaps brachiopods with their epithelial cells and extracellular hydrous phase control their Sr, Mg, Li and Na shell contents. This intriguing aspect deserves more research.

Section 7: Concluding summary

In Sections one to six, we presented: (1) the diversity of calcite crystal assembly solutions which are utilized by calcite-secreting extant brachiopod orders for shell formation, and (2) a summary of the current knowledge of brachiopod shell structure, micro-and nanostructure, texture and pattern of organic matrix distribution and organization.

In the present section, we place our findings related to microstructure and texture diversity of extant brachiopod shells in a broader context and discuss: (1) a possible adaptation of microstructure and texture to environments, (2) advantages gained for the organism from a shell material that has a composite nature and a hierarchical architecture, (3) determinants of brachiopod microstructure fabrication, and (4) the microstructure of Recent thecideides that we consider to be unique and distinct from the primary layer structure of terebratulide and rhynchonellide.

Microstructure, texture, lifestyle and environment

Modern, calcite-secreting brachiopods show indeterminate mineralization and growth; valves grow in both, length and thickness (Williams 1966; Rosenberg et al. 1988; Baumgarten et al. 2014). The shells of all extant calcite-secreting brachiopods consist of two, differently sized valves. For the species we discuss in this study (Table S1) size difference between the valves is most pronounced in cementing specimens (Craniida, Thecideida), while for species of taxa living attached to substrate by a pedicle (Terebratulida, Rhynchonellida) the difference in ventral and dorsal valve dimensions is less marked.

For the investigated species, we find major differences in shell microstructure and texture between taxa that live in sheltered/cryptic habitats and those that live in relatively open marine environments. *K. chathamensis, P. atlantica* (live in cryptic habitats), *N. anomala* (live in sheltered habitats) are cemented to the substrate and form shells with low crystal co-ordination, of an almost untextured calcite (Figs. 23, 24, 25, 26, 27, 28, 29, 31). The investigated terebratulide and rhynchonellide species live in open marine waters attached to the substrate by a pedicle and secrete shells with well to highly textured calcite (Figs. 19, 20, 21, 30, 31, 32).

When focussing only on the fibrous shell layer, characteristic relationships emerge between structural features of the fibers and environmental and ontogenetic conditions for both terebratulides as well as rhynchonellides (Ye et al. 2018a, b). Ye et al. (2018a, b) investigated adult specimens of six Recent brachiopod species living in three different habitats (Antarctica, the Pacific about New Zealand, Mediterranean Sea) for their fiber convexity, roundness and length. The following characteristics and relationships could be established: (1) there is no difference in morphometric features between fibers in ventral and dorsal valves, (2) there is a connection between morphological characteristics of fibers and ontogenetic development, and (3) there is a link between fiber morphometry and environmental conditions. The latter was, however, only observed when the comparison was made between cogeneric species that live in water with similar salinity, but different temperature and carbonate saturation state. Accordingly, the study of Ye et al. (2018a, b) demonstrates that Recent terebratulide and rhynchonellide brachiopods respond to changes in temperature and carbonate saturation state with subtle changes in microstructure and texture. Nonetheless, any specific brachiopod secretes only one type of fiber.

Peck and Harper (2010) investigated shell size variations of terebratulides and rhynchonellides with latitude and water depth. The study showed a relationship between maximal shell size and environmental conditions (latitude and depth) for the Terebratulida however, not for the Rhynchonellida.

Balthasar and coworkers (Balthasar et al. 2020) investigated, in addition to few Recent species, predominantly fossil (Ordovician and Silurian) taxa and observed a possible connection between shell thickness and environmental perturbations. According to this study, one might conclude that brachiopod shell thickness reflects some, predominantly, major changes in environmental conditions (Balthasar et al. 2020).

Composite nature and hierarchical architecture

Calcium and carbonate are abundant in seawater and are readily available to marine organisms. However, the pure carbonate phases, calcite and aragonite, are of little value as shell construction materials as they are brittle and break easily. For the hard tissue to be protective and functional, the structural biomineral has to be functionalized right from the outset of its formation. The two main means of biomaterial functionalization are the generation of (1) a hierarchical architecture and (2) fabrication of a hybrid composite material; the latter on all scale levels of the biological hard tissue.

1. Organisms employ a bottom-up construction process in fabricating their shell, tooth or skeleton. Material fabrication starts at the level of cells with the secretion of mineral and biopolymer components. As secreted by cells, the first-formed entities have to be small, even though the final product, e.g. the shell, is macro-sized. This specific characteristic is accomplished by utilizing hierarchical assembly principles (e.g. Dunlop and Fratzl 2010; Staudart 2012; Wegst et al. 2014). For Recent rhynchonellide and terebratulide fibrous shell layers, we recognize at least 5 levels of hierarchy: (1) nanometric calcite crystals (Fig. 18A), (2) crystallographically perfectly co-oriented calcite growth increments within fibers (80–100 nm sized, Fig. 18A–C), (3) individual fibers (Figs. 5A, 15C), (4) stacks of fibers (Figs. 3, 6E) the twisted plywood structure of the fibrous layer of the shell (Figs. 3, 5B, 6A). The entire shell that forms the sixth level of the hierarchy.
2. To fabricate a shell, tooth or skeleton of pure calcite or aragonite is biomechanically unsuitable, as it is the case for the formation of a tooth, skeleton or shell of biopolymers alone. To be protective and functional, the structural biomaterial has to be functionalized to satisfy the specific needs of the organism (Merkel et al. 2009; Schmahl et al. 2012). This is achieved with the formation of biopolymer-carbonate composites and various modes of crystal organizational arrangements, microstructures and textures. Phosphate-based biomaterials (e.g. phosphatic brachiopod shells) are composites as well, however, these materials show a gradation in phosphate mineral content (Merkel et al. 2007, 2009). Composite formation occurs on all scales of the hard tissue, from organic membrane bound and mineral/ion-filled vesicles to the macro-scale level of the shell. The latter consists of shell layers formed of a mineral component that incorporates an extracellular matrix (e.g. the fibrous and columnar shell layers of Rhynchonelliformea or the calcite layers within the shell of Craniiformea). Hence, when the biomineral is functionalized with biopolymers, the organic substance becomes incorporated into the mineral. This incorporation is an important and major characteristic that makes the biocarbonate different from its non-biologic calcite/aragonite counterpart. The biologic and non-biologic carbonate minerals have little in common, except (1) the crystal structure of the carbonate phase (calcite or aragonite) and (2) the gross chemical composition of the mineral.

On rare occasions, the inorganic microstructure alone, rather than a hybrid composite assembly, functionalizes the overall material properties of the carbonate biological hard tissue. We observe this in the primary shell layer of rhynchonellide and terebratulide brachiopods. The tightly interdigitating crystals with dendritic outlines, the jigsaw topology of grain boundaries, the polycrystalline assembly of dendritic calcite crystals form material properties that are characteristic for the primary shell layer. A layer with a specific microstructure, a high microhardness and increased resistence to abrasion, relative to the significantly softer subjacent fibrous layer (Griesshaber et al. 2007).

An important feature that distinguishes biogenic from non-biogenic calcite is the absence of (104) cleavage and the increased hardness of the biocalcite, relative to the inorganic equivalent. When not the result of a specific microstructure, an increase in hardness is imparted by the composite nature of the biomaterial, the intercalation of organic substance in the biologically secreted mineral (Merkel et al. 2009; Schmahl et al. 2012). In the composite hard tissue, the mineral component contributes stiffness, provides compressive and bending strength, hardness and abration resistance. The organic component provides morphogenetic control of the biocrystal (e.g. tablet, fiber, prism, Checa et al. 2016), tensile strength, flexibility, ductility (Wegst et al. 2014). As shown in previous sections, the extracellular matrix is a dominant feature of the fibrous shell layer of rhynchonellide and terebratulide brachiopods. The organic matrix makes the biological fibrous composite deformation tolerant, as: (1) it allows for dislodged fibers, (2) deviates and blunts cracks and (3) inhibits crack propagation.

Fibers of brachiopod shells are not just simple rods, but are sophisticated structures. They are variable in roundness, convexity, lengths and thickness (Ye et al. 2018a, b), have elaborate morphologies and are interleaved in three dimensions. Throughout the life of an organism, its structural material is subject to and has to sustain compressive, bending and shearing forces. As fibers within an organic matrix cannot be reorganized after secretion, they must be properly packed and oriented within the hard tissue right from the beginning of their formation. This is accomplished by the generation of stacks of parallel fibres, with the stacks being arranged in a twisted plywood-like structure (Figs. 3, 5B). Brachiopod fiber morphology is specific and unique (Fig. 5 and Simonet Roda et al 2019b). The one convex and the three concave sides allow for the staggered arrangement of the fibers and for the interleaved packing in and to stacks (Figs. 3, 4C, 6C, E, 11B, E). Hence, the specific morphological characteristics of brachiopod fibers, their packing into stacks and the twisted plywood arrangement of the stacks ensures that all components of the fibrous composite are interleaved in three dimensions and on all length scales. Simonet Roda et al. (2019a) noted that rhynchonellide/terebratulide brachiopod fiber arrangements resemble tablet arrangements of sheeted nacreous aragonite in bivalve shells (Fig. A7 in Simonet Roda et al. 2019a). Accordingly, the combination of staggered arrangements and twisted plywood architectures generates highly successful shell microstructures, whether formed by bivalve nacre or brachiopod fibrous shell layers.

Two-layered brachiopod shells consist of a stiff, hard and resilient, protective cap, the primary shell layer, constructed as a thin, surface sheet. Adjacent and inward is a massive, ductile but tough layer, the fibrous shell layer, consisting of a highly efficient fiber-composite structural material (e.g. Figures 3, 6A, C, E, S12A, and Schmahl et al. 2012).

Determinants of microstructure and texture

EBSD measurements of brachiopod shells over the last two decades demonstrate that the shells of the four extant calcite-secreting orders consist of seven types of biomineral units and biocrystals: (1) dendrites (Rhynchonellida, Terebratulida), (2) fibers (Rhynchonellida, Terebratulida), (3) columns (Terebratulida), (4) platelets (Craniida), (5) laminae (Craniida), (6) acicles (Thecideida), and (7) polygonal crystals (Thecideida). Fibers and platelets are intimately associated with an extracellular biopolymer matrix. Columnar layers of terebratulides and polygonal crystal assemblies of thecideides also contain organic matrices, however, the fabric of these is less regular, especially that of the thecideide shells. The matrix of thecideide shells is formed of submicrometer-sized polygonal calcite crystallites that are blended with micrometer-sized or even tens of micrometer-sized crystals. Randomly distributed organic membranes and networks of organic fibrils strengthen the cohesion of the shell material (Figs. 14, S6–S8). Dendrite-shaped crystals form the primary layer of rhynchonellide and terebratulide shells. No organic matter has been observed between interdigitating dendrites with SEM or with TEM, on etched or on unetched shell surfaces (Giesshaber et al. 2009).

An interesting case is the columnar shell layer of terebratulides. Organic membranes are intercalated into the columnar layer, often, delineating individual and neighboring columns. It has, in addition, been also demonstrated that columns form through a competitive growth process (Schmahl et al. 2012). Those observations pose an important question concerning the determinant that influences/controls columnar layer microstructure formation: (a) is it the organic matrix that guides mineral assembly? or (b) is it a competitive crystal growth process? Checa (2018) described determinants for microstructure formation in mollusc shells and demonstrated that microstructure fabrication can be influenced by (1) mainly physical, (2) mainly biological or (3) by both physical as well as biological determinants. For the columnar layer of brachiopods, the main determinant of column formation is growth competition, supported by a membraneous organic matrix, thus a mix of physical and biological determinants. Physical determinants only would operate (1) if the pattern organizes merely by crystal competition, whereas mixed physical plus biological determinants would have to be invoked (2) if the organic matrix is also responsible for the organization of the microstructural pattern. In the latter case, the pattern would follow the evolution of an emulsion between the fluid precursors of the organic and mineral phases. In addition, for the pattern to be continued, mantle cell recognition and differential secretion would have to occur, as it is the case for the columnar prismatic layers in bivalves (Checa et al. 2016; Checa 2018).

Column- and prism-shaped brachiopod crystals that form through crystal growth competition are the closest analogues to non-biologic carbonate (von Allmen et al. 2010). Further prominent examples of biocarbonates that form through competitive growth are myostracal shell layers of bivalves (Crippa et al. 2020a, b) and the carbonate hard tissue of the cephalopod *Argonauta argo* (Stevens et al. 2017). The latter biomaterials consist of highly co-oriented aragonite prisms or calcite crystallites with high MUD values for individual mineral units/biocrystals (MUD > 700). This is what we observed for the columns of *L. neozelanica* and *G. vitreus* (Fig. 21). MUD values for individual columns are close to 700 or above (Fig. 21A, C). High co-orientation strength of crystallites and high MUD values (well above 700) are characteristic for non-biological calcite and aragonite precipitated directly from solution (e.g. Yin et al. 2019).

Castro-Claros et al. (2021) investigated calcium transport to myostracal and non-myostracal shell layers in the bivalves *Anomia ephippium* and *Ostrea stentina*. The authors observed that during mineralization of the myostracum, mantle cells are *not in contact* with the myostracal shell, while when the ostracum and the hypostracum are mineralized, mantle cells are *directly adjacent* to the shell. Castro-Claros et al. (2021) suggest that two modes of shell secretion are in operation in both these bivalves: (1) Ca transport by vesicles at myostracal prism formation and (2) mineralization in direct contact with mantle cells at ostracum and hypostracum formation. Thus, the above mentioned bivalves utilize, at least, two different mineralization processes when they form their shell. It is important to note that the two modes of shell mineralization are mirrored by differences in carbonate microstructure. (1) Myostracal aragonite assembly resembles that of the non-biological mineral counterpart, whereas (2) ostracum and hypostracum shell microstructures are highly sophisticated, hierarchical and diverse.

Simonet Roda et al. (2019a, b) demonstrated that the primary shell layer of the terebratulide brachiopod *M. venosa*, even though being in close contact with the secreting cells, is secreted by cell extensions only, the latter being devoid of cell nuclei. In contrast, the mineralization of fibers, during secretion also in close contact with the cells, occurs through mantle epithelial cells that contain cell nuclei and other organelles. This review clearly demonstrated that primary and fibrous shell layers have highly different microstructural arrangements and biopolymer contents. Furthermore, three-layered terebratulide shells have an additional microstructure: an assembly of columns with microstructural features

highly distinct from those of the primary and fibrous layers. This might indicate that another mode of mineralization is applicable for the columnar shell layer secretion. The columnar shell layer forms through competitive growth, a process that is little dependent on microstructure or, especially, the controlling influence of an organic component. Accordingly, and most probably, three-layered terebratulide brachiopods are not only able to (1) exert different modes of calcite secretion when they form their shell but also to (2) apply, more or less simultaneously, distinct types of determinants for shell fabrication: (1) biological determinants that are in control for forming the fibrous microstructure where mineralization is fully controlled by the activity of the mantle cells [contact recognition connected to differential subcellular secretion of organic and mineral components and cell cooperation (Simonet Roda et al. 2019a, b)] and, (2) physical determinants (growth by crystal competition) when forming columnar microstructures.

Unique microstructure of modern thecideide shells

Modern terebratulide and rhynchonellide brachiopods form layered shells. Descriminants between the layers are the microstructures of the mineral and the fabric of the organic components. For the shell of these taxa the molecular arrangement of ions forming a plane in calcite is linked to the macroscopic morphology of the shell via the orientation pattern of the calcite *c*- and *a**-axes (Fig. 21A, and Schmahl et al. 2004). Both calcite crystallites as well as the occluded organic components have well organized structures and fabrics.

These characteristics are not present in Recent thecideide shells (this study, and Goetz et al. 2009). Instead, the hierarchical architecture typical of terebratulide and rhynchonellide shell calcite (up to 6 levels of hierarchy) was not detected in Recent thecideide shells. The latter form composite shells with calcite and organic components with little ordered arrangements (Figs. 10, 14, 23, 24). A further distinction between Recent thecideide and terebratulide/rhynchonellide shells is the distribution pattern of organic material within the shell. With the exception of the primary shell layer, terebratulide and rhynchonellide fibrous and columnar calcite occludes an extracellular matrix that delineates the mineral units (fibres, columns) from each other. In addition, we know that the fibers intercalate some amount of organic substance in the form of a network of fibrils (Fig. 15F). Accordingly, in terebratulide/rhynchonellide shells the distribution pattern of organic material is structured and hierarchical, another feature that we do not observe in Recent thecideide shells. In the latter, much organic material is intercalated into the calcite (membranes, fibrils) however, without any structured distribution pattern, consisting essentially of an extracellular matrix filled with mineral. The mineral component in Recent thecideide shells consists of a groundmass of submicrometer-sized calcite crystallites with interspersed irregularly-shaped micrometer-sized crystals (Figs. 23, S14). These calcite crystals do not have a dendritic structure typical for the primary shell layer of terebratulides and rhynchonellides. Nor do we see in thecideides strong interdigitation of neighboring crystals, as it is the case for the primary shell layer of Terebratulida and Rhynchonellida.

In summary, our review demonstrates that the microstructure and texture of Recent thecideides is a unique structure amongst extant taxa, specific to this brachiopod order (Simonet Roda et al. 2021). It is dissimilar to the microstructure and texture of the primary layer of Recent rhynchonellide and terebratulide brachiopods; the latter consists of interlocked crystals with dendritic boundaries, being devoid of organic substance and having a strong texture. These contrast all structural characteristics we find for the hard tissue of Recent Thecideida.

Our geochemical results (Figs. 33, 34) substantiate the distinctness between thecideide and terebratulide shells: (1) *P. atlantica* (thecideide) secretes high-Mg calcite, *M. venosa* (terebratulide) forms its shell of low-Mg calcite, (2) the range in Li, Na, Mg, Sr concentration is larger for *M. venosa* shells, in comparison to what we observe for *P. atlantica* valves. Even though, oxygen isotope results for inner ventral valve sections of *P. atlantica* (thecideide) fall within the $\delta^{18}O$ equilibrium zone (this study, and Brand et al. 2003). This result could be interpreted that parts of thecideide shells might be appropriate as archives for environmental reconstruction. However, the drawback is that thecideide shell fabric is not sub-structured into layers, sections, regions. Thus, the problem is, where in the thecideide shell do we base the distinction between outer and inner shell portions, between valve sections precipitated in equilibrium or in disequilibrium with ambient seawater? Even if this distinction could be made for thecideide shells, localization between different shell portions will vary for each specimen and in some cases might not be possible. In addition, due to their high-Mg calcite shells, thecideides are more prone to diagenetic overprinting, relative to low-Mg calcite shelled brachiopods. Thus, in contrast to terebratulides and rhynchonellides, their unstructured shell fabric does not allow for a distinction between (1) overprinted shells that lost their pristine microstructure due to diagenesis or simply (2) a possibly pristine but little organized shell fabric, that is an intrinsic feature of representatives of Recent thecideide taxa.

Supplementary Information The online version contains supplementary material available at https://doi.org/10.1007/s00227-021-03962-4.

Acknowledgements We thank Dr. C. Lüter for the *Kakanuiella chathamensis* specimens. We thank Dr. F. Nindiyasari and J. Huber for microtome preparation and etching of many shell samples; M. Zenkert for preparation of some brachiopod shells for EBSD measurements.

We thank Dr. H. Jurikova for taking care of culturing Recent *Magellania venosa* and *Pajaudina atlantica* in aquaria at GEOMAR Helmholtz Zentrum für Meeresforschung, Kiel, Germany. We, in particular, express our thanks to Prof. P. Walter and Dr. A. Ziegler for letting us to use for many years the laboratory equipment at the Center for Electron Microscopy, University of Ulm. We thank Pierre Burckel for his help with ICP-MS analyses. We thank Dr. N. Lagos for the *Tegula atra* specimens and Dr. S. Hahn for the *Mytilus edulis* species. Finally, we want to express our thanks to Prof. J. Veizer and Dr. R. Neuser with whom we started EBSD measurements on carbonate biological hard tissues of marine organisms.

Author contributions EG and MSR initiated this article. MSR and EG performed the EBSD measurements, AFM, FE-SEM and STEM imaging and EBSD data analysis. HG provided the microtome sections for STEM imaging. AL, UB, LA, AB, FY, DH and VH provided shell material. CR-B, SM provided the geochemical data. WS contributed to the interpretation of EBSD data. LA, EH, AB, UB, WWS contributed and improved significantly the discussion. All authors, MSR, EG, LA, CR-B, EH, MAB, SM, FY, DH, VH, AE, HG, UB, AL, WWS contributed to the final version of the manuscript.

Funding Open Access funding enabled and organized by Projekt DEAL. This project received funding from the European Union's Horizon 2020 research and innovation programme under Grant agreement no 643084 and the German Research Council Programmes GR 9/1234 and SCHM 930/11-2.

Data availability The datasets generated during and/or analysed during the current study are available from the corresponding author on request.

Declarations

Conflict of interest We have no conflict of interest.

Ethical approval All applicable international, national and/or institutional guidelines for sampling, care and experimental use of organisms have been followed and all necessary approvals have been obtained. Details about permissions and documentary evidence are available on request.

References

Al-Aasm IS, Veizer JJ (1982) Chemical stabilization of low-magnesium calcite: an example of brachiopods. J Sed Petrol 52:1101–1109

Angiolini L, Jadoul F, Leng MJ, Stephenson MH, Rushton J, Cheney S, Crippa G (2009) How cold were Early Permian glacial tropics? Testing sea-surface temperature using the oxygen isotope composition of rigorously screened brachiopod shells. Geol Soc 166:933–945

Auclair AC, Joachimski MM, Lécuyer C (2003) Deciphering kinetic, metabolic, and environmental controls on stable isotope fractionations between seawater and the shell of *Terebratalia transversa* (Brachiopoda). Chem Geol 202:59–78

Bajnai D, Fiebig J, Tomašových A, Milner Garcia S, Rollion-Bard C, Raddatz J, Löffler N, Primo-Ramos C, Brand U (2018) Assessing kinetic fractionation in brachiopod calcite using clumped isotopes. Sci Rep 8:533

Baker PG (1990) The classification, origin and phylogeny of thecideidine brachiopods. Palaeontology 33:175–191

Baker PG (2006) Thecideida. In: Kaesler RL (ed) Treatise on invertebrate paleontology Part H. Brachiopoda 5 (revised), Geological Society of America, Boulder, and University of Kansas Press, Lawrence, Kansas, pp 1938–1943

Balthasar U, Jin J, Hints L, Cusack M (2020) Brachiopod shell thickness links environment and evolution. Paleontology 63:171–183

Baumgarten S, Laudien J, Jantzen C, Haussermann V, Försterra G (2014) Population structur, growth and production of a recent brachiopod from the Chilean fjord region. Mar Ecol 35:401–413

Beck WC, Grossman EL, Morse JW (2005) Experimental studies of oxygen isotope fractionation in the carbonic acid system at 15, 25, and 40 °C. Geochim Cosmochim Acta 69:3493–3503

Bevelander G, Nakahara H (1969) An electron miscroscope study of the formation of the nacreous layer in the shell of certain bivalve molluscs. Calc Tissue Res 3:84–92

Bitner MA (2010) Biodiversity of shallow-water brachiopods from New Caledonia, SW Pacific, with description of a new species. Sci Marina 74:643–657

Bitner MA (2019) Recent brachiopods from the Tonga islands, SW Pacific: taxonomy and biogeography. Riv Ital Paleontol Stratigr 125:587–608

Brand U, Logan A, Hiller N, Richardson J (2003) Geochemistry of modern brachiopods: applications and implications for oceanography and paleoceanography. Chem Geol 198:305–334

Brand U, Logan A, Bitner MA, Griesshaber E, Azmy K, Buhl D (2011) What is the ideal proxy of Palaeozoic seawater chemistry? Mem Assoc Australas Palaeontol 41:9–24

Brand U, Bitner MA, Logan A, Azmy K, Crippa G, Angiolini L, Colin P, Griesshaber E, Harper EM, Taddei Ruggiero E, Häussermann V (2019) Brachiopod-based oxygen-isotope thermometer: update and review. Riv Ital Paleont Strat 125:775–787

Brock KJ (1993) The crystal forms of calcite. Min Rec 24:451–461

Castro-Claros JD, Checa A, Lucena C, Pearson JR, Salas C (2021) Shell-adductor muscle attachment and Ca^{2+} transport in the bivalves *Ostrea stentina* and *Anomia ephippium*. Acta Biomater 120:249–262

Carlson SJ (1995) Phylogenetic relationships among extant brachiopods. Cladistics 11:131–197

Carlson SJ (2007) Recent research on brachiopod evolution. In: Selden PA (ed) Treatise on invertebrate paleontology Part H. Brachiopoda 6, Geological Society of America, Boulder, and University of Kansas Press, Lawrence, Kansas, pp 2878–2900

Carlson SJ (2016) The evolution of Brachiopoda. Annu Rev Earth Planet Sci 44:409–438

Cartwright JHE, Checa AG (2007) The dynamics of nacre self-assembly. J R Soc Interface 4:491–504

Carpenter SJ, Lohmann KC, Holden P, Walter LM, Hoston T, Halliday AN (1991) $\delta^{18}O$ values, $^{87}Sr/^{86}Sr$ and Sr/Mg ratios of late Devonian abiotic marine calcite: implications for the composition of ancient seawater. Geochim Cosmochim Acta 55:1991–2010

Carpenter SJ, Lohmann KC (1995) $\delta^{18}O$ and $\delta^{13}C$ values of modern brachiopod shells. Geochim Cosmochim Acta 59:3749–3764

Casella LA, Griesshaber E, Simonet Roda M, Ziegler A, Mavromatis V, Henkel D, Laudien J, Häussermann V, Neuser RD, Angiolini L, Dietzel M, Eisenhauer A, Immenhauser A, Brand U, Schmahl WW (2018) Micro- and nanostructures reflect the degree of diagenetic alteration in modern and fossil brachiopod shell calcite: a multi-analytical screening approach (CL, FE-SEM, AFM, EBSD). Palaeogeogr Palaeoclimatol Palaeoecol 502:13–30

Checa A (2018) Physical and biological determinants of the fabrication of molluscan shell microstructures. Front Mar Sci 5:353

Checa AG, Gaspard D, González-Segura A, Ramírez-Rico J (2009) Crystallography of the calcitic foliated-like and seminacre microstructures of the brachiopod *Novocrania*. Cryst Growth Des 9:2464–2469

Checa AG, Macías-Sánchez E, Harper EM, Cartwright JHE (2016) Organic membranes determine the pattern of the columnar prismatic layer of mollusc shells. Proc R Soc B 283:20160032. https://doi.org/10.1098/rspb.2016.0032

Checa A, Yáñez-Avila M, González-Segura A, Varela-Feria F, Griesshaber E, Schmahl WW (2019) Bending and branching of calcite laths in the foliated microstructure of pectinoidean bivalves occurs at coherent crystal lattice orientation. J Struct Biol 205:7–17

Crippa G, Griesshaber E, Checa AG, Harper E, Simonet Roda M, Schmahl WW (2020a) Orientation patterns of the aragonitic crossed-lamellar, myostracal and fibrous microstructures of modern *Glycymeris* shells. J Struct Biol 212:107653

Crippa G, Griesshaber E, Checa AG, Harper EM, Simonet Roda M, Schmahl WW (2020b) SEM, EBSD, laser confocal microscopy and FE-SEM data from modern *Glycymeris* shell layers. Data Brief 33:106547

Cross EL, Peck LS, Harper EM (2015) Ocean acidification does not impact shell growth or repair of the Antarctic brachiopod *Liothyrella uva* (Broderip, 1833). J Exp Mar Biol Ecol 462:29–35

Cross EL, Peck LS, Lamare MD, Harper EM (2016) No ocean acidification effects on shell growth and repair in the New Zealand brachiopod *Calloria inconspicua* (Sowerby, 1846). ICES J Mar Sci 73:920–926

Cross EL, Harper EM, Peck LS (2018) A 120-year record of resilience to environmental change in brachiopods. Glob Change Biol 24:2262–2271

Cusack M, Williams A (2007) Biochemistry and diversity of brachiopod shells. In: Selden PA (ed) Treatise on invertebrate paleontology. Part H, Brachiopoda 1, Geological Society of America, Boulder, Colourado and University of Kansas Press, Lawrence, Kansas, pp 2373–2395

Cusack M, Dauphin Y, Chung P, Pérez-Huerta A, Cuif JP (2008) Multiscale structure of calcite fibres of the shell of the brachiopod *Terebratulina retusa*. J Struct Biol 164:96–100

Curry GB, Brunton CH (2007) Stratigraphic distribution of brachiopods. In: Selden PA (ed) Treatise on invertebrate paleontology. Part H, revised, Brachiopoda. Geological Society of America and Paleontological Institute, Boulder, Colourado, and Lawrence, Kansas, pp 2901–3081

Delaney ML, Popp BN, Lepzelter CG, Anderson TF (1989) Lithium-to calcium ratios in modern, Cenozoic and Paleozoic articulate brachiopod shells. Paleoceanography 4:681–691

Dunlop JWC, Fratzl P (2010) Biological composites. Annu Rev Mater Res 40:1–24

Emig CC (1997a) Biogeography of the inarticulated brachiopods. In: Kaesler RL (ed) Treatise on invertebrate paleontology. Part H. Brachiopoda. Geological Society of America and University of Kansas. Boulder, Colorado, and Lawrence, Kansas, pp 497–502

Emig CC (1997b) Ecology of the inarticulated brachiopods. In: Kaesler RL (ed) Treatise on invertebrate paleontology. Part H. Brachiopoda. Geological Society of America and University of Kansas. Boulder, Colorado, and Lawrence, Kansas, pp 473–495

Emig CC, Bitner MA, Álvarez F (2013) Phylum Brachiopoda. Zootaxa 3703:75–78

Emig CC (2017) Atlas of Antarctic and sub-Antarctic Brachiopoda. Carnets de Géologie CG2017 B03

England J, Cusack M, Dalbeck P, Pérez-Huerta A (2007) Comparison of the crystallographic structure of semi nacre and nacre by electron backscatter diffraction. Cryst Growth Des 7:307–310

Engler O, Randle V (2009) Introduction to texture analysis: macrotexture, microtexture, and orientation mapping. CRC Press, Boca Raton, p 488

Finnegan S, Rasmussen CMØ, Harper DAT (2016) Biogeographic and bathymetric determinants of brachiopod extinction and survival during the Late Ordovician mass extinction. Proc Royal Soc B 283:20160007

Garbelli C, Angiolini L, Jadoul F, Brand U (2012) Micromorphology and differential preservation of Upper Permian brachiopod low-Mg calcite. Chem Geol 299:1–10

Garbelli C, Angiolini L, Brand U, Jadoul F (2014) Brachiopod fabric, classes and biogeochemistry: implications for the reconstruction and interpretation of seawater carbon—isotope curves and records. Chem Geol 371:60–67

Gaspard D, Nouet J (2016) Hierarchical architecture of the inner layers of selected extant rhynchonelliform brachiopods. J Struct Biol 196:197–205

Goetz AJ, Griesshaber E, Neuser RDL, Harper E, Schmahl WW (2009) Calcite morphology, texture and hardness in the distinct layers of rhynchonelliform brachiopod shells. Eur J Mineral 21:303–315

Goetz AJ, Steinmetz DR, Griesshaber E, Zaefferer S, Raabe D, Kelm K, Irsen S, Sehrbrock A, Schmahl WW (2011) Interdigitating biocalcite dendrites form a 3-D jigsaw structure in brachiopod shells. Acta Biomater 7:2237–2243

Goetz AJ, Griesshaber E, Abel R, Fehr T, Ruthensteiner B, Schmahl WW (2014) Tailored order: the mesocrystalline nature of sea urchin teeth. Acta Biomater 10:3885–3898

Griesshaber E, Schmahl WW, Neuser RD, Job R, Bluem M, Brand U (2005) Microstructure of brachiopod shells—an inorganic/organic fibre composite with nanocrystalline protective layer. In: Katti K, Ulm FJ, Hellmich C, Viney C (eds) Mechanical properties of bio-inspired and biological materials, MRS symposium proceedings series, vol 844, pp 99–104

Griesshaber E, Schmahl WW, Neuser R, Pettke T, Blüm M, Mutterlose J, Brand U (2007) Crystallographic texture and microstructure of terebratulide brachiopod shell calcite: an optimized materials design with hierarchical architecture. Am Mineral 92:722–734

Griesshaber E, Kelm K, Sehrbrock A, Mader W, Mutterlose J, Brand U, Schmahl WW (2009) Amorphous calcium carbonate in the shell material of the brachiopod *Megerlia truncata*. Eur J Mineral 21:715–723

Griesshaber E, Schmahl WW, Ubhi HS, Huber J, Nindiyasari F, Maier B, Ziegler A (2013) Homoepitaxial meso- and microscale crystal co-orientation and organic matrix network structure in *Mytilus edulis* nacre and calcite. Acta Biomater 9:9492–9502

Griesshaber E, Yin X, Ziegler A, Kelm K, Checa A, Eisenhauer A, Schmahl WW (2017) Patterns of mineral organization in carbonate biological hard materials. In: Heuss-Aßbichler S, Amthauer G, John M (eds) Highlights in applied mineralogy. De Gruyter, Berlin, pp 245–272

Harper DAT, Drachen A (2010) The Orthida: the rise and fall of a great Palaeozoic clade. Spec Pap Palaentol 84:107–117

Harper DAT, Renbin Z, Jisuo J (2015) The Great Ordovician Biodiversification Event: reviewing two decades of research on diversity's big bang illustrated by mainly brachiopod data. Palaeoworld 24:75–85

Harper DAT, Popov LE, Holmer LE (2017) Brachiopods: origin and early history. Palaeontology 60:609–631

He WH, Shi GR, Zhang KX, Yang T-L, Shen S-Z, Zhang Y (2019) Brachiopods around the Permian–Triassic boundary of South China. New records of the great dying in South China. Springer, Berlin

Holmer LE, Skovsted CB, Brock GA, Popov LE (2011) An early Cambrian chileate brachiopod from South Australia and its phylogenetic significance. Australas Palaeontol Mem 41:289–294

Immenhauser A, Schöne BR, Hoffmann R, Niedermayr A (2015) Mollusc and brachiopod hard parts: intricate archives of their marine environment. Sedimentology 63:1–59

James MA, Ansell AD, Collins MJ, Curry GB, Peck LS, Rhodes MC (1992) Biology of living brachiopods. Adv Mar Biol 28:175–387

Jurikova H, Gutjar M, Wallmann K, Flögel S, Liebetrau V, Posenato R, Angiolini L, Garbelli C, Brand U, Wiedenbeck M, Eisenhauer A (2020) Permian-Triassic mass extinction pulses driven by major marine carbon cycle perturbations. Nature Geosci 13:745–750

Logan A (2007) Geographic distribution of extant articulated brachiopods. In: Kaesler RL (ed) Treatise on invertebrate paleontology. Part H, Brachiopoda 6 (revised) Geological Society of America, Boulder, Colourado and University of Kansas Press, Lawrence, Kansas, pp 2822–2855

Lorens RB (1981) Sr, Cd, Mn and Co distribution coefficients in calcite as a function of calcite precipitation rate. Geochim Cosmochim Acta 45:553–561

Lowenstam H (1961) Mineralogy, O^{18}/O^{16} ratios and strontium and magnesium content of recent and fossil brachiopods and their bearing on the history of the oceans. J Geol 69:241–260

Lüter C (2005) The first modern species of the unusual brachiopod *Kakanuiella* (Thecideidae) from New Zealand deep waters. Syst Biodivers 3:105–111

McConnaughey T (1989) ^{13}C and ^{18}O isotopic disequilibrium in biological carbonates: II. In vitro simulation of kinetic isotope effects. Geochim Cosmochim Acta 53:163–171

Merkel C, Griesshaber E, Kelm K, Neuser R, Jordan G, Logan A, Mader W, Schmahl WW (2007) Micromechanical properties and structural characterization of modern inarticulated brachiopod shells. J Geophys Res 112:G02008

Merkel C, Deuschle J, Griesshaber E, Enders S, Steinhauser E, Hochleitner R, Brand U, Schmahl WW (2009) Mechanical properties of modern calcite- (*Mergerlia truncata*) and phosphate-shelled brachiopods (*Discradisca stella* and *Lingula anatina*) determined by nanoindentation. J Struct Biol 168:396–408

Milner Garcia S (2018) Evaluation of the biomineralization and chemical differentiation in brachiopods. Dissertation, Sorbonne Université, Paris

Morse JW, Bender ML (1990) Partition coefficients in calcite: examination of factors influencing the validity of experimental results and their application to natural systems. Chem Geol 82:265–277

Nakahara H (1991) Nacre formation in bivalve and gastropod molluscs. In: Suga S, Nakahara H (eds) Mechanisms and phylogeny of mineralization in biological systems. Springer, Berlin, pp 343–350

Nebelsick JD, Bassi D, Rasser MW (2011) Cryptic relicts from the past: Paleoecology and taphonomy of encrusting thecideid brachiopods in Paleogene carbonates. Ann Naturhist Mus Wien 113:525–542

Parkinson D, Curry GB, Cusack M, Fallick AE (2005) Shell structure, patterns and trends of oxygen and carbon stable isotopes in modern brachiopod shells. Chem Geol 219:193–235

Payne J, Clapham M (2012) End-Permian mass extinction in the oceans: an ancient analog for the 21st century? Annu Rev Earth Planet Sci 40:89–111

Peck L (2007) Brachiopods and climate change Brachiopods and climate change. Earth Environ Sci Trans R Soc Edinb 98:451–456

Peck LS, Harper EM (2010) Variation in size of living articulated brachiopods with latitude and depth. Mar Biol 157:2205–2213

Peck LS, Brockington S, Brey T (1997) Growth and metabolism in the Antarctic brachiopod *Liothyrella uva*. Philos Trans R Soc Lond Biol Sci 352:851–858

Pérez-Huerta A, Cusack M, England J (2007) Crystallography and diagenesis in fossil craniid brachiopods. Palaeontology 50:757–763

Peter NJ, Griesshaber E, Reisecker Ch, Hild S, Oliveira MVG, Ziegler A, Schmahl WW, Arzt E, Schneider AS (2021) Microstructure, texture and material property relationships in mollusc shells. Acta Biomat (submitted)

Richards PR (1999) The four twin laws of calcite and how to recognize them. Rocks and Minerals 74:308–317

Richardson JR (1997a) Ecology of articulated brachiopods. In: Kaesler RL (ed) Treatise on invertebrate palaeontology. Part H, Brachiopoda 1. Geological Society of America, Boulder, Colourado and University of Kansas Press, Lawrence, Kansas, pp 441–462

Richardson JR (1997b) Biogeography of articulated brachiopods. In: Kaesler RL (ed) Treatise on invertebrate palaeontology. Part H, Brachiopoda 1. Geological Society of America, Boulder, Colourado and University of Kansas Press, Lawrence, Kansas, pp 463–472

Rollion-Bard C, Mangin D, Champenois M (2007) Development and application of oxygen and carbon isotopic measurements of biogenic carbonates by ion microprobe. Geostand Geoanal Res 31:39–50

Rollion-Bard C, Marin-Carbonne J (2011) Measurements of SIMS matrix effects on oxygen isotopic compositions in carbonates. J Anal at Spectrom 26:1285–1289

Rollion-Bard C, Chaussidon M, France-Lanord C (2011) Biological control of internal pH in scleractinian corals: implications on paleo-pH and paleo-temperature reconstructions. C R Geosci 343:397–405

Rollion-Bard C, Saulnier S, Vigier N, Schumacher A, Chaussidon M, Lécuyer C (2016) Variability in magnesium, carbon and oxygen isotope compositions of brachiopod shells: implications for paleoceanographic studies. Chem Geol 423:49–60

Rollion-Bard C, Milner Garcia S, Burckel P, Angiolini L, Jurikova H, Tomašových A, Henkel D (2019) Assessing the biomineralization processes in the shell layers of modern brachiopods from oxygen isotopic composition and elemental ratios: implications for their use as paleonvironmental proxies. Chem Geol 524:49–66

Romanin M, Crippa G, Ye F, Brand U, Bitner MA, Gaspard D, Häussermann V, Laudien JA (2018) Sampling strategy for recent and fossil brachiopods: 1321 selecting the optimal shell segment for geochemical analyses. Riv Ital Di Paleontol e Stratigr 124:343–359

Rosenberg GD, Hughes WW, Tkachuck RD (1988) Intermediary metabolism and shell growth in the brachiopod *Terebratalia transversa*. Lethaia 21:219–230

Rudwick MJS (1959) The growth and form of brachiopod shells. Geol Mag 96:1–24

Rudwick MJS (1970) Living and fossil brachiopods. Hutchinson University Library, London

Shiino Y, Suzuki Y (2010) The ideal hydrodynamic form of the concavo-convex productide brachiopod shell. Lethaia 44:329–343

Shiino Y, Angiolini L (2014) Hydrodynamic advantages in the free-living spiriferide brachiopod *Pachycyrtella omanensis*: functional insight into adaptation to high-energy flow environments. Lethaia 47:216–228

Schmahl WW, Griesshaber E, Neuser R, Lenze A, Job R, Brand U (2004) The microstructure of the fibrous layer of terebratulide brachiopod shell calcite. Eur J Mineral 16:693–697

Schmahl WW, Griesshaber E, Merkel C, Kelm K, Deuschle J, Neuser RD, Goetz AJ, Sehrbrock A, Mader W (2008) Hierarchical fibre composite structure and micromechanical properties of

phosphatic and calcitic brachiopod shell biomaterials—an overview. Mineral Mag 72:541–562
Schmahl WW, Griesshaber E, Kelm K, Goetz A, Jordan G, Ball A, Xu D, Merkel C, Brand U (2012) Hierarchical structure of marine shell biomaterials: biomechanical functionalization of calcite by brachiopods. Z Kristallogr Cryst Mater 227:793–811
Simonet Roda M, Ziegler A, Griesshaber E, Yin X, Rupp U, Greiner M, Henkel D, Häusermann V, Eisenhauer A, Laudien J, Schmahl WW (2019a) Terebratulide brachiopod shell biomineralization by mantle epithelial cells. J Struct Biol 207:136–157
Simonet Roda M, Griesshaber E, Ziegler A, Rupp U, Yin X, Henkel D, Häussermann V, Laudien J, Brand U, Eisenhauer A, Checa AG, Schmahl WW (2019b) Calcite fibre formation in modern brachiopod shells. Sci Rep 9:598
Simonet Roda M (2021) Pathways of biomineralization and microstructure evolution in brachiopod shells. Ph.D. Thesis submitted to the Department of Earth and Environment Sciences LMU Munich, Munich, Germany
Simonet Roda M, Griesshaber E, Angiolini L, Harper David DAT, Jansen U, Bitner MA, Henkel D, Manzanero E, Müller T, Tomasovych A, Eisenhauer A, Ziegler A, Schmahl WW (2021) The evolution of thecideide microstructures and textures: traced from Triassic to Holocene. Lethaia. https://doi.org/10.1111/let.12422
Staudart AR (2012) Towards high-performance bioinspired composites. Adv Mater 24:5024–5044
Stevens K, Griesshaber E, Casella LA, Iba Y, Mutterlose J (2017) Belemnite biomineralization, development and geochemistry: the complex rostrum of *Neohibolites minimus*. Paleogeogr Paleoclimatol Paleoecol 468:388–402
Stojakivic D (2012) Electron backscatter diffraction in materials characterization. Proc Appl Ceram 6:1–13
Schwartz AJ, Kumar M, Adams BL (2000) Electron backscatter diffraction in materials science. Kluwer Academic/Plenum Publishers, New York, p 339
Takayanagi H, Asami R, Abe O, Miyajima T, Kitagawa H, Sasaki K, Iryu Y (2013) Intraspecific variations in carbon-isotope and oxygen-isotope compositions of a brachiopod *Basiliola lucida* collected off Okinawa-jima, southwestern Japan. Geochim Cosmochim Acta 115:115–136
Tretsch H (1950) Observations on Vickers microhardness in calcite. Mikroskopie 5:172–183
Ullmann CV, Frei R, Korte C, Lüter C (2017) Element/Ca, C and O isotope ratios in modern brachiopods: species-specific signals of biomineralization. Chem Geol 460:15–24
Ushatinskaya GT (2008) Origin and dispersal of the earliest brachiopods. Paleontol J 42:776–791 ((**English translation**))
Veizer J, Ala D, Azmy K, Bruckschen P, Buhl D, Bruhn F, Carden GAF, Diener A, Ebneth S, Godderis Y, Jasper T, Korte C, Pawellek F, Podlaha OG, Strauss H (1999) $^{87}Sr/^{86}Sr$, $\delta^{13}C$ and $\delta^{18}O$ evolution of Phanerozoic seawater. Chem Geol 161:59–88
Von Allmen K, Nägler TF, Pettke T, Hippler D, Griesshaber E, Logan A, Eisenhauer A, Samankassou E (2010) Stable isotope profiles (Ca, O, C) through modern brachiopod shells of *T. septentrionalis* and *G. vitreus*: implications for calcium isotope paleo-ocean chemistry. Chem Geol 269:210–219
Wegst UGK, Bai H, Saiz E, Tomsia AP, Ritchie RO (2014) Bioinspired structural materials. Nat Mater 14:23–36
Watkins JM, Nielsen LC, Reyerson FJ, DePaolo DJ (2013) The influence of kinetics on the oxygen isotope composition of calcium carbonate. Earth Planet Sci Lett 375:349–360
Williams A (1966) Growth and structure of the shell of living articulate brachiopods. Nature 211:1146–1148
Williams A, Wright AD (1970) Shell structure of the Craniacea and other calcareous inarticulate Brachiopoda. Spec Pap Palaentol 7:1–51
Williams A (1973) The secretion and structural evolution of the shell of Thecideidine brachiopods. Philos Trans R Soc Lond B 264:439–478
Williams A, Carlson SJ, Brunton CHC, Holmer LE, Polov LE (1996) A supra-ordinal classification of the Brachiopoda. Philos Trans R Soc B 35:1171–1193
Williams A (1997) Shell structure. In: Kaesler RL (ed) Treatise on Invertebrate Palaeontology. Part H, Brachiopoda 1 (Revised). Geological Society of America, Boulder, Colourado and University of Kansas Press, Lawrence, Kansas, pp 267–320
Williams A, Carlson SJ (2007) Affinities of brachiopods and trends in their evolution. In: Selden PA (ed) Treatise on invertebrate paleontology, Part H, Brachiopoda 6 (Revised). Geological Society of America, Boulder, Colourado and University of Kansas Press, Lawrence, Kansas, pp 2822–2877
Williams A, Cusack M (2007) Chemico structural diversity of the brachiopod shell. In: Selden PA (ed) Treatise on invertebrate paleontology. Part H, Brachiopoda 6 (Revised), Geological Society of America, Boulder, Colourado and University of Kansas Press, Lawrence, Kansas, pp 2397–2521
Wilkinson AJ, Britton TB (2012) Strains, planes, and EBSD in materials science. Mater Today 15(9):366–374
Yamamoto K, Asami R, Iryu Y (2010) Within-shelf variations in carbon and oxygen isotope compositions of two modern brachiopods from subtropical shelf environments off Amami-o-shima, southwestern Japan. Geochem Geophys Geosyst 11:1–16
Yamamoto K, Asami R, Iryu Y (2013) Correlative relationships between carbon–and oxygen-isotope records in two cool temperate brachiopod species off Otsuchi Bay, northeastern Japan. Paleontol Res 17:12–26
Ye F, Crippa G, Angiolini L, Brand U, Capitani G, Cusack M, Garbelli C, Griesshaber E, Harper EM, Schmahl WW (2018a) Mapping of recent brachiopod microstructure: a tool for environmental studies. J Struct Biol 201:221–236
Ye F, Crippa G, Garbelli C, Griesshaber E (2018b) Microstructural data of six modern brachiopod species: SEM, EBSD, morphometric and statistical analyses. Data Brief 18:300–318
Ye F, Jurikova H, Angiolini L, Brand U, Crippa G, Henkel D, Laudien J, Hiebenthal C, Šmajgl D (2019) Variation in brachiopod microstructure and isotope geochemistry under low pH–ocean acidification–conditions. Biogeosciences 16:617–642
Yin X, Griesshaber E, Fernández-Díaz L, Ziegler A, García-García FJ, Schmahl WW (2019) Influence of gelatin-agarose composites and Mg on hydrogel carbonate aggregate formation and architecture. Cryst Growth Des 19:5696–5715
Yin X, Griesshaber E, Checa A, Nindijasari-Behal F, Sanchez-Almazo I, Ziegler A, Schmahl WW (2021) Calcite crystal orientation patterns in the bilayers of laminated shells in benthic rotaliid foraminifera. J Struct Biol. https://doi.org/10.1016/j.jsb.2021.107707
Zeebe RE, Wolf-Gladrow D (2001) CO_2 in seawater: equilibrium, kinetics, isotopes. Elsevier oceanography book series, vol 65. Gulf Professional Publishing, Houston